

**THÈSE DE DOCTORAT
DE L'UNIVERSITÉ DE LILLE**

Laboratoire de Mécanique multiphysique et multiéchelle - FRE 2016

Présenté par

Bei Han

pour obtenir le grade de

DOCTEUR DE L'UNIVERSITÉ LILLE

Domaine

GÉNIE CIVIL

Sujet de la thèse

**Étude expérimentale du calcaire et la constitution de
modèle micro-macro pour les roches typiquement poreuses**

Soutenue le 13 septembre 2018 devant le jury composé de :

D. HOXHA	PR	PRISME, Université Orléans	<i>Rapporteur</i>
M.SOULEY	HDR	INERIS	<i>Rapporteur</i>
J. SULEM	PR	NAVIER, Ecole des Ponts ParisTech	<i>Examineur</i>
A. ABOU CHAKRA	MCF	INSA Toulouse	<i>Examinatrice</i>
W.Q.SHEN	MCF	LaMcube, Université de Lille	<i>Co-encadrant</i>
J.F. SHAO	PR	LaMcube, Université de Lille	<i>Directeur de thèse</i>

LaMcube-L'UNIVERSITÉ DE LILLE

Abstract

In this work, a series of experimental investigations has been performed on the basic mechanical behavior, permeability evolution and effects of pore pressure on plastic deformation and failure of a medium-porosity limestone, Anstrude limestone. The obtained results allow to identifying two basic plastic deformation mechanisms, the plastic shearing and pore collapse, and their effects on the permeability evolution, as well as the effects of pore pressure on plastic deformation and failure of water saturated Anstrude limestone. Based on experimental data, the validity of effective stress concept for plastic yielding and failure strength is discussed. For modelling the mechanical and poromechanical behaviors of porous rock, based on a recent Gurson-type model of porous material with a Mises–Schleicher matrix [Shen et al., 2015], a micromechanics-based model is firstly proposed to describe the mechanical behavior of porous rocks. Considering that the high-porosity rock exhibits a volumetric compaction under low confining pressure, a non-associated model is then proposed for porous rock. At first, the proposed model is applied to describe a typical high-porosity chalk, Lixhe chalk. Both the mechanical and poromechanical behaviors of oil and water saturated chalk are studied by adopting the proposed model. Numerical simulations show that the proposed model describes correctly the main features of the mechanical behaviors of the porous chalk with effect porosity. On considering the mechanical behavior of porous limestone, the model is then extended to describe the mechanical behavior of studied limestone by taking the effect of porosity evolution into account in the hardening effect of solid matrix. From a high-porosity chalk to a medium porosity limestone, the proposed model is finally verified in different loading conditions through comparisons between the numerical predictions and experimental data for both drained and undrained tests.

Résumé

Dans ce travail, une série d'études expérimentales ont été effectuées sur le comportement mécanique de base, l'évolution de la perméabilité et les effets de la pression interstitielle sur la déformation plastique et la rupture d'un calcaire à porosité moyenne, calcaire Anstrude. Les résultats obtenus permettent d'identifier deux mécanismes fondamentaux de déformation plastique, le cisaillement plastique et l'effondrement de structure et leurs effets sur l'évolution de la perméabilité, ainsi que les effets de la pression interstitielle sur la déformation plastique et la rupture du calcaire Anstrude saturé en eau. Basé sur des données expérimentales, la validité du concept de contrainte effective pour le limite plastique et la résistance à la rupture est discutée. Pour modéliser les comportements mécaniques et poromécaniques des roches poreuses, à partir d'un modèle récent de matériau poreux de type Gurson avec matrice Mises-Schleicher [Shen et al., 2015], un modèle basé sur la micromécanique est d'abord proposé pour décrire le comportement mécanique des roches poreuses. Considérant que la roche à haute porosité présente un compactage volumétrique sous faible pression de confinement, un modèle non associé est alors proposé pour la roche poreuse. Dans un premier temps, le modèle proposé est appliqué pour décrire une craie avec une porosité typiquement élevé, la craie de Lixhe. Les comportements mécaniques et poromécaniques de la craie saturée d'huile et d'eau sont étudiés en adoptant le modèle proposé. Des simulations numériques montrent que le modèle proposé décrit correctement les principales caractéristiques des comportements mécaniques et poromécaniques de la craie poreuse. En considérant le comportement mécanique du calcaire poreux, le modèle est ensuite étendu pour décrire le comportement mécanique et poromécanique du calcaire étudié en prenant en compte l'effet de l'évolution de la porosité dans l'effet de durcissement de la matrice solide. pour la craie avec une porosité élevé et même pour le calcaire avec une porosité moyenne, le modèle proposé est vérifié dans différentes conditions de charge par des comparaisons entre les prédictions numériques et les données expérimentales pour les essais drainés et non drainés à la fin.

Remerciement

Je voudrais d'abord exprimer ma plus sincère gratitude à mon superviseur principal, le Professeur Jianfu Shao, pour ses précieux conseils, patiences, confidences et courages durant mes trois années de recherche et c'est un grand honneur pour moi d'être l'un de ses étudiants.

Je voudrais également remercier mon co encadrant, Monsieur WanQing Shen, pour son soutien, sa motivation et son enthousiasme tout au long de ma recherche.

Je suis profondément reconnaissant des commentaires de Mme Ariane Abou Chakra, du Professeur Dashnor Hoxha, du , de Monsieur Mountaka Souley comme les membre de jury de ma soutenance et rapporteur et examinateur de mon mémoire de thèse. Ma sincère gratitude va au Professeur Jean Sulem en tant que jury du président.

Mes remerciement vont également à l'ensemble du personnel de LaMcube pour son soutien moral et matériel qui m'a permis de mener à bien ce travail.

Enfin j'exprime toute ma gratitude à ma famille et mes amis pour leurs encouragements et leurs attentions lors de la réalisation de ce travail

Table Of Contents

General Introduction	iii
I Experimental Investigation on Mechanical Behavior of limestone	1
1 Introduction	4
2 Tested material and testing procedure	5
3 Experimental results	7
4 Discussion on deformation plastic and effect water flow	8
5 Conclusion	13
II Influence of Pore Pressure on Plastic Deformation of Limestone	15
1 Introduction	17
2 Experimental procedure and results	18
3 Effects of pore pressure	21
4 Discussions on effective stress and pore pressure	23
5 Conclusion	25
III Micromechanics-Based Model for Porous Rocks	29
1 Introduction	29
2 Elastic properties of porous rocks	31
3 Micromechanics-based model for porous rocks	32
3.1 Macroscopic yield criterion of porous rocks	32
3.2 Hardening function	34
3.3 Evolution of porosity	35
3.4 Plastic multiplier	36
4 Sensibility analysis of the model	37
4.1 Influences of parameters on the initial yield strength	37
4.2 Effect of confining pressure	40
4.3 Comparison between associated and non-associated models	41
5 Conclusion	47
IV Applications for Porous Rocks	49
1 Introduction	49
2 Simulations of drained mechanical behavior of Lixhe chalk	51

2.1	Basic mechanical behaviors of porous chalks	51
2.2	Simulation of drained laboratory tests	63
3	Simulations of undrained mechanical behavior of Lixhe chalk	66
3.1	General framework of the poroplastic modelling	66
3.2	Extension to poroplastic modelling	68
3.3	Simulation results of undrained laboratory tests	70
4	Simulations of mechanical behaviors Anstrude limestone	75
4.1	Hardening function for porous limestone	75
4.2	Simulation of drained laboratory tests	77
4.3	Simulations of undrained triaxial tests of porous limestone	81
5	Conclusion	86
V Conclusions and Perspectives		87
Bibliography		91

General Introduction

Porous rocks are frequently encountered in various engineering problems such as petroleum engineering, mining industry, geotechnical engineering, geological sequestration of carbon and residual gas. The characterization of mechanical behavior, poromechanical behavior and permeability evolution of porous rocks is an essential issue for the integrity analysis in these fields. Experimental data on the different porous limestones showed a very complex behavior of this material. Due to the high porosity, the deformation and failure process of porous rocks are very sensitive to confining pressure. Two distinct mechanisms of plastic deformation can be identified, the plastic pore collapse and plastic shearing. The pore collapse is related to the irreversible collapse of pores, under high confining pressure, leading to a strong plastic volume compaction and a reduction of porosity. The plastic shearing is more conventional for materials with internal friction, generally leading to a plastic volumetric dilatancy and an increase of porosity. The plastic deformation can also induce permeability change in porous rocks due to the modification of microstructure. Experimental studies show that the volumetric dilatation induced by plastic shear will enhance permeability under relatively low confining pressures, and that the volumetric compaction induced by pore collapse results in permeability diminution. However, the permeability evolution is complex, especially when there is an interaction between two plastic mechanisms. The effects of the pore pressure on the mechanical behavior of porous limestone should be investigated. The pore pressure can affect the mechanical behavior of porous rock with different effects. Especially, the effect of a constant pore pressure, the effect of pore pressure increase and the coupling effect of plastic deformation and pore pressure variation should be investigated. The experimental results could be used

for validating the effective stress concept for plastic yielding and failure strength. Modeling of the mechanical behavior is essential for understanding the comportment of porous rocks. Based on a recent Gurson-type model of porous material with a Mises–Schleicher matrix [Shen et al., 2015], a micromechanics-based plastic model will be proposed to describe the elastoplastic behaviors of porous rocks, such as a high-porosity chalk and a medium-porosity limestone. This present dissertation consists of four chapters: The first chapter concerns the experimental investigations of mechanical behavior and permeability evolution of Anstrude limestone under compression. Two series of tests with and without permeability measurement were carried out. The object of the tests without permeability measurement is to characterize the basic mechanical behavior of studied limestone. And the main purpose of the tests with permeability measurement is to bring an in-depth analysis of correlation between plastic deformation process and permeability evolution. The experimental investigation of the effects of pore pressure on mechanical behavior is the subject of the second chapter. Three different groups of laboratory tests were performed. The effects of pore pressure, including the effect of constant pore pressure, the effect of pore pressure increase and the coupling effect of pore pressure variation and plastic deformation, were studied. And the main purpose of the tests is to verify the effective stress concept for plastic yielding and failure strength of Anstrude limestone. In the third chapter, based on a recent Gurson-type model of porous material with a Mises–Schleicher matrix [Shen et al., 2015], a micromechanics-based plastic model is proposed for the description of elastoplastic behavior of porous rocks. Two plastic parameters of the equivalent solid matrix, the plastic yield stress and the pressure-sensitive coefficient, and the porosity are used as the fundamental parameters in the macroscopic plastic yield function. Considering that the high-porosity rock exhibits a volumetric compaction under low confining pressure, a non-associated model is then proposed for high porous rock. The last chapter is devoted to describe the elastoplastic behaviors of two porous rocks, a high-porosity chalk and a medium porosity limestone. Firstly, the proposed model is applied to describe the drained mechanical behaviors of a high-porosity chalk saturated by oil and water respectively. The influences of water saturation will be studied as a weakening effect

taken into account in modeling. And then, the proposed model is extended to describe the poroplastic coupling effect by using the plastic effective stress concept, and the poroplastic behaviors of high-porosity chalk will be studied. Finally, based on the mechanical and poromechanical behaviors of porous limestone, the proposed model is improved for a medium-porosity limestone by taking the effect of porosity evolution on the hardening law. The simulations of the mechanical behaviors with effect porosity of studied limestone will be carried out with the improved model. Therefore, in this work, the elastoplastic behaviors of two porous rocks, a high-porosity chalk and a medium porosity limestone, are studied on basis of the proposed model.

Chapter I

Experimental Investigation on Mechanical Behavior and Permeability Evolution of a Porous Limestone Under Compression

Contents

1	Introduction	4
2	Tested material and testing procedure	5
3	Experimental results	7
4	Discussion on deformation plastic and effect water flow	8
5	Conclusion	13

Summary

This chapter presents an experimental investigation on the mechanical behavior and permeability evolution of a typical porous limestone, the Anstrude limestone. Hydrostatic and triaxial compression tests are first performed under drained condition to study the basic mechanical behavior of the porous rock. Permeability measurement under both

hydrostatic and triaxial compression is carried out for investigating effects of stress state on the permeability evolution along the axial direction of sample.

Due to the relative high porosity, the deformation and failure process of porous limestone are very sensitive to confining pressure. The experimental results have confirmed that the studied limestone has two modes of plastic deformation: the plastic pore collapse and plastic shearing. Under low effective confining pressures (3, 6 and 10 MPa), the basic behavior of porous limestone is elastic brittle or elastoplastic brittle. An elastic limit can be identified and it increases with the effective confining pressure. The brittle failure occurs with a material softening, and a peak deviatoric stress can be observed. The failure state of sample is clearly characterized by a peak deviatoric stress, which significantly increases with the confining pressure. With regard to the plastic volumetric strain, there is a clear transition from volumetric compaction to dilatancy during the deviatoric loading due to the plastic shearing. Under high confining pressures, for instance above 10 MPa, no peak stress can be identified until a relatively large value of axial strain; with increase of the confining pressure, an elastic–plastic response with a more and more important strain hardening phase can be observed. The initial elastic limit which obviously decreases with the confining pressure; in contrast, the onset of plastic shearing and the deviatoric stress corresponding to the transition from compaction to dilatancy increase with the increase in confining pressure. In regard to the plastic volumetric strain transition, after the elastic limit stress, there is an important volumetric compaction due to the plastic pore collapse, followed by a clear transition from compaction to dilatancy with the increase in deviatoric stress. The plastic dilatancy is mainly induced by the plastic shearing process while the plastic compaction is induced by the plastic pore collapse. Therefore, under a high confining pressure, the plastic pore collapse and plastic shearing are inherently coupled.

The plastic deformation can induce permeability change in porous rocks due to the modification of microstructure. Under low confining pressures, the permeability diminution in the elastic phase is controlled by deviatoric stress. After the onset of plastic shearing, the deviatoric stress induces a plastic volumetric dilatation and a permeability increase. When the deviatoric stress reaches the peak strength or after the onset of shear

bands, the permeability slightly decreases. Under high confining pressures, the deviatoric stress also induces a permeability diminution before the onset of plastic pore collapse. After the onset of pore collapse, the deviatoric stress leads to a plastic volumetric compaction and permeability decrease. When the deviatoric stress reaches the onset of plastic shearing, the two plastic mechanisms are in competition, the permeability continuously decreases but with a reduced rate. Finally, after the compaction–dilatation transition, the plastic shearing dominates the deformation process while the pore collapse still controls the permeability evolution.

Experimental Investigation on Mechanical Behavior and Permeability Evolution of a Porous Limestone Under Compression

B. Han^{1,2} · S. Y. Xie² · J. F. Shao^{1,2}

Received: 21 June 2015 / Accepted: 2 May 2016 / Published online: 13 May 2016
© Springer-Verlag Wien 2016

Abstract This paper presents an experimental investigation on the mechanical behavior and permeability evolution of a typical porous limestone, the Anstrude limestone. Hydrostatic and triaxial compression tests are first performed under drained condition to study the basic mechanical behavior of the porous rock. Permeability measurement under both hydrostatic and triaxial compression is carried out for investigating effects of stress state on the permeability evolution along the axial direction of sample. The obtained results allow to identifying two basic plastic deformation mechanisms, the plastic shearing and pore collapse, and their effects on the permeability evolution. Under low confining pressures, the permeability diminution in the elastic phase is controlled by deviatoric stress. After the onset of plastic shearing, the deviatoric stress induces a plastic volumetric dilatation and a permeability increase. When the deviatoric stress reaches the peak strength or after the onset of shear bands, the permeability slightly decreases. Under high confining pressures, the deviatoric stress also induces a permeability diminution before the onset of plastic pore collapse. After the onset of pore collapse, the deviatoric stress leads to a plastic volumetric compaction and permeability decrease. When the deviatoric stress reaches the onset of plastic shearing, the two plastic mechanisms are in competition, the permeability continuously decreases but with a reduced rate. Finally, after the compaction–dilatation transition, the

plastic shearing dominates the deformation process while the pore collapse still controls the permeability evolution.

Keywords Plastic deformation · Pore collapse · Plastic shearing · Failure · Permeability · Limestone · Porous rocks

1 Introduction

Porous rocks are frequently encountered in various engineering problems such as petroleum engineering, mining industry, geotechnical engineering, geological sequestration of carbon and residual gas. The characterization of mechanical behavior and permeability evolution of porous rocks is an essential issue for the integrity analysis in these fields. In such a context, different kinds of porous rocks have so far been investigated. Laboratory tests, essentially including hydrostatic compression test, oedometric test and triaxial compression test, have been carried out under both drained and undrained conditions. According to previous studies (Paterson 1958; Byerlee 1968; Fredrich et al. 1989; Zhang et al. 1990; Shao and Henry 1991; Wong et al. 1992, 1997; Homand and Shao 2000; Collin et al. 2002; Xie and Shao 2006, 2012, 2015; Baud et al. 1999; Xie et al. 2011, just to mention a few), the deformation and failure process of porous rocks are very sensitive to confining pressure. Two distinct mechanisms of plastic deformation can be identified, the plastic pore collapse and plastic shearing. The plastic behavior is further affected either by intrinsic microstructural variables such as grain size and porosity and extrinsic factors including interstitial pressure, temperature and fluid chemistry.

The plastic deformation can also induce permeability change in porous rocks due to the modification of microstructure. Some experimental studies were devoted to

✉ J. F. Shao
jian-fu.shao@polytech-lille.fr

¹ College of Civil Engineering and Architecture, Hubei University of Technology, Wuhan 430068, China

² Laboratory of Mechanics of Lille, UMR CNRS 8107, University of Lille, 59655 Villeneuve d'Ascq, France

the characterization of permeability evolution in saturated porous rocks (Zhu and Wong 1997; Zhu et al. 1997; Lion et al. 2004; Fortin et al. 2005; Ghabezloo et al. 2009; Hu et al. 2010). These previous studies have shown that the permeability change is intimately related to mechanical loading path. In particular, the effect of confining pressure on the permeability evolution has been studied in laboratory by Zhu et al. (1997). In general, the increase in effective confining pressure can successively result in micro-crack closure, elastic compaction of pores and plastic pore collapse, leading to concomitant decreases in porosity and permeability. The effect of deviatoric stress on the permeability evolution is more complicated. Results from triaxial compression tests show that porous rocks may exhibit both volumetric compaction and dilatation in response to deviatoric stress under different confining pressures. As a consequence, the deviatoric stress can reduce or enhance permeability. Under relatively low confining pressures, porous rocks will typically dilate and fail by shear banding or brittle faulting. The volumetric dilatation will enhance permeability. Under relatively high confining pressures, porous rocks will generally compact due to plastic pore collapse. The volumetric compaction results in permeability diminution (Zhu and Wong 1997). However, the permeability evolution is not always consistent with deformation process, especially due to interaction between two plastic mechanisms.

In this paper, a complementary experimental study is performed on the mechanical behavior and permeability evolution of porous rocks. The main purpose is to bring an in-depth analysis of correlation between plastic deformation process and permeability evolution. To this end, hydrostatic and triaxial compression tests are performed with and without permeability measurement on a typical porous limestone. The comparisons between two series of tests allow to investigating the permeability evolution in relation to plastic deformation process.

2 Tested Material and Testing Procedure

2.1 Description of Porous Limestone

In the present work, the experimental investigation is performed on the Anstrude limestone which is an oolitic limestone of Bathonian strata of middle Jurassic age and is drilled from a quarry located at Bierry les Belles Fontaines, in Bourgogne (France). The petrographic study shows that the limestone is almost monomineralic with calcite as the main component and appears as an assemblage of ooids of 100–1000 μm width made of concentric spheres of calcite. The macroscopic pore space is mainly located between the external envelopes of ooids and is never observed at the

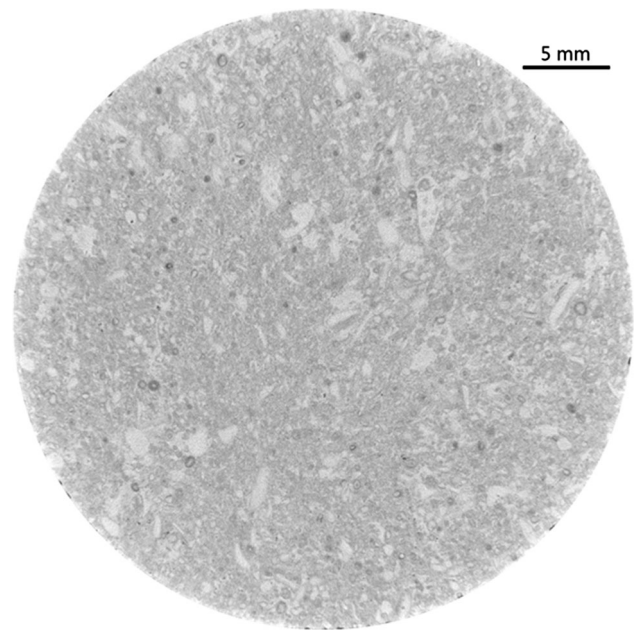


Fig. 1 Tomographic image of transverse cross section of a cylinder sample of Anstrude limestone

sparite grain boundaries (Lion et al. 2004). Generally, the Anstrude limestone is a relatively homogeneous and isotropic material at the sample scale, as shown in Fig. 1. Its mineralogical composition is calcite (>98 %), and quartz (<2 %). Its average porosity is about 20 % and the initial permeability about $6 \times 10^{-16} \text{ m}^2$. The morphology of this rock results in a continuous pore network, which constitutes the connected porosity for interstitial fluid flow. The limestone can be considered as a porous medium in the sense of Biot's theory.

2.2 Experimental Device

The laboratory tests are performed on cylindrical samples of 37.5 mm in diameter and 75 mm in length. The samples are drilled from a big block without macroscopic cracks. According to the average size of mineral grains, this sample size seems to be large enough to represent a representative volume element of the limestone. The saturation condition is an important factor for the determination of permeability. For this purpose, the sample is first saturated with water in vacuum condition before each test. The sample is then inserted inside a rubber jacket and thus isolated from confining fluid. It is placed between two porous steel pads, in order to obtain a uniform distribution of fluid pressure at the inlet and outlet faces of the sample. In addition, after the application of confining pressure, the saturation of the sample is again verified by a water injection procedure. Two types of laboratory tests are performed in this study: hydrostatic compression tests and

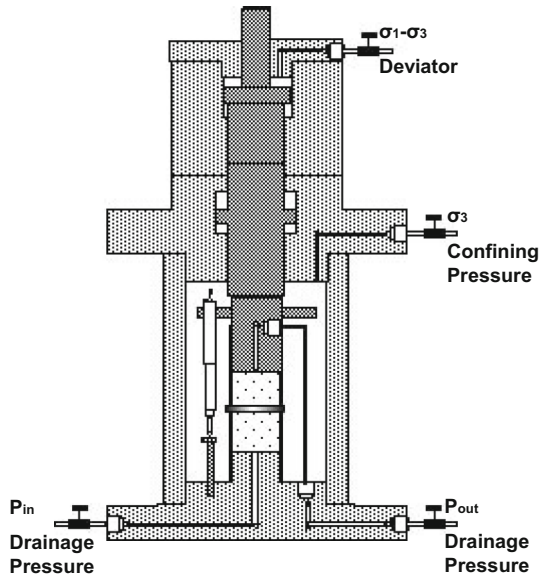


Fig. 2 Schematic presentation of the autonomous and auto-compensated triaxial system

conventional triaxial compression tests with and without permeability measurement. All the tests are conducted in drained conditions. Thermal effects are not studied here and all the tests are carried out under an isothermal condition with an average room temperature of $20 \pm 2 \text{ }^\circ\text{C}$.

All the tests are conducted by using the home-designed autonomous and auto-compensated triaxial testing system. The schematic illustration of the testing system is shown in Fig. 2. It is mainly composed of a cylindrical cell and three high-pressure generators with a maximum capacity of 60 MPa each, the first one for deviatoric stress loading, the second one for confining pressure application and the third one for interstitial pressure injection and monitoring. There are four pressure transducers, respectively, for measuring confining pressure, deviatoric stress, and inlet and outlet interstitial pressure. In addition, a backpressure regulator is used to control the outlet interstitial pressure. The axial strain is measured by two LVDT transducers, which are placed between the bottom and top platens inside the cell (Fig. 2). The radial (or lateral) strain is measured by a home-designed strain ring placed at the middle height of sample.

2.3 Hydrostatic and Triaxial Compression Testing Procedure

The drained hydrostatic compression test is performed to determine the bulk compressibility and the onset of pore collapse of porous limestone. The test is conducted in two steps. At the first step, an initial confining pressure P_{c0} and an interstitial pressure p are first applied to the sample. At

the second step, maintaining the interstitial pressure at a constant value, the confining pressure P_c is increased up to a desired value with a prescribed rate.

The drained triaxial test is also performed in two steps. The confining pressure P_c and interstitial pressure p are first applied to the sample up to a desired value. Then, the deviatoric stress $(\sigma_1 - \sigma_3)$ is increased with a prescribed axial strain rate until sample failure or a large axial strain while the confining pressure and interstitial pressure are kept at the constant values.

2.4 Permeability Measurement Procedure

According to the range of permeability, two different techniques are usually used for the measurement of rock permeability, the steady-state flow method and pulse test technique (Hu et al. 2010). For materials with relatively high permeability (say $>10^{-16} \text{ m}^2$), the steady-state flow method is generally preferred for its simple experimental procedure and direct interpretation method. For rocks with low and very low permeability, an indirect method, the pulse test method, is generally needed (Brace et al. 1968). In the case of the porous limestone studied here, its initial permeability is estimated at the order of 10^{-16} m^2 . The steady-state flow method is thus adopted. The principle of the test is very simple. It consists in the injection of water from the inlet surface of sample with a constant pressure p_{in} while the pressure at the outlet surface p_{out} is also kept constant. A constant pressure difference between the two ends of sample ($\Delta p = p_{in} - p_{out}$) is then applied. The constant injection pressure is obtained by adjusting the injection flow rate Q while the constant outlet pressure is maintained with the help of a backpressure regulator. Applying the linear Darcy's law by neglecting the gravity force, the average permeability of sample (noted as k) can be easily determined by:

$$k = \frac{Q\mu L}{\Delta p A} \tag{1}$$

The coefficient μ denotes the dynamic fluid viscosity. L and A are the length and cross section of the sample, respectively. During each test, the injection flow rate is measured at different time steps, and therefore, the permeability evolution of sample with loading process can be evaluated.

Note that the permeability determination is based on the assumption of a linear interstitial pressure distribution in the sample. Therefore, the mechanical loading rate should be small enough in order to avoid fluid over pressure and then affect the pressure distribution. On the other hand, the pressure gradient generates a non-uniform distribution of interstitial pressure inside the sample. The effective stresses are not uniform, and each test should be interpreted as a

boundary value problem. Therefore, in order to simplify the experimental interpretation and to consider each test as a uniform test, the pressure gradient should be small enough. The detailed values of loading rate and pressure gradient will be given later in the paper. Finally, due to the technical limitation of the experimental device, only the axial permeability of sample is measured.

3 Experimental Results

In this section, the main results obtained from hydrostatic and triaxial compression tests are presented. More detailed discussions on these results will be given in the next section. The tests without permeability measurement are performed with an interstitial pressure of 5 MPa. The tests with permeability measurement are also performed with an average interstitial pressure of 5 MPa. The injection water pressure is $p_{in} = 5.2$ MPa, and the outlet pressure is $p_{out} = 4.8$ MPa. The average pressure difference is then $\Delta p = 0.4$ MPa.

3.1 Drained Hydrostatic Compression Tests

The drained hydrostatic tests are realized with different initial effective confining pressures, 2 MPa for the test with permeability measurement and 4 MPa for the test without permeability measurement, respectively. The loading rate of hydrostatic stress is 5×10^{-3} MPa/s. The volumetric strain (ϵ_v) is calculated from the measured values of axial strain (ϵ_1) and lateral strain (ϵ_3) by the relation $\epsilon_v = -\epsilon_1 + 2\epsilon_3$. The volumetric strain versus effective hydrostatic stress curves are shown in Fig. 3 for the tests with and without permeability measurement. The basic mechanical behaviors of the limestone in two tests are similar. The volumetric strain continuously compacts with the effective hydrostatic stress. Further, the volumetric strain curve is

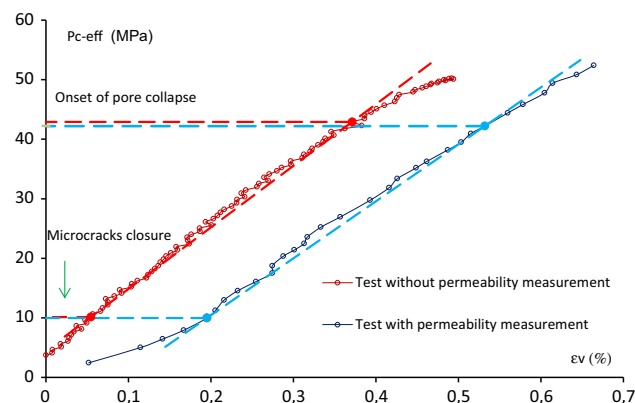


Fig. 3 Volumetric strain versus effective hydrostatic stress in hydrostatic compression tests with 5 MPa interstitial pressure (with and without permeability measurement)

composed of three different phases: a nonlinear concave phase with a decreasing compaction rate due to progressive closure of micro-cracks, a quasi-linear phase corresponding to elastic compaction of pores and a nonlinear phase with increasing compaction rate indicating the onset of plastic pore collapse.

3.2 Drained Triaxial Tests

All the triaxial tests with and without permeability measurement are conducted under an axial strain controlled condition. The prescribed axial strain rate is 5×10^{-6} /s which is considered as low enough to avoid excessive interstitial overpressure. For the triaxial tests without permeability measurement, seven different values of effective confining pressure are used, namely 3, 6, 10, 15, 25, 35 and 50 MPa. For the tests with permeability measurement, six different effective confining pressures are used, for instance 3, 6, 10, 20, 35 and 50 MPa. The obtained stress–strains curves are presented in Fig. 4. The basic trends of mechanical responses of the limestone are similar for two series of triaxial compression tests. The mechanical behavior of limestone changes from an elastoplastic brittle type to an elastoplastic ductile type with the increase in

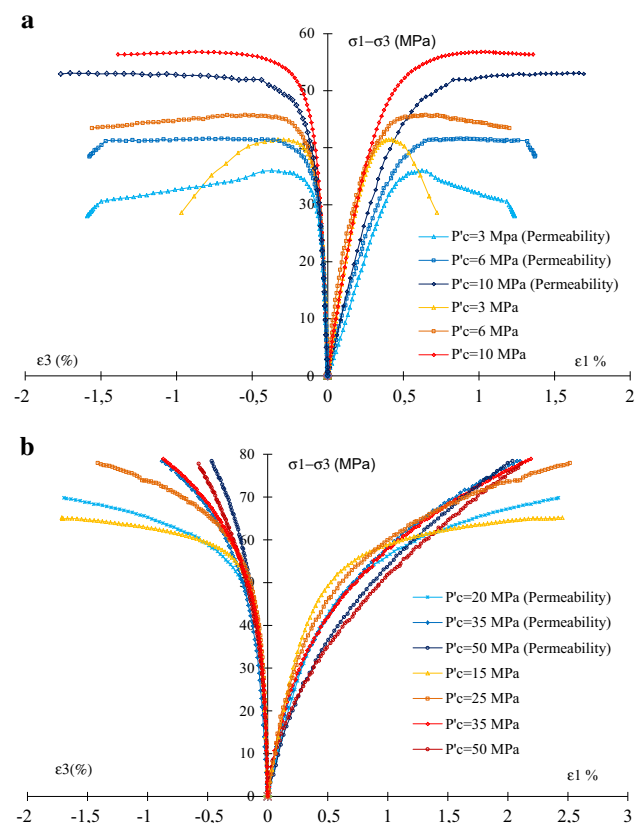


Fig. 4 Stress–strain curves obtained in triaxial compression tests under different confining pressures (with and without permeability measurement). **a** Low confining pressures, **b** high confining pressures

confining pressure. These results show a strong influence of effective confining pressure on the mechanical behavior of the limestone. In particular, under a low confining pressure, the mechanical behavior of the limestone seems affected by the fluid flow process for permeability measurement.

3.3 Permeability Evolution in Hydrostatic Test

The permeability evolution in hydrostatic stress is shown in Fig. 5. One can see that the permeability continuously decreases with effective hydrostatic stress. The permeability variation can also be characterized by three distinct phases. In the first phase, the permeability decreases with a decreasing rate. In the second phase, the rate of permeability decrease is quasi-constant. And in the third phase, the permeability decreases with an accelerated rate.

3.4 Permeability in Triaxial Compression Test

In Fig. 6, the evolutions of permeability during the triaxial compression tests are presented as functions of axial strain for the different values of effective confining pressure. It is clear that the permeability evolutions can be distinguished into two groups. Under a low confining pressure, the permeability decreases at the beginning of deviatoric loading and then increases with the deviatoric stress or axial strain. Under a high confining pressure, the permeability also decreases with the deviatoric stress or axial strain during the first loading stage but continues to slightly decrease or becomes quasi-constant during the second stage. The evolution of permeability is generally related to volumetric strain. For this purpose, the evolutions of volumetric strain in different tests are plotted in Fig. 7. It is found that the permeability evolution is clearly correlated with the volumetric strain under a low confining pressure. But there is no clear correlation under a high confining pressure. Therefore, the analysis of permeability evolution should include other factors, as discussed in the next section.

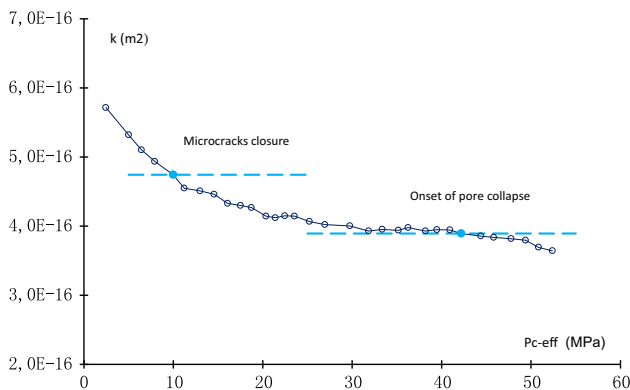


Fig. 5 Permeability versus effective hydrostatic stress of in the hydrostatic compressive test

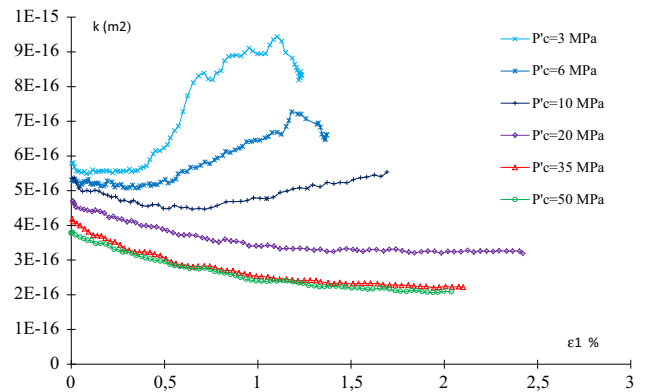


Fig. 6 Permeability versus axial strain curves in the triaxial compression tests with permeability measurement

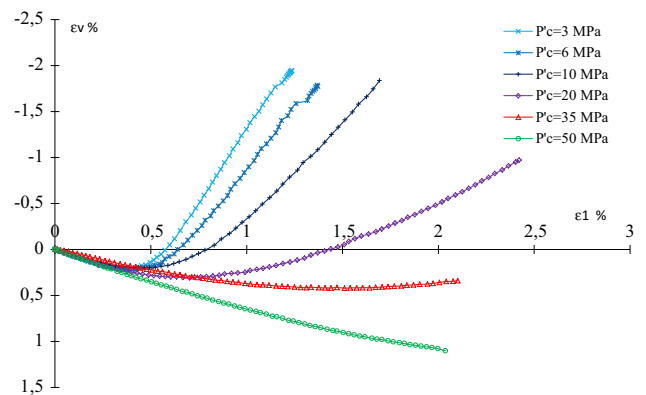


Fig. 7 Volumetric strain versus axial strain in the triaxial compression tests with permeability measurement

4 Discussions

Based on the experimental results presented above, some specific features are discussed here. In particular, it is proposed to investigate effects of confining pressure on plastic deformation process, plastic mechanisms involved in the transition from compaction to dilatancy and in the transition from brittle to ductile behavior, effects of plastic deformation on permeability evolution, effects of water injection process on mechanical behavior and impacts of the experimental results obtained here on constitutive modeling and permeability evolution modeling.

4.1 Effect of Confining Pressure on Plastic Deformation Process

4.1.1 Plastic Deformation Under Hydrostatic Compression

According to previous studies on different porous rocks (Zhang et al. 1990; Shao and Henry 1991; Homand and Shao 2000), a typical stress strain curve of a porous rock is

generally composed of three phases. This is also confirmed by the present study on the limestone. The first concave phase corresponds to the closure of initial micro-cracks. The second phase shows a linear elastic behavior. When the effective hydrostatic stress reaches some limit value, the plastic pore collapse occurs in the third phase and produces an important volumetric compaction. The volumetric compaction results in an increase in contact surfaces between solid grains and enhances plastic hardening. As a consequence the volumetric compaction rate progressively decreases. In the present work, due to the capacity limitation of experimental device, the effective hydrostatic stress is increased up to 50 MPa only. However, it is still possible to identify two first phases and to observe the beginning of pore collapse phase. The drained bulk modulus is determined from the elastic phase by $K_b = \left(\frac{\Delta\sigma_m}{\Delta\varepsilon_v}\right)_{\Delta p=0}$, and one obtains the values of 9.6 and 10.3 GPa, respectively, for the tests with and without permeability measurement. The corresponding values of pore collapse threshold are 42.2 and 42.9 MPa. One can see that the values are quasi-identical for two hydrostatic tests. This means that the water flow process does not affect the mechanical behavior of limestone under hydrostatic compression.

4.1.2 Plastic Deformation Under Triaxial Compression

The plastic deformation process under triaxial compression is complex and strongly influenced by confining pressure. For the tests under low effective confining pressures, for instance below 10 MPa, an elastic limit can be identified and it increases with the confining pressure (see Fig. 4a). The failure state of sample is clearly characterized by a peak deviatoric stress, which significantly increases with the confining pressure. Under a very low confining pressure (for instance 3 MPa), the limestone exhibits an elastic–plastic brittle behavior. The sample failure is marked by a sharp strain softening phase. This is physically generated by the coalescence of micro-cracks producing the splitting of sample. With the increase in confining pressure, the peak stress progressively becomes less pronounced and even disappears. Inclined shear bands are observed by the visual inspection of the tested samples. In addition, after the elastic limit, there is a clear transition from volumetric compressibility to dilatancy during the deviatoric loading. The term dilatancy is here used to refer to the development of an incremental volumetric dilation during plastic deformation process (Wong et al. 1997). In order to better investigate the plastic volumetric strain transition, a refined volumetric strain curve is presented in Fig. 8 for the test without permeability measurement under an effective confining pressure of 3 MPa. An elastic reference line of the volumetric strain is added, based on the extrapolation

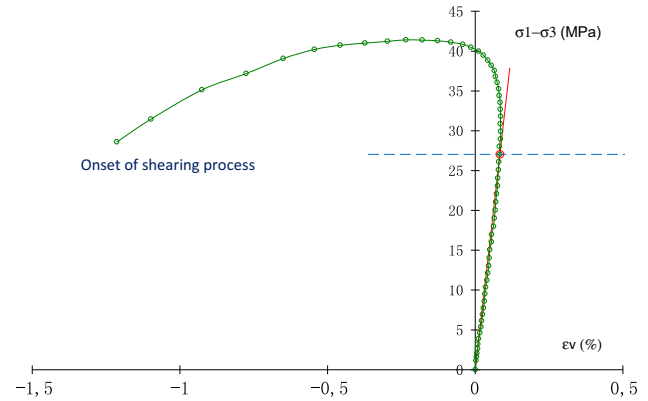


Fig. 8 Detailed volumetric strain versus deviatoric stress curve obtained in the triaxial compression test with an effective confining pressure of 3 MPa (8 MPa confining pressures and 5 MPa interstitial pressure)

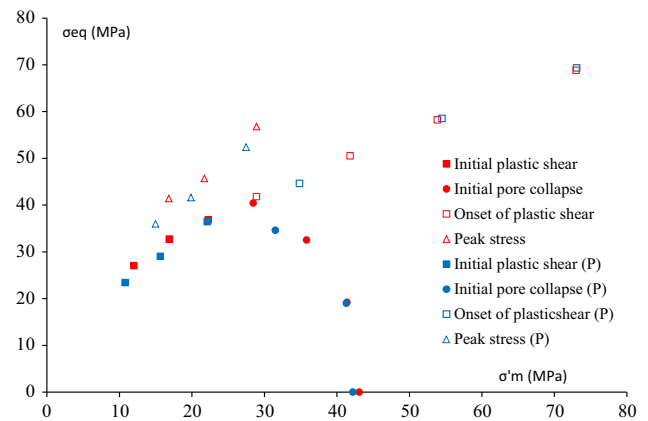


Fig. 9 Comparisons of plastic yield stress and peak stress between the samples with water flow (blue) and without water flow (red) (σ^{eq} is the deviatoric stress and $\sigma'_m = \sigma_m - p$ is the effective compressive mean stress) (color figure online)

of the approximately linear part of the volumetric strain curve. It is found that under such a confining pressure, the plastic volumetric dilatancy threshold nearly coincides with the plastic shearing threshold. It is known that the volumetric dilatancy in brittle rocks under compressive stresses is generally related to normal opening of micro-cracks during frictional sliding along rough crack surfaces (Horii and Nemat-Nasser 1985). This confirms that the frictional shearing is the main plastic process under triaxial compression with a low confining pressure.

In Fig. 9, the values of deviatoric stress, respectively, corresponding to the initial threshold of plastic shearing and to the peak stress are plotted for the different values of confining pressure. Both the initial plastic threshold and peak stress significantly increase with confining pressure. Further, for two series of triaxial tests, the initial plastic shearing stress locus and the failure stress locus are of linear form.

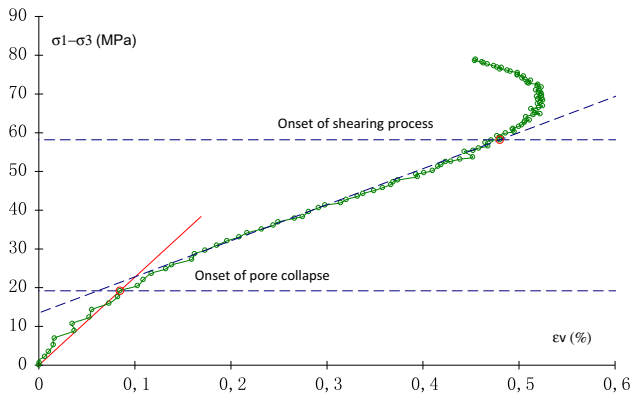


Fig. 10 Detailed volumetric strain versus deviatoric stress curve obtained in the triaxial compression test with an effective confining pressure of 35 MPa (40 MPa confining pressure and 5 MPa interstitial pressure)

For the tests under high effective confining pressures, for instance above 10 MPa, no peak stress can be identified until a relatively large value of axial strain (see Fig. 4b). The limestone exhibits an elastic–plastic ductile behavior. It is not easy to identify the initial elastic limit which obviously decreases with confining pressure. After the elastic limit stress, there is an important volumetric compaction due to the plastic pore collapse, followed by a clear transition from compaction to dilatancy. The volumetric strain is strongly influenced by the effective confining pressure. In contrast to the elastic limit stress, the deviatoric stress corresponding to the transition from compaction to dilatancy increases with the increase in confining pressure. Visual inspection of the tested samples does not reveal any obvious signs of strain localization, even though the volumetric dilatancy is clearly observed. An amplified volumetric strain curve is presented in Fig. 10 for the test without permeability measurement under an effective confining pressure of 35 MPa. Two reference lines are plotted in this figure. The first one defines the elastic strain slope and the second line defines the average slope of the quasi-linear part of volumetric strain curve during the pore collapse process. With the help of these two lines, it is easy to identify the pore collapse threshold and the plastic shearing threshold. It is found that a plastic volumetric compaction phase is firstly observed due to the pore collapse process, which is followed by a volumetric dilatancy phase with the increase in deviatoric stress. Therefore, under a high confining pressure, the plastic pore collapse and plastic shearing are inherently coupled. The stress values corresponding to the onset of plastic shearing and pore collapse are plotted in Fig. 9. One can see that the onset stress of plastic shearing increases with effective confining pressure while the onset of pore collapse decreases. Further, it is found that the plastic shearing

stress locus under high confining pressures is also defined by a quasi-linear line as that under low confining pressures.

4.2 Analysis of Compaction–Dilatancy Transition

The evolution of volumetric strain versus deviatoric stress is shown in Fig. 11 for all triaxial tests without permeability measurement. It is clear that the evolution of volumetric strain depends on effective confining pressure. The volumetric strain evolves from elastic compaction to plastic dilatancy under a low confining pressure. However, under a high confining pressure, the volumetric strain evolves from elastic compaction to plastic compaction and finally to plastic dilatancy. The plastic dilatancy is mainly induced by the plastic shearing process while the plastic compaction is induced by the plastic pore collapse.

In Fig. 12, the volumetric strain for the test with an effective confining pressure of 3 MPa is decomposed into an elastic part and a plastic part and they are, respectively, plotted versus deviatoric stress and axial strain. One can see that the compaction to dilatancy transition appears as soon as the plastic shearing starts. This transition can be easily identified by the point where the volumetric strain rate becomes greater than that of elastic strain.

In a similar way, the volumetric strain for the test with an effective confining pressure of 35 MPa is analyzed in Fig. 13. In this case, the pore collapse onset is identified by the deviation point of the total volumetric strain from the elastic one. The plastic shearing occurs when the deviatoric stress reaches a limit value. The plastic shearing produces a volumetric dilatancy and it is in competition with the plastic pore collapse which produces a volumetric compaction. As a result, the compaction–dilatancy transition occurs when the deviatoric stress is high enough. It is important to note that under a high effective confining pressure, the failure of limestone occurs by a diffuse destruction of matrix-pore structure without producing a peak deviatoric stress. Therefore, it seems that under a high effective confining pressure, the mechanical behavior of limestone under high deviatoric stress is mainly controlled by the plastic shearing process. However, under some intermediate confining pressure, for instance 10 and 15 MPa, both plastic mechanisms are activated at the same time and strongly coupled. It is generally difficult to distinguish the relative contributions of the two mechanisms. Generally, with the increase in deviatoric stress, the plastic shearing will progressively dominate the mechanical behavior.

4.3 Effect of Plastic Deformation on Permeability Evolution

Under a hydrostatic compression, the permeability of limestone continuously decreases due to plastic volumetric

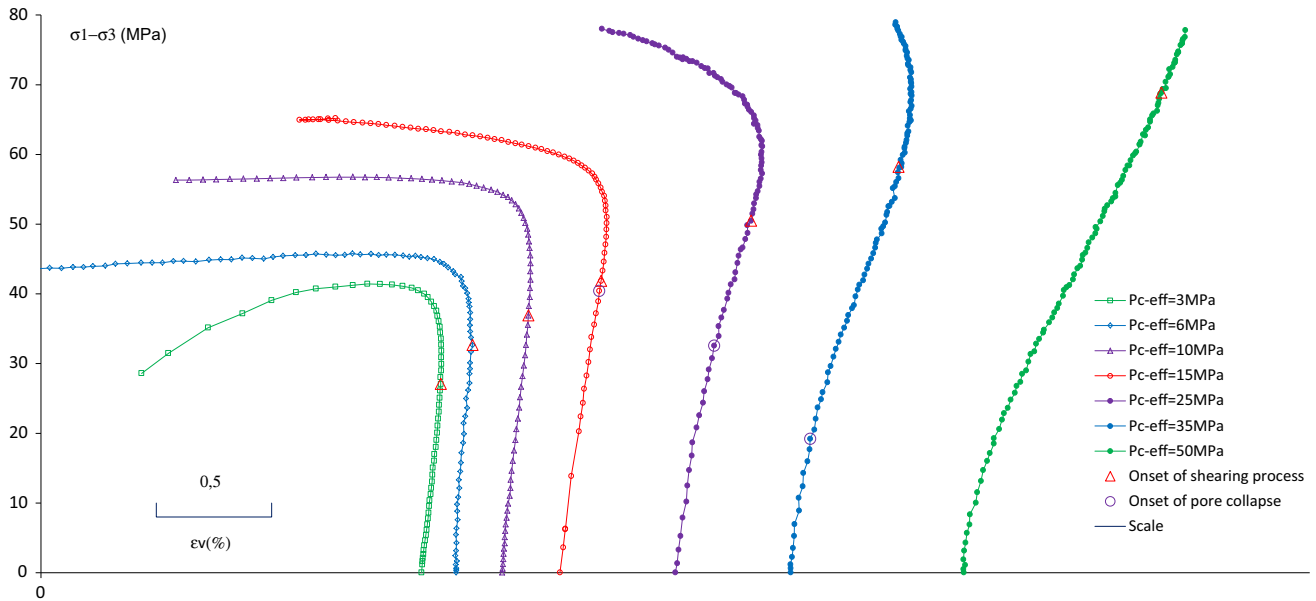


Fig. 11 Evolutions of volumetric strain versus deviatoric stress in water saturated samples under different confining pressures

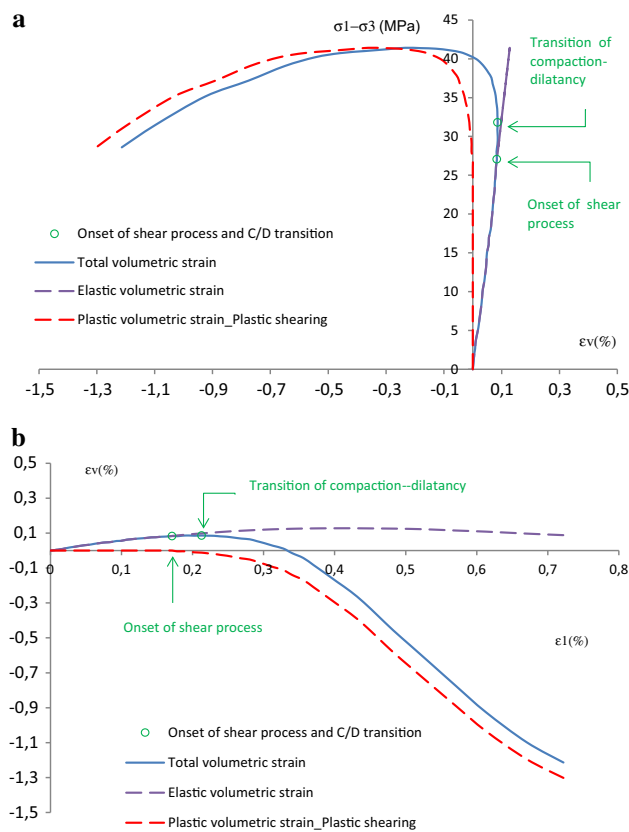


Fig. 12 Decomposition of volumetric strain for the triaxial test under an effective confining pressure of 3 MPa. **a** Evolution of volumetric strain with deviatoric stress, **b** evolution of volumetric strain with axial strain

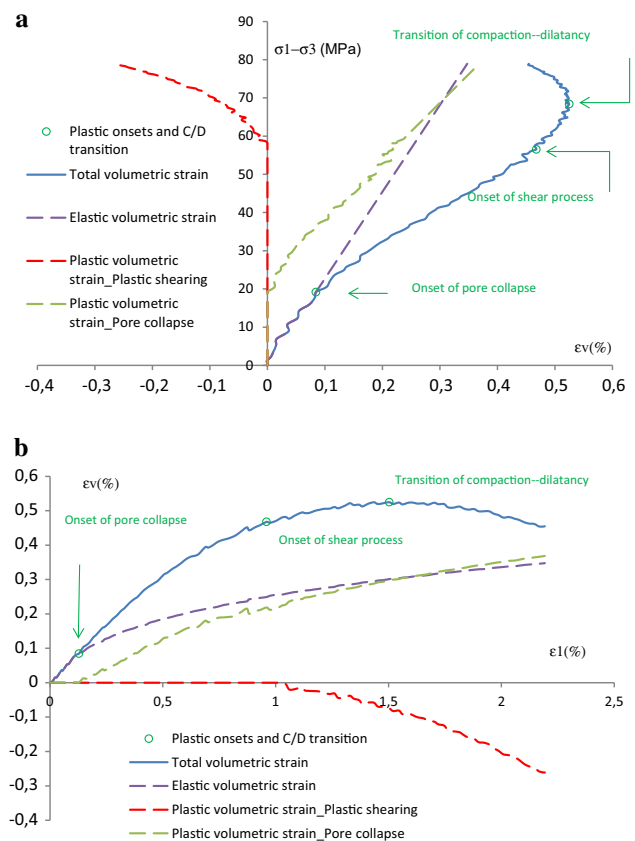


Fig. 13 Decomposition of volumetric strain for the triaxial test under an effective confining pressure of 35 MPa. **a** Evolution of volumetric strain with deviatoric stress, **b** evolution of volumetric strain with axial strain

compaction. The emphasis is here put the permeability evolution in triaxial compression tests.

One first considers the permeability evolution under a low effective confining pressure, for instance 3, 6 and 10 MPa. The stress–strain and permeability–strain curves obtained in the test with 3 MPa effective confining pressure are plotted in Fig. 14. It seems that the permeability evolution is characterized by three stages. In this first stage corresponding to the linear elastic deformation process, the permeability slightly decreases when the deviatoric stress increases. In the second stage, an increase in permeability is observed with the onset of plastic shearing. In the last stage, the permeability slightly decreases. Similar results are also observed for the tests with an effective confining pressure of 6 and 10 MPa (not reported here). The reason of permeability decrease in the last stage is quite complex. In most rocks, there is the formation of localized strain bands or micro-crack coalescence bands when the deviatoric stress approaches the peak stress. The overall permeability of sample is affected by the deformation inside such bands. In the case of highly compacted shear bands, the overall permeability will decrease as that reported in Zhu and Wong (1997). At the same time, the volumetric strain is dominated by the plastic dilatancy under a low confining pressure. Therefore, it is not easy to find a correlation between the volumetric strain and permeability evolution after the onset of localized strain bands due to the non-uniform distribution of strain inside the sample.

Consider now the permeability evolution under a high effective confining pressure, namely 20, 35 and 50 MPa. The stress–strain and permeability–strain curves obtained in the triaxial compression test under 35 MPa effective confining pressure are presented in Fig. 15. The permeability evolution can also be decomposed into three stages. In the first stage related to the elastic deformation process, as for a low confining pressure, the permeability slightly

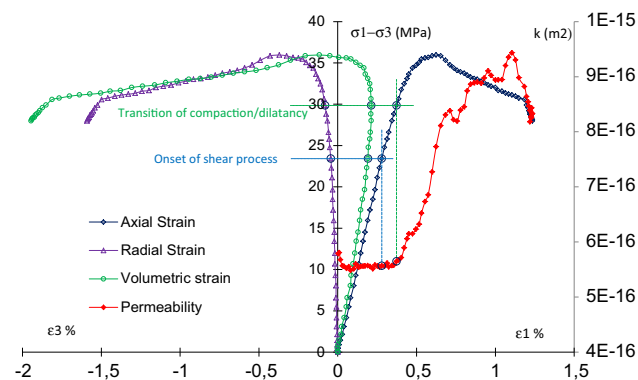


Fig. 14 Stress–strain and permeability–strain curves obtained in the triaxial compression test under an effective confining pressure of 3 MPa (8 MPa confining pressure and 5 MPa interstitial pressure)

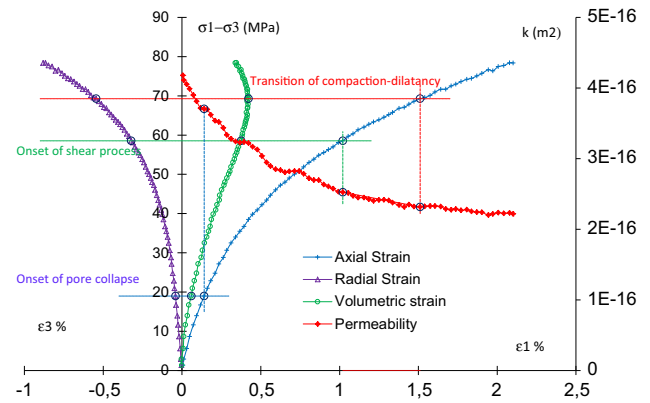


Fig. 15 Stress–strain and permeability–strain curves obtained in the triaxial compression test under an effective confining pressure 35 MPa (40 MPa confining pressure and 5 MPa interstitial pressure)

decreases. At the second stage, the permeability continuously decreases due to the plastic pore collapse as far as the onset of plastic shearing occurs. In the last stage, the plastic shearing process is activated and produces the compaction to dilatancy transition. The permeability becomes quasi-constant. The permeability evolution observed in this work is in agreement with those observed on various sandstones (Zhu and Wong 1997; Zhu et al.1997). Therefore, the permeability under a relatively high confining pressure is affected by two competitive plastic deformation processes. The quasi-constant permeability during the last stage can be seen as a result of such a competition. The plastic shearing will dominate the mechanical behavior of limestone under high deviatoric stress and produce a volumetric dilatancy. But the overall permeability of the sample will not increase due to the pore collapse process. Therefore, the results obtained here seem to show that there is no direct correlation between the permeability evolution and the cumulated volumetric strain.

4.4 Effect of Water Flow on Mechanical Behavior

In this work, the tests with permeability measurement are performed on samples subjected a water flow (see Figs. 3, 4). By comparing the stress–strain curves obtained in these tests with those obtained in the tests without water flow, effects of water flow on the mechanical behavior of limestone can be studied. In Fig. 9, the values of the pore collapse onset stress and the peak deviatoric stress are plotted for the two series of tests. There is no significant difference for the hydrostatic compression tests and triaxial compression tests performed under a high confining pressure. However, for the triaxial tests with a low confining pressure, there are some slight decreases in the peak deviatoric stress and in the drained bulk modulus for the samples with water flow. But there is no significant

difference for the pore collapse onset stress and for the plastic shearing onset stress. For a quantitative description, the failure surface of the limestone is described by the classical linear Mohr–Coulomb criterion. Based on the peak stresses obtained from the tests with a low confining pressure, the following values are obtained, respectively, for the cohesion $C = 9.7$ MPa and the frictional angle $\phi = 31.6^\circ$ for the samples without water flow, and $C = 7.9$ MPa, $\phi = 32.7^\circ$ for the samples with water flow. There is a decrease in cohesion and a slight increase in friction angle. It appears that the failure stress of limestone or the plastic shearing process is affected by the water flow process. However, the in-depth analysis of water flow effects on the mechanical behavior of the limestone is behind the topic of this paper and will be discussed in future works.

4.5 Impact on Constitutive Modeling

According to the experimental results presented in this work and those reported in previous works, the limestone exhibits two plastic deformation processes, the plastic pore collapse and plastic shearing. These two processes should be taken into account in constitutive modeling. The plastic shearing is a common process for most cohesive–frictional materials. Classical models based on Mohr–Coulomb and Drucker–Prager criteria are generally developed by choosing an appropriate hardening and eventually softening law. A non-associated plastic potential is generally needed for a better description of the plastic compaction–dilatancy transition. However, the special feature of porous rocks is the strong pressure sensitivity. That means that a linear yield surface is not suitable for the description of plastic shearing and a nonlinear yield surface should be defined. On the other hand, the plastic collapse is a specific property of porous rocks like the limestone studied here. This process plays an essential role in many engineering applications such as subsidence analysis of oil reservoir. Therefore, a particular attention should be paid to the modeling of such a plastic process. Two different kinds of approaches can be adopted. In the first kind of approaches, plastic models with two distinct yield surfaces are developed and the plastic pore collapse is described by a cap model. In the second kind of approaches, plastic models with a single closed yield surface are proposed. For example, a plastic model based on the Gurson's criterion has been recently proposed for porous chalks (Xie and Shao 2006). It is worth noticing that recent developments from nonlinear homogenization techniques provide a very interesting and promising way to develop plastic models for porous rocks. For instance, some micro-mechanics based elastic–

plastic models have been proposed for porous rocks by Lin et al. (2011) and Shen et al. (2013).

As mentioned above, there is a complex coupling between permeability evolution and plastic deformation. The permeability evolution is mainly controlled by the plastic shearing process under a low confining pressure but by the plastic pore collapse under a high confining pressure. In contrast to the coupling between permeability and micro-cracking process for brittle rocks (Shao et al. 2005; Jiang et al. 2010), the modeling of permeability evolution for porous rocks should be based on the description of these two plastic processes.

5 Conclusions

In this paper, the mechanical behavior and permeability evolution of a typical porous limestone have been investigated. Two series of hydrostatic and triaxial compression tests have been performed, respectively, with and without permeability measurement.

The experimental results obtained have confirmed the effect of confining pressure on plastic behavior and failure property in most porous rocks. Two plastic processes should be identified: plastic pore collapse and deviatoric plastic shearing. The transition from brittle to ductile behavior can be explained as an effect of the pore collapse with the increase in confining pressure.

In triaxial compression tests with a low confining pressure, the volumetric strain evolves from an elastic compaction to a plastic dilatancy due to the plastic shearing process. Under a high confining pressure, the volumetric strain first evolves from an elastic compaction to the plastic compaction due to the pore collapse and then to a plastic dilatancy due to the plastic shearing process. Therefore, the compaction to dilatancy transition is essentially controlled by the shearing process under both low and high confining pressures.

The permeability evolution is also affected by the two plastic processes. The permeability decreases under hydrostatic compression due to the volumetric compaction induced by the pore collapse. Under the triaxial compression with a low confining pressure, the permeability is enhanced by the volumetric dilatancy which induced by the plastic shearing. However, under a high confining pressure, the permeability evolution is strongly affected by the pore collapse process and continues to decrease or becomes nearly constant even after the compaction–dilatancy transition.

The experimental data presented in this work provide useful data for the formulation and validation of constitutive models devoted to porous rocks. This will be considered in future works.

References

- Baud P, Schubnel A, Wong TF (1999) Dilatancy, compaction, and failure mode in Solnhofen limestone. *J Geophys Res* 105(B8):19289–19303
- Brace WF, Walsh JB, Frangos WT (1968) Permeability of granite under high pressure. *J Geophys Res* 73:2225–2236
- Byerlee JD (1968) Brittle–ductile transition in rocks. *J Geophys Res* 73(14):4741–4750
- Collin F, Cui YJ, Schroeder C, Charlier R (2002) Mechanical behaviour of Lixhe chalk partly saturated by oil and water: experimental and modeling. *Int J Numer Anal Methods Geomech* 26:897–924
- Fortin J, Schubnel A, Guéguen Y (2005) Elastic wave velocities and permeability evolution during compaction of Bleuswiller sandstone. *Int J Rock Mech Min Sci* 42:873–889
- Fredrich JT, Evans B, Wong TF (1989) Micromechanics of the brittle to plastic transition in Carrara marble. *J Geophys Res* 94:4129–4145
- Ghabezloo S, Sulem J, Guedon S, Martineau F (2009) Effective stress law for the permeability of a limestone. *Int J Rock Mech Min Sci* 46:297–306
- Homand S, Shao JF (2000) Mechanical behaviour of a porous chalk and water/chalk interaction, part I. Experimental study. *Oil Gas Sci Technol* 55(6):591–598
- Horii H, Nemat-Nasser S (1985) Compression-induced microcrack growth in brittle solids: axial splitting and shear failure. *J Geophys Res* 90(B4):3105–3125
- Hu DW, Zhou H, Zhang F, Shao JF (2010) Evolution of poroelastic properties and permeability in damaged sandstone. *Int J Rock Mech Min Sci* 47(6):962–973
- Jiang T, Shao JF, Xu WY, Zhou CB (2010) Experimental investigation and micromechanical analysis of damage and permeability variation in brittle rocks. *Int J Rock Mech Min Sci* 47:703–713
- Lin J, Kondo D, Shao JF (2011) A two scale model of porous rocks with Drucker–Prager matrix: application to a sandstone. *Mech Res Commun* 38:602–606
- Lion M, Skoczylas F, Ledésert B (2004) Determination of the main hydraulic and poro-elastic properties of a limestone from Bourgogne, France. *Int J Rock Mech Min Sci* 41:915–925
- Paterson MS (1958) Experimental deformation and faulting in Wombeyan marble. *Geol Soc Am Bull* 69:465–476
- Shao JF, Henry JP (1991) Development of an elastoplastic model for porous rock. *Int J Plast* 7:1–13
- Shao JF, Zhou H, Chau KT (2005) Coupling between anisotropic damage and permeability variation in brittle rocks. *Int J Numer Anal Meth Geomech* 29:1231–1247
- Shen WQ, Kondo D, Dormieux L, Shao JF (2013) A closed-form three scale model for ductile rocks with a plastically compressible porous matrix. *Mech Mater* 59(2013):73–86
- Wong TF, Szeto H, Zhang J (1992) Effect of loading path and porosity on the failure mode of porous rocks. *Appl Mech Rev* 45(8):281–293
- Wong TF, David C, Zhu W (1997) The transition from brittle faulting to cataclastic flow in porous sandstone: mechanical deformation. *J Geophys Res* 102:3009–3025
- Xie SY, Shao JF (2006) Elastoplastic deformation of a porous rock and water interaction. *Int J Plast* 22:2195–2225
- Xie SY, Shao JF (2012) Experimental investigation and poroplastic modelling of saturated porous geomaterials. *Int J Plast* 39:27–45
- Xie SY, Shao JF (2015) An experimental study and constitutive modeling of saturated porous rocks. *Rock Mech Rock Eng* 48:223–234
- Xie SY, Shao JF, Xu WY (2011) Influences of chemical degradation on mechanical behaviour of a limestone. *Int J Rock Mech Min Sci* 48:741–747
- Zhang J, Wong T-F, Davis DM (1990) Micromechanics of pressure-induced grain crushing in porous rocks. *J Geophys Res* 95:341–352
- Zhu W, Wong TF (1997) The transition from brittle faulting to cataclastic flow: permeability evolution. *J Geophys Res* 102:3027–3041
- Zhu W, Montesi LGJ, Wong TF (1997) Shear-enhanced compaction and permeability reduction: triaxial extension tests on porous sandstone. *Mech Mater* 25:199–214

Chapter II

Influence of Pore Pressure on Plastic Deformation and Strength of Limestone Under Compressive Stress

Contents

1	Introduction	17
2	Experimental procedure and results	18
3	Effects of pore pressure	21
4	Discussions on effective stress and pore pressure	23
5	Conclusion	25

Summary

This chapter is devoted to experimental investigation of effects of pore pressure on plastic deformation and failure of a water saturated limestone. The experimental study is composed of three different groups of laboratory tests. The basic mechanical behavior of the rock is first characterized by drained triaxial compression tests on water-saturated samples without pore pressure. The results are compared with those obtained in a previous study from triaxial compression tests on saturated samples with a constant pore pressure. In the second group, water injection tests under a confining pressure of 20 MPa and


different values of deviatoric stress are realized to study the effect of pore pressure increase. Finally, undrained triaxial compression tests are carried out for investigating the coupling effect of plastic deformation and pore pressure variation.

The experimental results have shown that the effects of pore pressure on mechanical behavior are complex. Comparing the experimental results of drained triaxial tests without pore pressure and with pore pressure of 5 MPa, effects of constant pore pressure on mechanical behavior have been investigated. For the tests with pore pressure of 5MPa, both plastic deformation and strength are lower than those without pore pressure for a same effective confining pressure, especially for the tests under low confining pressure. The water injection induces an increase in pore pressure and then a decrease in effective confining pressure. This enhances the plastic shearing process, volumetric dilatancy and shearing failure. Further only the plastic shearing is activated in such a loading path. The pore pressure evolution in undrained triaxial tests is also influenced by two plastic processes. Under low confining pressure, the deviatoric stress induces plastic dilatancy due to shearing process and then a decrease in pore pressure. But under high confining pressure, the deviatoric stress induces a plastic compaction due to pore collapse and enhances the increase in pore pressure. The pore collapse dominates the pore pressure evolution during the first stage of loading, while the plastic shearing dominates the peak strength and pore pressure evolution during the second stage.

Based on the experimental results, finally, the validity of effective stress concept for plastic yielding and failure strength is discussed.



Influence of pore pressure on plastic deformation and strength of limestone under compressive stress

B. Han^{1,2} · W. Q. Shen² · S. Y. Xie² · J. F. Shao^{1,2} 

Received: 8 August 2017 / Accepted: 17 April 2018
© Springer-Verlag GmbH Germany, part of Springer Nature 2018

Abstract

This study is devoted to experimental investigation of effects of pore pressure on plastic deformation and failure of a water-saturated limestone. The experimental study is composed of three different groups of laboratory tests. The basic mechanical behavior of the rock is first characterized by drained triaxial compression tests on water-saturated samples without pore pressure. The results are compared with those obtained in a previous study from triaxial compression tests on saturated samples with a constant pore pressure. In the second group, water injection tests under a confining pressure of 20 MPa and different values of deviatoric stress are realized to study the effect of pore pressure increase. Finally, undrained triaxial compression tests are carried out for investigating the coupling effect of plastic deformation and pore pressure variation. Based on experimental data, the validity of effective stress concept for plastic yielding and failure strength is discussed.

Keywords Effective stress · Limestone · Plastic deformation · Poroelasticity · Pore pressure · Porous rocks

1 Introduction

Porous rocks are generally saturated by one or several fluids. Under mechanical loading and temperature change, important variation of pore pressure can be generated. For many engineering applications, it is important to study effects of pore pressure on deformation behavior and mechanical strength of porous rocks. Since the Biot's theory of poroelasticity [2], a great number of studies have been performed on experimental investigation of elastic behavior of saturated porous rocks. The poroelasticity has been extended to nonlinear rheology [3], anisotropic materials [6, 8, 35], to materials with induced damage by microcracks [32, 45, 48]. Different experimental techniques have been proposed for the measurement of poroelastic parameters in saturated porous materials [4, 15, 17, 20, 29]. Poroelastic theory has also been

successively applied to the analysis of deformation, instability and failure in various engineering contexts [26]. Some studies have been devoted to undrained poroelastic response to deviatoric stress change and to effect of temperature-induced pore pressure on the strength of porous rocks [21, 22]. Using homogenization techniques, poroelastic coefficients have been determined as responses of microstructure [12, 23].

On the other hand, most porous rocks also exhibit plastic deformation. Extensive experimental studies are available on the characterization of plastic deformation in porous rocks [1, 11, 16, 33, 39, 42]. In general, two plastic deformation processes can be identified, the irreversible collapse of voids and the plastic shearing related to frictional sliding between mineral grains. The plastic behavior of porous rocks is also strongly influenced by confining pressure. There is a clear transition from brittle to ductile behavior when the confining pressure increases [5, 28, 40]. Various constitutive models have also been developed for porous rocks. In general, one can find models either with a single yield surface or with two distinct yield surfaces to describe the two plastic processes. However, the description of plastic deformation and failure strength with pores pressure variation in porous materials is still an open issue.

✉ J. F. Shao
jian-fu.shao@polytech-lille.fr

¹ College of Civil Engineering and Architecture, Hubei University of Technology, Wuhan 430068, China

² CNRS, LaMcube, FRE 2016, University of Lille, 59000 Lille, France

A number of previous studies have been so far performed to investigate effects of pore pressure variation on plastic yielding, earthquake rupture dynamics, nucleation of slip-weakening rupture instability and other features [13, 14, 19, 36, 37, 46, 48]. The concept of effective stress is generally involved for both elastic and plastic fields [7, 34, 43, 47]. However, the existence and validity of effective stress concept for plastic deformation and failure strength in saturated and partially saturated materials are still an open issue [9, 19, 38, 42, 46]. With the help of nonlinear homogenization techniques, some micro-mechanical studies have been reported on the effective stress concept for plastic yield and strength criteria in saturated materials [10, 24]. In addition, one can also find experimental studies on chemical effects of pore fluids on mechanical properties of porous rocks [7, 16, 31, 41, 44]. It is found that the plastic yield and strength criteria are affected by physical and chemical processes in pore fluids such as dissolution, wettability, capillary force and other factors.

In our previous study [14], we have investigated the basic mechanical behavior and the effect of plastic deformation on the permeability evolution of a saturated limestone in drained triaxial compression tests with a constant pore pressure of 5 MPa. As an extension to the previous study, the objective of this paper is to study the effect of constant or varying pore pressure on plastic deformation and failure strength of saturated porous rocks by performing a series of new laboratory tests. For this purpose, the same limestone as that used in Han et al. [14] is selected in the present work. The experimental program is composed of three groups of laboratory tests. A series of drained triaxial compression tests are first performed on water-saturated samples without pore pressure but with different values of confining pressure, which are chosen in a special way so that the values of effective confining pressure (defined as the difference between confining pressure and pore pressure) are the same as those used in the previous study. The effect of a constant pore pressure on plastic deformation and failure strength is therefore discussed. Then, another series of triaxial compression tests are carried out by injecting water into samples at different levels of deviatoric stress. The objective is to investigate the consequence of pore pressure increase on plastic deformation and failure. Finally, undrained triaxial compression tests are realized in order to study the coupling effect between plastic deformation and pore pressure variation.

2 Experimental procedure and results

The present study is performed on Anstrude limestone from Bourgogne in France. This rock has been previously investigated by Lion et al. [20] and Han et al. [14]. The lithology, microstructure and mineralogy of this rock have been characterized in the previous papers. Anstrude limestone is composed of about 98% calcite and 2% quartz, with an average porosity of 20% and an initial permeability of about $6 \times 10^{-16} \text{ m}^2$. The experimental scatter is a common phenomenon in laboratory tests. It is mainly caused by the natural scatter of samples and by the differences of testing procedure. In order to reduce the experimental scatter, the tests presented in this paper are carried out with the same procedures. The hard task is to reduce the natural scatter of samples. For this purpose, the samples used in the previous study of Han et al. [14] and in the present study are all carefully drilled from a homogeneous block without macroscopic cracks. If some abnormal results are obtained from a test, a second test is performed to verify the results.

The following methodology is adopted. The basic mechanical behavior of Anstrude limestone has been studied in Han et al. [14] through a series of drained triaxial compression tests on saturated samples with a constant pore pressure of 5 MPa. In the present work, the emphasis is put on the effect of pore pressure on plastic deformation and failure strength of the limestone. For this purpose, three groups of laboratory tests will be performed. In the first group, drained triaxial compression tests are performed on saturated samples without pore pressure. (Or the pore pressure is equal to zero.) The values of confining pressure are especially selected so that the values of effective confining pressure, which is defined as the difference between nominal confining pressure and pore pressure, are identical for two series of tests, respectively, performed with 0 and 5 MPa pore pressure. In this way, we shall identify the effect of a constant pore pressure on plastic deformation and failure strength of limestone. In the second group of tests, the pore pressure is increased by injecting water into samples at different levels of deviatoric stress until failure at a selected confining pressure. The purpose of these tests is to investigate the mechanical responses of limestone to pore pressure increase. Finally, in the third group, a series of undrained triaxial compression tests are realized with different confining pressures in order to capture the coupling process between the evolution of pore pressure during deviatoric stress loading, plastic deformation and failure behavior.

All the tests are performed using a custom-designed autonomous and auto-compensated triaxial testing device. This is mainly composed of a cylindrical cell and three

pressure generators and a computer monitoring system. It is possible to independently apply and monitor confining pressure, axial stress, inlet and outlet pore pressures. The axial strain is measured by two LVDT transducers, which are placed between the bottom and top platens inside the cell. The radial (or lateral) strain is measured by a custom-designed strain ring placed at the middle height of sample. The detailed presentation of the device and strain measurement techniques was given in Han et al. [14]. All the samples, used in the previous study [14] and in this study, were carefully drilled from a big block without macroscopic cracks and homogeneous at the sample scale. The size of cylindrical samples is 37.5 mm in diameter and 75 mm in length. All tests will be performed in a room with a temperature controlled around 20 ± 2 °C.

2.1 Triaxial compression tests with a constant pore pressure

The drained triaxial tests with a constant pore pressure are performed by three steps. The confining pressure (noted as $P_c = \sigma_3$) is increased to a selected value in the first step. The pore pressure (noted as P_i) is then increased by water injection to a desired value in the second step. At the third step, the axial stress (noted as σ_1) is finally applied with a given axial strain rate (noted as $d\varepsilon_1/dt$) in order to capture post-peak response of sample. The axial strain rate is chosen as slow as possible so that the over-pore pressure does not create a significant disturbance of the prescribed uniform pore pressure inside the sample. In the present study, the axial strain rate was selected as 5×10^{-6} /s. Note that in the previous study [14], a series of drained triaxial compression tests with a constant pore pressure of $P_i = 5$ MPa have been performed with seven different confining pressures such as 8, 11, 15, 20, 30, 40 and 55 MPa. In order to capture the effect of a constant pore pressure, in the present study, drained triaxial compression tests are performed on saturated samples but without pore pressure ($P_i = 0$ MPa). Seven specific values of confining pressure are selected: 3, 6, 10, 15, 25, 35 and 50 MPa. These values are selected in a way that the effective confining pressures defined as the difference between confining pressure and pore pressure ($P_c - P_i$) are identical for the two series of tests, respectively, performed in the previous and present studies. Therefore, the results obtained from the two series of tests can be compared and their differences can be used to interpret the effect of pore pressure. In Fig. 1, we present the deviatoric stress defined as $(\sigma_1 - \sigma_3)$ versus the axial strain and lateral strain (noted as ε_3). In this figure, the stress–strain curves are presented in two separate groups, respectively, for “low” and “high” confining pressures. The definition of low and high confining pressures is relatively subjective and mainly based on the general trend of

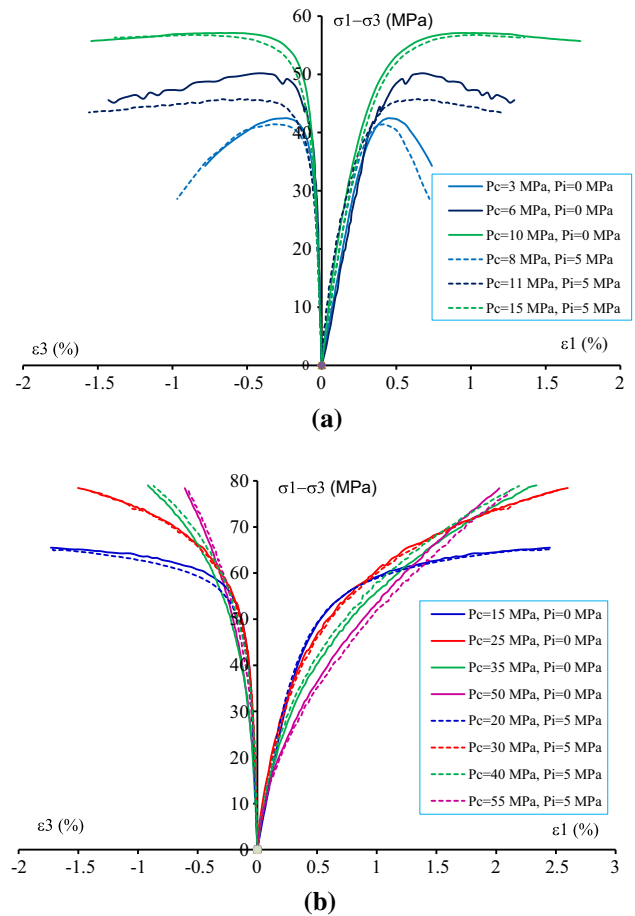


Fig. 1 Comparisons of stress–strain curves between drained triaxial compression tests with a constant pore pressure ($P_i = 5$ MPa) [14] and without pore pressure ($P_i = 0$). **a** ‘Low’ confining pressures, **b** ‘high’ confining pressures

mechanical behavior. For the tests under “low” confining pressures, the basic behavior of limestone is typically elastic brittle or elastoplastic brittle, and the failure state of sample can be clearly identified by a peak stress. In contrast, for the tests under “high” confining pressures, the basic behavior of limestone is elastoplastic ductile, and no peak stress can be defined until a relatively large axial strain. Detailed discussions on the effect of constant pore pressure will be given in the next section.

2.2 Water injection tests

In these tests, the sample is first subjected to a classical drained triaxial compression loading without initial pore pressure. When the deviatoric stress reaches a selected value and the strains become stable (green points in Fig. 2), an increase in pore pressure is generated by injecting water into the sample until the peak deviatoric stress is obtained (blue points in Fig. 2). After the peak stress, the water injection is continued with the same flow rate and the axial

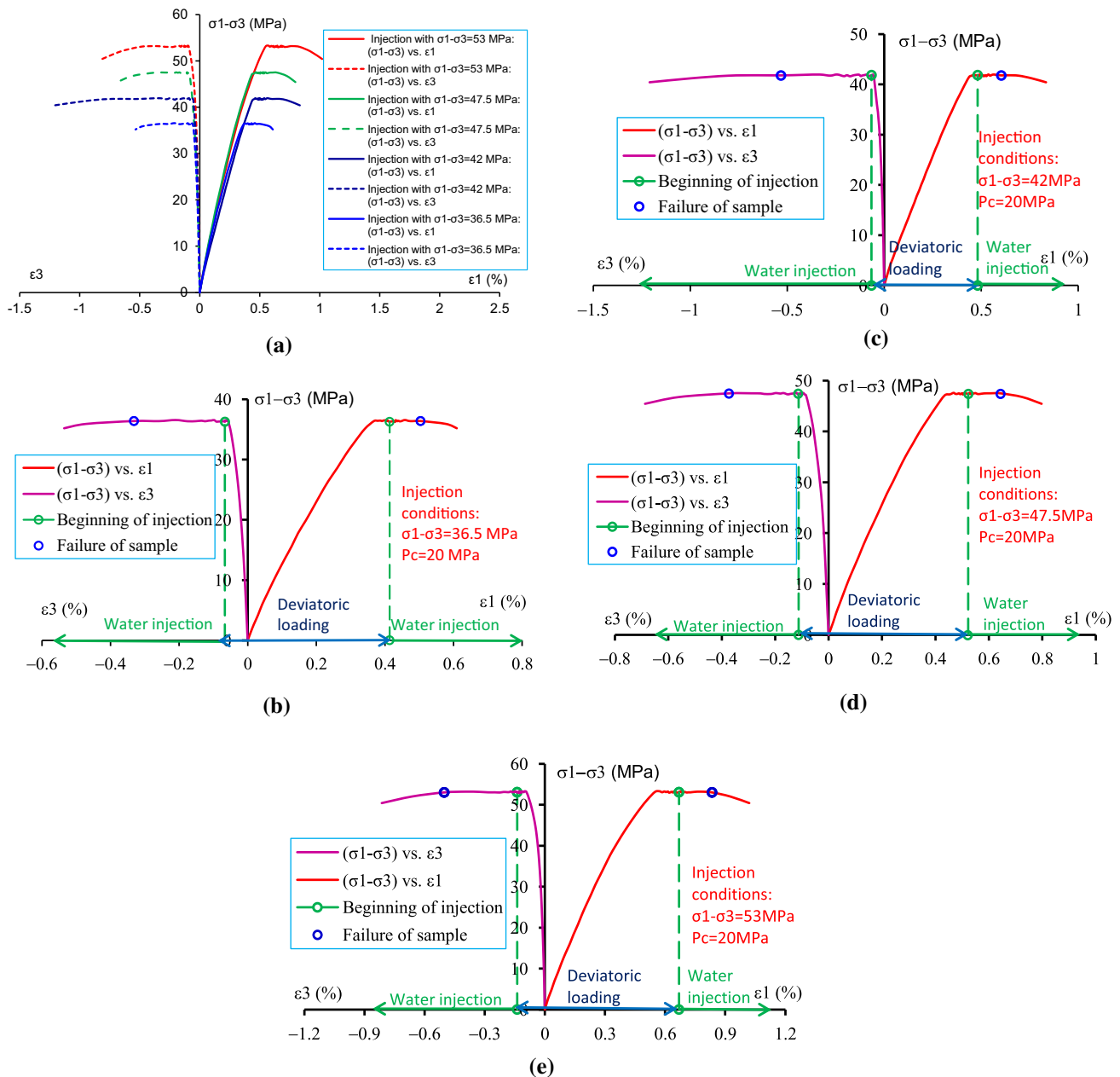


Fig. 2 Overall curves (a) and individual curves (b–e) of deviatoric stress versus axial and lateral strains during triaxial compression tests with water injection at different values of deviatoric stress and under a confining pressure of 20 MPa

strain is controlled by the corresponding pressure generator. It is thus possible to capture the post-peak behavior of sample during the water injection test (after the blue points in Fig. 2). Four tests are performed under a confining pressure of 20 MPa and with the deviatoric stresses of 36.5, 42.0, 47.5 and 53 MPa, respectively. The water is injected from the inlet point, while the outlet point is closed. The water injection flow rate is 0.003 ml/s. Both the inlet and outlet pressures are measured during the injection. The inlet pore pressure is slightly higher than the outlet one, but the difference is less than 0.1 MPa due to the relatively

high permeability of limestone and the small injection rate. The overall and individual curves of deviatoric stress versus axial and lateral strains are presented in Fig. 2. The variations of pore pressure are shown as functions of the axial and lateral strains in Fig. 3.

2.3 Undrained triaxial compression tests

The undrained triaxial compression test is performed in three steps. The selected confining pressure is first applied. An initial pore pressure is then set up in order to insure a

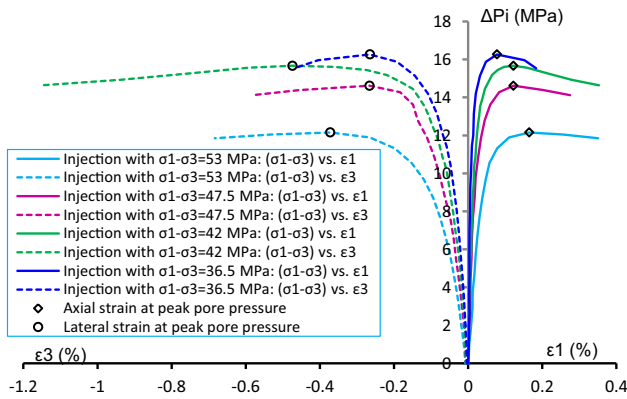


Fig. 3 Variations of axial and lateral strains with pore pressure increase during triaxial compression tests with water injection phase at different values of deviatoric stress and under a confining pressure of 20 MPa

good saturation state and to better measure variation of pore pressure during test. Finally, the axial stress is applied while the pore fluid circuit is closed from the exterior of sample. Fours tests are performed with four different confining pressures (6, 10, 23 and 38 MPa) and an initial pore pressure of 3 MPa. The axial strain rate is the same as that used in drained tests. In Fig. 4, we present the deviatoric stress versus the axial and lateral strains as well as the pore pressure, respectively.

3 Effects of pore pressure

As discussed in the previous study [14], the basic mechanical behavior of Anstrude limestone is characterized by two plastic deformation processes: pore collapse and plastic shearing. The effective mean stress threshold for pore collapse is about 44 MPa. Under low effective confining pressures (3, 6 and 10 MPa), the plastic shearing is the dominant process producing the strain softening in the post-peak regime and volumetric dilatancy. On the other hand, under high effective confining pressures (25, 35 and 50 MPa), the pore collapse plays an essential role and is responsible for volumetric compaction and ductile failure process. For an intermediate effective confining pressure such 15 MPa, there is a competition between the two plastic processes and it represents the transition point from brittle to ductile behavior of material. In this section, we shall discuss the effect of a constant pressure on two plastic deformation processes and failure strength of limestone.

3.1 Influence of a constant pore pressure

According to Fig. 1, for the effective confining pressures higher than 10 MPa, the stress–strain curves obtained, respectively, from tests without pore pressure and those

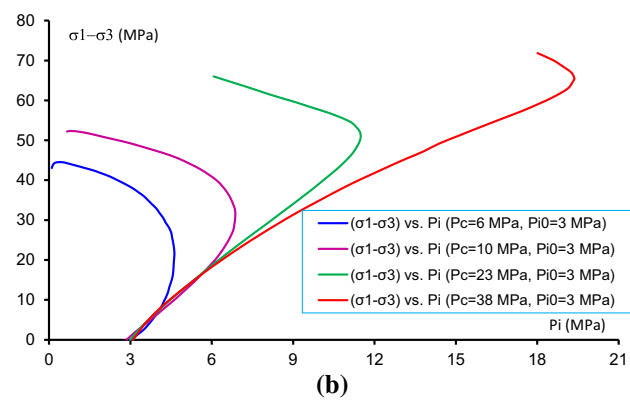
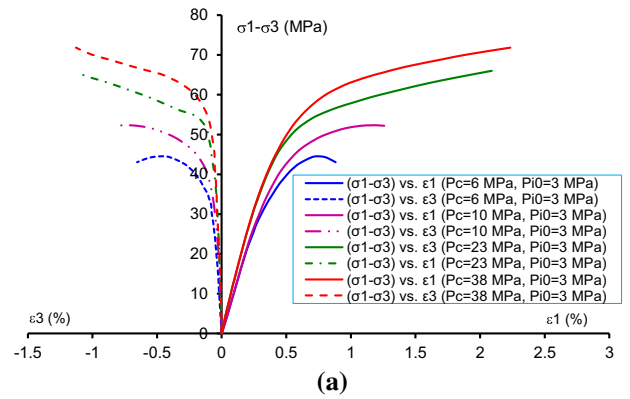


Fig. 4 Deviatoric stress versus axial and lateral strains as well as pore pressure in undrained triaxial compression tests with different confining pressures and an initial pore pressure of 3 MPa. **a** Deviatoric stress versus axial and lateral strains, **b** deviatoric stress versus pore pressure

with a constant pore pressure of 5 MPa [14] are nearly identical. However, for two low effective confining pressures (3 and 6 MPa), it seems that the peak deviatoric stress of samples with pore pressure is slightly lower than that of samples without pore pressure for a same value of effective confining pressure. In order to quantify the effect of pore pressure, we have determined the stress threshold, respectively, for the initial plastic shearing in the tests with low confining pressures, the pore collapse and onset of plastic shearing in the tests under high confining pressures. Under a low confining pressure, after the elastic limit, there is a clear transition from volumetric compressibility to dilatancy during the deviatoric loading. In order to better investigate the plastic volumetric strain transition, an elastic reference line is added on the basis of the extrapolation of the approximately linear part of the deviatoric stress versus volumetric strain curve. It is found that the plastic volumetric dilatancy threshold nearly coincides with the plastic shearing threshold. Under a high confining pressure, after the elastic limit stress, there is an important volumetric compaction due to the plastic pore collapse, followed by a clear transition from compaction to

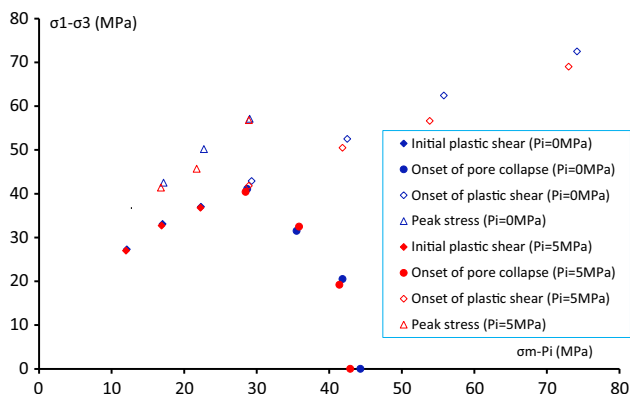


Fig. 5 Comparisons of stress threshold for plastic shearing, pore collapse and peak deviatoric stress obtained in triaxial compression tests without and with pore pressure in the diagram of deviatoric stress versus mean stress ($\sigma_m - p_i$)

dilatancy. Therefore, two reference lines can be added on the deviatoric stress versus volumetric strain curve. The first one defines the elastic strain slope, and the second line defines the average slope of the quasi-linear part of the curve during the pore collapse process. With the help of these two lines, it is easy to identify the pore collapse threshold and the plastic shearing threshold. The more detailed description for the determination of the onset points was presented in Han et al. [14]. The obtained results are presented in the diagram of deviatoric stress versus effective mean stress ($\sigma_m - P_i$, $\sigma_m = (\sigma_1 + 2\sigma_3)/3$), as shown in Fig. 5. Except the small difference of peak strength mentioned before, the onset of pore collapse and plastic shearing are almost not affected by the pore pressure. These results indicate that the mechanical behavior of limestone in triaxial compression tests is approximately controlled by the effective confining pressure defined according to the effective stress of Terzaghi. More detailed discussions about the effective stress concept will be given in the next section.

3.2 Analysis of water injection tests

In Fig. 6, the loading paths during the water injection tests are indicated by the horizontal lines in the diagram of deviatoric stress ($\sigma_1 - \sigma_3$) versus effective mean stress ($\sigma_m - P_i$). In this figure, the initial shearing threshold surface, the pore collapse surface and the peak strength surface are also illustrated. The corresponding variations of axial and lateral strains are presented in Fig. 3. It is seen that the mechanical responses of limestone during the water injection phase are dependent on the values of deviatoric stress of injection point, respectively, equal to 36.5, 42, 47.5 and 53 MPa. When the deviatoric stress is low, e.g., 36.5 MPa, the water injection point is in the elastic domain. The water injection process should generate

elastic tensile strains at both the axial and lateral directions. This is the case for the lateral strain as shown in Fig. 3. However, one gets a compressive axial strain. This is not verified by the isotropic poroelastic theory. There are several possible reasons to explain such a compressive strain induced by the water injection. Based on some previous studies [27], the water injection can enhance the pressure solution process in limestone and induce a weakening of both elastic modulus and mechanical strength of material. Therefore, if such a weakening effect exists, the water injection can induce a decrease in plastic yield stress of limestone and then generate additional plastic strains. Due to the applied deviatoric stress, the additional axial plastic strain should be compressive. However, additional investigations are needed to confirm the weakening effect of water injection in limestone. With the increase in pore pressure due to water injection (moving to the left on the diagram), the plastic shearing surface is reached as shown in Fig. 3. When the peak strength surface is finally reached, there is a material softening and a diminution of pore pressure. Moreover, the diminution of pores pressure is directly related to an important volumetric dilatancy. For higher levels of deviatoric stress (42, 47.5 and 53 MPa), the injection point is behind the initial pore collapse surface. This means that the material is in the plastic domain when the water injection is started. However, during the water injection phase, due to the increase in pore pressure before peak strength, there is an elastic unloading with respect to the pore collapse surface. However, when the plastic shearing surface is reached, the plastic deformation occurs but only due to the shearing process. Therefore, the plastic deformation during the water injection phase is dominated by the plastic shearing process.

3.3 Analysis of undrained tests

In Fig. 7, we present the curves of deviatoric stress versus axial and lateral strains as well as pore pressure versus axial strain separately for each value of confining pressure. In Fig. 8, the stress paths during the undrained tests are illustrated with respect to the initial plastic shearing surface, pore collapse surface and peak strength surface. It can be seen that the mechanical response of limestone during undrained triaxial compression tests is also influenced by confining pressure, in particular in terms of pore pressure, volumetric dilatancy and peak strength.

Let us first consider two tests under a low confining pressure (6 and 10 MPa). In the initial elastic zone, there are quasi-linear relations between strains, pore pressure increase and deviatoric stress. When the plastic shearing surface is reached, plastic deformation occurs with the shearing process. The plastic deformation produces a slight

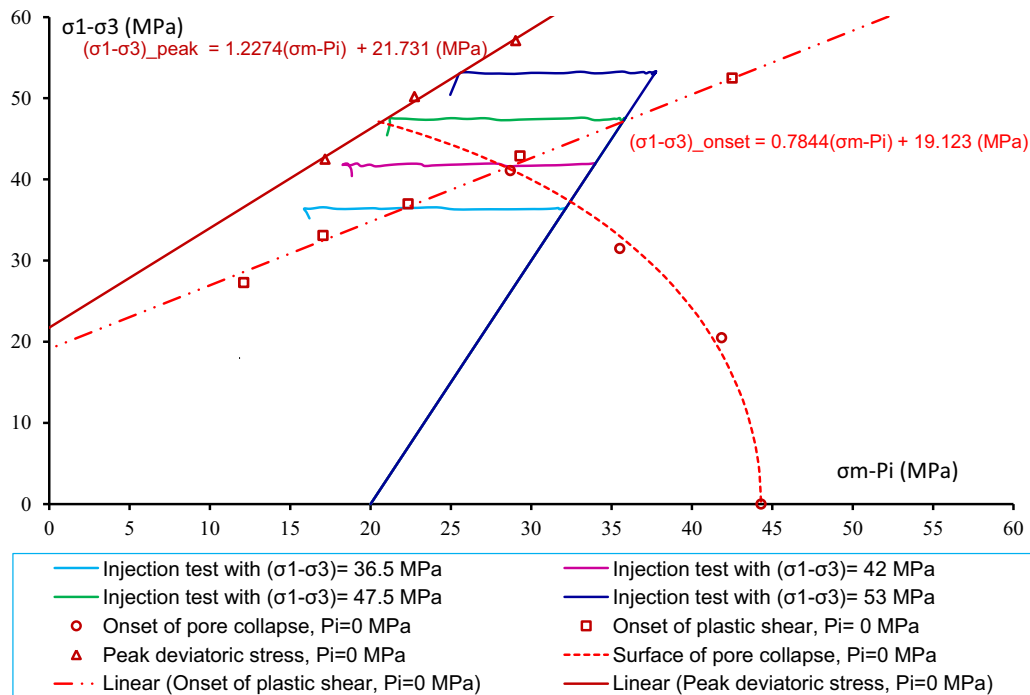


Fig. 6 Stress paths in water injection tests with respect to initial plastic shearing surface, pore collapse surface and peak deviatoric stress surface determined from triaxial compression tests without pore pressure

volumetric dilatancy but the total volumetric strain remains compressive. The pore pressure should continue to increase but with a reduced rate. Some scatters from this theoretical prediction are found on the experimental data obtained. It seems that the pore pressure drop starts before the volumetric compressibility–dilatancy transition point is reached. This may be attributed to possible heterogeneous distribution of pore pressure inside the sample. After the onset of volumetric dilatancy, the plastic strains become more significant and the pore pressure decreases quickly. The peak strength surface is then reached, and the peak deviatoric stress is obtained. The peak strength is more pronounced when the confining pressure is lower, and this indicates the transition from brittle to ductile behavior. The pore pressure continues to decrease during the post-peak regime and finally approaches zero. One obtains some residual stress–strain regime. Note that in these two tests, the pore collapse surface is never reached. Therefore, the plastic deformation is entirely controlled by the shearing process.

For the test under a high confining pressure (38 MPa), after an initial elastic phase, the plastic pore collapse surface is reached before reaching the shearing surface. The two plastic processes have a competitive influence on pore pressure evolution. The pore collapse process produces a volumetric compaction. As a consequence, one gets a significant increase in pore pressure. When the plastic shearing is reached, a volumetric dilatancy is produced and

the rate of pore pressure increase is reduced. The volumetric compressibility–dilatancy transition is then observed, and one observes a quasi-constant phase of pore pressure. Finally, the pore pressure decreases with the increase in volumetric dilatancy. In this case, the plastic pore collapse process plays an essential role in the pore pressure evolution while the material failure is controlled by the plastic shearing.

For the test with an intermediate confining pressure (20 MPa), both two plastic processes are also activated. However, the plastic shearing is reached before the plastic pore collapse. Even if the plastic shearing process produces a volumetric dilatancy, the overall volumetric strain remains compacting and the pore pressure continues to increase. Progressively, the plastic shearing process becomes dominant with respect to pore collapse. One obtains the transition from compressibility to dilatancy and the decrease in pore pressure.

4 Discussions

The presence of fluid can affect the mechanical behavior of rock through both chemical and mechanical interactions [28]. As mentioned above, there are some differences of plastic yield and failure surfaces between tests without and with pore pressure. For a better understanding of such differences, the experimental results obtained are now

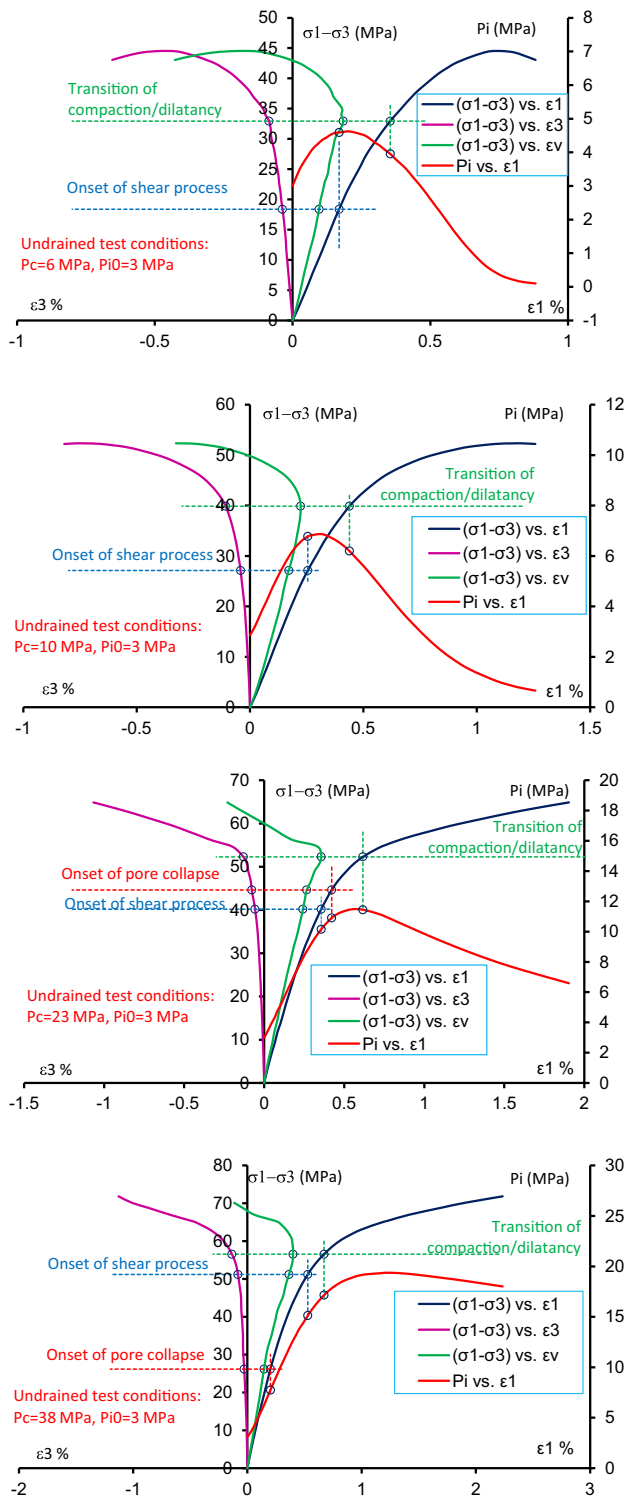


Fig. 7 Variations of strains and pore pressure in undrained triaxial compression tests under different confining pressures and an initial pore pressure of 3 MPa

analyzed in terms of effective stress concept and chemical effect of pore fluid.

4.1 Discussion on effective stress concept for plasticity

Based on a macroscopic kinematic assumption, Coussy [8] has introduced the concept of effective stress for poroelasticity theory by the relation $\sigma_{ij}^p = \sigma_{ij} - \beta p \delta_{ij}$, with $\beta \leq 1$ being the plastic effective stress coefficient, which is physically different with the Biot's coefficient for poroelasticity theory.

In Fig. 5, the threshold stresses for plastic shearing, pore collapse and peak strength are presented, respectively, from the tests without pore pressure ($p_i = 0$) and with a constant pore pressure ($p_i = 5$ MPa). One can see that the pore collapse threshold obtained from the test with $p_i = 5$ MPa is slightly lower than that from the test with $p_i = 0$. By assuming the validity of plastic effective stress concept and by neglecting for the moment any chemical effect of water on limestone, one can easily deduce $\beta < 1$ for the studied limestone. Following this concept, the effective confining pressure ($P_c - \beta p_i$) in a test with $P_{c1}, p_i > 0$ should be higher than that in a test with $P_{c2}, p_i = 0$ if $P_{c1} - p_i = P_{c2}$. As a consequence, the plastic shearing threshold for the test with $p_i > 0$ should be higher than that of the test with $p_i = 0$. This theoretical prediction is not verified by the experimental data in Fig. 5. Indeed, the initial plastic shearing surface issued from tests with $p_i = 5$ MPa is slightly lower than that issued from those with $p_i = 0$. A similar result can be obtained about the peak strength surface. The peak strength of samples with pore pressure is generally lower than that in samples without pore pressure. The stress paths followed in the water injection tests are shown in Fig. 6. One can make the same remark as the tests with a constant pressure. For instance, for the tests performed with low deviatoric stress levels (36.5 and 42 MPa), it is clear that the peak deviatoric stresses obtained in the water injection tests are lower than that obtained the triaxial compression tests without pore pressure. As a conclusion, it seems that the effect of pore pressure on plastic deformation and strength cannot be explained by the mechanical effect only. It seems that the presence of pore fluid induces a chemical degradation which affects both plastic yield stress and peak strength.

4.2 Discussion on degradation effect of pore pressure

The objective here is not to present a detailed study on physical and chemical reactions between water and limestone. We just want to discuss the effects of pore pressure increase on plastic deformation and strength of limestone. However, it is useful to mention some possible physical and chemical processes between water and limestone

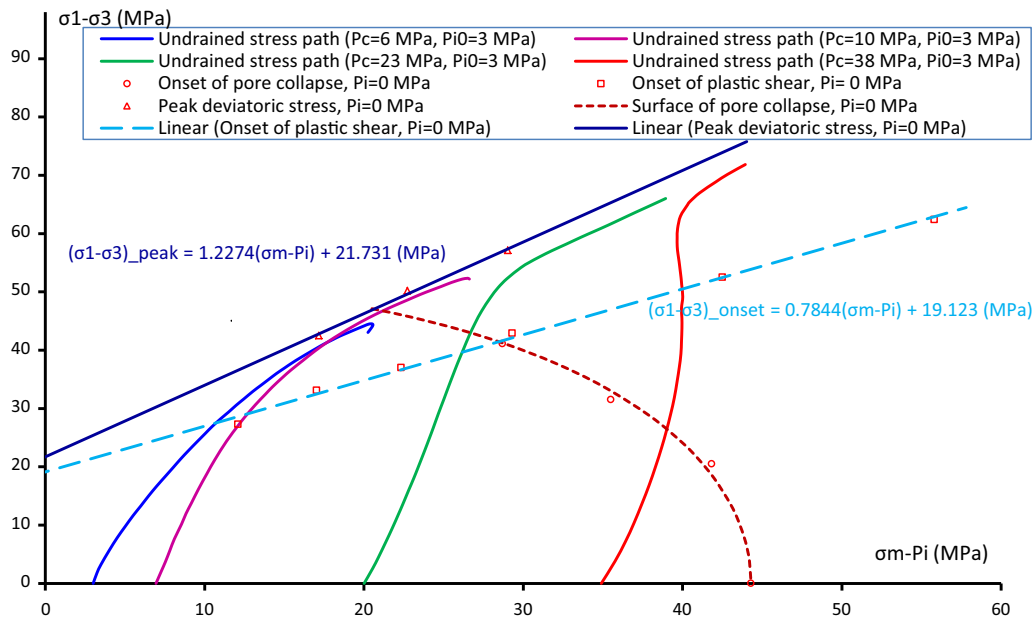


Fig. 8 Stress paths in undrained triaxial compression tests with respect to initial plastic shearing surface, pore collapse surface and peak deviatoric stress surface determined from triaxial compression tests without pore pressure

observed in some previous studies. One can invoke the dissolution of contact surfaces by the inter-granular pressure solution [18, 25, 30, 31, 44]. It was found that the effect of chemical dissolution is generally amplified by the increase in pore pressure [27]. For the limestone studied here, as presented above, under a low effective confining pressure, the mechanical behavior of limestone is clearly affected by the increase in pore pressure. In contrast, the mechanical behavior under a high effective confining pressure seems not affected by the increase in pore pressure. In order to confirm this result with a higher pore pressure, we have performed two additional triaxial compression tests with a constant pore pressure of 18 MPa and two confining pressures of 33 and 53 MPa, respectively. In Fig. 9, the obtained results are compared with those obtained from the tests with $P_c = 15$ MPa, $p_i = 0$ and $P_c = 20$ MPa, $p_i = 5$ MPa, and with $P_c = 35$ MPa, $p_i = 0$ and $P_c = 40$ MPa, $p_i = 5$ MPa, respectively. It is clear that the peak strength for the test with $P_c = 33$ MPa, $p_i = 18$ MPa is lower than that with $P_c = 20$ MPa, $p_i = 5$ MPa, which is again lower than that with $P_c = 15$ MPa, $p_i = 0$, as shown in the deviatoric stress–volumetric strain curves. For the three tests with an effective confining pressure of 35 MPa, the deviatoric stress versus axial strain curves are almost identical. However, the deviatoric stress versus volumetric strain curves show a clear difference. It is clear that the compaction–dilatation transition for the test with $P_c = 53$ MPa, $p_i = 18$ MPa is lower than that with $P_c = 40$ MPa, $p_i = 5$ MPa, which is again lower than that with $P_c = 35$ MPa, $p_i = 0$. At the same time, the plastic

volumetric strain due to pore collapse is amplified by the increase in pore pressure. Therefore, the presence of pore fluid could induce a degradation effect on the plastic yielding and failure strength of limestone and this degradation effect is amplified when the pore pressure is higher.

5 Conclusions

Effects of pore pressure on both plastic deformation and strength of saturated limestone have been investigated in this work. The experimental results have confirmed that the plastic deformation is characterized by pore collapse and shearing. The pore collapse is responsible for volumetric compaction, while the shearing induces a volumetric dilatancy. The plastic deformation is dominated by the pore collapse process under high confining pressures but by the shearing process under low ones. There is a transition from brittle to ductile behavior with the increase in confining pressure.

The water injection induces an increase in pore pressure and then a decrease in effective confining pressure. This enhances the plastic shearing process, volumetric dilatancy and shearing failure. Further only the plastic shearing is activated in such a loading path.

The pore pressure evolution in undrained triaxial tests is also influenced by two plastic processes. At a low confining pressure, the deviatoric stress induces plastic dilatancy due to shearing process and then a decrease in pore pressure. But at a high confining pressure, the deviatoric stress

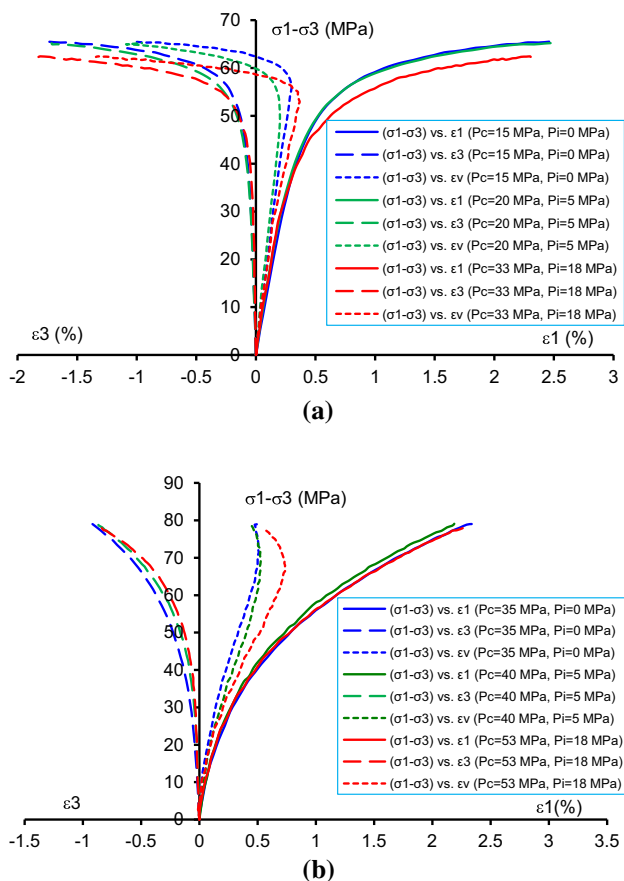


Fig. 9 Stress–strain curves in triaxial compression tests with and without pore pressure but under two same values of $(P_c - P_i)$ for different values of pore pressure (0, 5 and 18 MPa). **a** ‘Effective’ confining pressure $(P_c - P_i) = 15$ MPa, **b** ‘effective’ confining pressure $(P_c - P_i) = 35$ MPa

induces a plastic compaction due to pore collapse and enhances the increase in pore pressure. The pore collapse dominates the pore pressure evolution during the first stage of loading, while the plastic shearing dominates the peak strength and pore pressure evolution during the second stage.

The concept of effective stress for plastic deformation and peak strength has been revisited. It is found that the validity of the classical Terzaghi’s effective stress concept was not fully verified. The plastic yield stress and peak strength in the samples with pore pressure are generally lower than those in the samples without pore pressure for a same effective confining pressure. It seems that the scatter with the effective stress concept can be attributed to a degradation effect of pore fluid pressure. The presence of pore fluid can induce a decrease in plastic yield stress and peak strength, and the degradation effect is amplified by the increase in pore pressure. However, further investigations are still needed to identify and quantify the origins of degradation effect by pore fluid pressure in limestone.

References

- Baud P, Schubnel A, Wong TF (1999) Dilatancy, compaction, and failure mode in Solnhofen limestone. *J Geophys Res* 105(B8):19289–19303
- Biot MA (1941) General theory of three dimensional consolidation. *J Appl Phys* 12:155–164
- Biot MA (1973) Non-linear and semi-linear rheology of porous solids. *J Geophys Res* 78:4924–4937
- Boutéca M, Guéguen Y (1999) Mechanical properties of rocks: pore pressure and scale effects. *Rev IFP* 54(6):703–714
- Byerlee JD (1968) Brittle–Ductile transition in rocks. *J Geophys Res* 73(14):4741–4750
- Cheng AHD (1997) Material coefficients of anisotropic poroelasticity. *Int J Rock Mech Min Sci* 34(2):199–205
- Collin F, Cui YJ, Schroeder C, Charlier R (2002) Mechanical behaviour of Lixhe chalk partly saturated by oil and water: experimental and modeling. *Int J Numer Anal Methods Geomech* 26:897–924
- Coussy O (1995) *Mechanics of porous continua*. Wiley, Chichester
- Coussy O (2004) *Poromechanics*. Wiley, Hoboken
- De Buhan P, Dormieux L (1996) On the validity of the effective stress concept for assessing the strength of saturated porous materials: a homogenization approach. *J Mech Phys Solids* 44:1649–1667
- De Gennaro V, Delage P, Priol G, Collin F, Cui YJ (2004) On the collapse behaviour of oil reservoir chalk. *Géotechnique* 54:415–420
- Dormieux L, Kondo D, Ulm F-J (2006) *Microporomechanics*. Wiley, Hoboken
- French ME, Boutt DF, Goodwin LB (2012) Sample dilation and fracture in response to high pore fluid pressure and strain rate in quartz-rich sandstone and siltstone. *J Geophys Res* 117:B03215. <https://doi.org/10.1029/2011JB008707>
- Han B, Xie SY, Shao JF (2016) Experimental investigation on mechanical behavior and permeability evolution of a porous limestone under compression. *Rock Mech Rock Eng* 49:3425–3435
- Hart DJ, Wang HF (2001) A single test method for determination of poroelastic constants and flow parameters in rocks with low hydraulic conductivities. *Int J Rock Mech Min Sci* 38(4):577–583
- Homand S, Shao JF (2000) Mechanical behaviour of a porous chalk and water/chalk interaction, part I. Experimental study. *Oil Gas Sci Technol* 55(6):591–598
- Hu DW, Zhou H, Zhang F, Shao JF (2010) Evolution of poroelastic properties and permeability in damaged sandstone. *Int J Rock Mech Min Sci* 47(6):962–973
- Jeschke AA, Dreybrodt W (2002) Dissolution rates of minerals and their relation to surface morphology. *Geochim Cosmochim Acta* 66(17):3055–3062
- Kerbouche R, Shao JF, Skoczylas F (1995) On the poroplastic behaviour of porous rock. *Eur J Mech A Solids* 14:577–587
- Lion M, Skoczylas F, Ledéret B (2004) Determination of the main hydraulic and poro-elastic properties of a limestone from Bourgogne, France. *Int J Rock Mech Min Sci* 41:915–925
- Lisabeth HP, Zhu W (2015) Effect of temperature and pore fluid on the strength of porous limestone. *J Geophys Res Solid Earth* 120:6191–6208. <https://doi.org/10.1002/2015JB012152>
- Lockner DA, Stanchits SA (2002) Undrained poroelastic response of sandstones to deviatoric stress change. *J Geophys Res* 107(B12):2353. <https://doi.org/10.1029/2001JB001460>
- Lydzba D, Shao JF (2000) Study of poroelasticity material coefficients as response of microstructure. *Mech Cohesive Frict Mater* 5:149–171

24. Lydzba D, Shao JF (2002) Stress equivalence principle for saturated porous media. *C R Mécanique* 330:297–303
25. Lydzba D, Pietruszczak S, Shao JF (2007) Intergranular pressure solution in chalk; a multiscale approach. *Comput Geotech* 34:291–305
26. Ma X, Zoback MD (2017) Laboratory experiments simulating poroelastic stress changes associated with depletion and injection in low-porosity sedimentary rocks. *J Geophys Res Solid Earth* 122:2478–2503. <https://doi.org/10.1002/2016JB013668>
27. Macdonald RW, North NA (1974) The effect of pressure on the solubility of CaCO_3 , CaF_2 , and SrSO_4 in water. *Can J Chem* 52(18):3181–3186
28. Paterson MS, Wong TF (2005) *Experimental rock deformation—the brittle field*, 2nd edn. Springer, Berlin
29. Pimienta L, Fortin J, Yves Gueguen Y (2017) New method for measuring compressibility and poroelasticity coefficients in porous and permeable rocks. *J Geophys Res Solid Earth* 122:2670–2689. <https://doi.org/10.1002/2016JB013791>
30. Raj R (1982) Creep in polycrystalline aggregates by matter transport through a liquid phase. *J Geophys Res* 87:4731–4739
31. Risnes R, Madland MV, Hole M, Kwabiah NK (2005) Water weakening of chalk—mechanical effects of water–glycol mixtures. *J Petrol Sci Eng* 48:21–36
32. Shao JF (1997) Poroelastic behaviour of brittle rock materials with anisotropic damage. *Mech Mater* 30:41–53
33. Shao JF, Henry JP (1991) Development of an elastoplastic model for porous rock. *Int J Plast* 7:1–13
34. Stover SC (2003) A one-dimensional analytically based approach for studying poroplastic and viscous consolidation: application to Woodlark Basin, Papua New Guinea. *J Geophys Res* 108(B9):2448. <https://doi.org/10.1029/2001JB000466>
35. Thompson M, Willis JR (1991) A reformulation of the equations of anisotropic poroelasticity. *J Appl Mech ASME* 58:612–616
36. Viesca RC, Rice JR (2012) Nucleation of slip-weakening rupture instability in landslides by localized increase of pore pressure. *J Geophys Res* 117:B03104. <https://doi.org/10.1029/2011JB008866>
37. Viesca RC, Templeton EL, Rice JR (2008) Off-fault plasticity and earthquake rupture dynamics: 2. Effects of fluid saturation. *J Geophys Res* 113:B09307. <https://doi.org/10.1029/2007JB005530>
38. Warpinski NR, Teuffel LW (1993) Laboratory measurements of the effective-stress law for carbonate rocks under deformation. *Int J Rock Mech Min Sci Geomech Abstr* 30(7):1169–1172
39. Wong TF, Szeto H, Zhang J (1992) Effect of loading path and porosity on the failure mode of porous rocks. *Appl Mech Rev* 45(8):281–293
40. Wong TF, David C, Zhu W (1997) The transition from brittle faulting to cataclastic flow in porous sandstone: mechanical deformation. *J Geophys Res* 102:3009–3025
41. Xie SY, Shao JF (2006) Elastoplastic deformation of a porous rock and water interaction. *Int J Plast* 22:2195–2225
42. Xie SY, Shao JF (2012) Experimental investigation and poroplastic modelling of saturated porous geomaterials. *Int J Plast* 39:27–45
43. Xie SY, Shao JF (2015) An experimental study and constitutive modeling of saturated porous rocks. *Rock Mech Rock Eng* 48:223–234
44. Xie SY, Shao JF, Xu WY (2011) Influences of chemical degradation on mechanical behaviour of a limestone. *Int J Rock Mech Min Sci* 48:741–747
45. Xie N, Zhu QZ, Shao JF, Xu LH (2012) Micromechanical analysis of damage in saturated quasi brittle materials. *Int J Solids Struct* 49:919–928
46. Yamada SE, Schatz JF, Abou Sayed A, Jones AH (1981) Elastoplastic behavior of porous rock under undrained condition. *Int J Rock Mech Min Sci Geomech Abstr* 18:177–179
47. Yarushina VM, Podladchikov YY (2015) (De)compaction of porous viscoelastoplastic media: model formulation. *J Geophys Res Solid Earth* 120:4146–4170. <https://doi.org/10.1002/2014JB011258>
48. Zhang J, Wong T-F, Davis DM (1990) Micromechanics of pressure-induced grain crushing in porous rocks. *J Geophys Res* 95:341–352

Publisher's Note

Springer Nature remains neutral with regard to jurisdictional claims in published maps and institutional affiliations.

Chapter III

Micromechanics-Based Model for Porous Rocks with Pressure-Sensitive Matrix

Contents

1	Introduction	29
2	Elastic properties of porous rocks	31
3	Micromechanics-based model for porous rocks	32
3.1	Macroscopic yield criterion of porous rocks	32
3.2	Hardening function	34
3.3	Evolution of porosity	35
3.4	Plastic multiplier	36
4	Sensibility analysis of the model	37
4.1	Influences of parameters on the initial yield strength	37
4.2	Effect of confining pressure	40
4.3	Comparison between associated and non-associated models	41
5	Conclusion	47

1 Introduction

Porous rocks, such as chalk, limestone and sandstone are typical rocks with relative high porosity, and it is frequently encountered in various engineering problems such as

geotechnical engineering, mining engineering, petroleum industry, etc. The deformation and failure behaviours of porous rocks are essential in understanding and analysing those engineering problems. For example, in petroleum industry domain, many stability problems of wellbore and reservoirs occur in high porosity chalk reservoirs. A famous is the subsidence problem of Ekofisk field, North Sea, Norway [Wiborg and Jewhurst, 1986], and the petroleum reservoir chalk is porous chalk from Late Cretaceous to early Paleogene in age. Since the problem revealed, the deformation and failure behaviours, as well as the constitutive modelling of porous rocks have received considerable attention, for better understanding the mechanism of deformation and failure of porous chalk, a great number of studies have been performed on different kinds of chalk by petroleum operators and research communities, as ([Elliott and Brown, 1985], [Shao and Henry, 1991], [Risnes and Flaageng, 1999], [Homand and Shao, 2000]; [Risnes, 2001], [Talesnick et al., 2001], [Collin et al., 2002],[Schroeder, 2003], [De Gennaro et al., 2004]; [Xie and Shao, 2006], [Xie and Shao, 2012], [Xie and Shao, 2015], [Han et al., 2016],[Han et al., 2018], just to mention a few). The experimental results show that the mechanical behaviour of porous chalk are determined by the mineral composition and microstructural variables such as grain size and porosity, and affected by the extrinsic factors including temperature, the physical and chemical characterises of pore fluid. Moreover, the experimental results reveal the basic mechanical behaviour of porous rocks, such as pressure-sensitivity, and two plastic mechanisms. Thus, the porous rocks can be characterized by two coupled plastic deformation mechanisms: the plastic shear mechanism at low confining pressures and the plastic pore collapse mechanism at high confining pressures. Accordingly, the two plastic mechanisms should be taken into account in the modelling of mechanical behaviour of porous rocks.

Phenomenological and micromechanics-based models have been proposed for porous rocks by taking these two plastic mechanisms into account. Phenomenological elastoplastic models with two yield surfaces have been formulated ([DiMaggio and Sandler, 1971]; [Lade, 1977]; [Desai, 1980]; [Gens, 1993]; [Lade, 1997]; [Desai, 2000]; [Perić and Ayari, 2002];[Collin et al., 2002];[Xie and Shao, 2006]). In such models, a cap yield surface is used to describe the pore collapse deformation, while a modified Mohr–Coulomb type criterion is adopted to interpret the plastic shearing and failure. The advantage of such models is that two plastic deformation mechanisms are distinctly taken into account by two yield surfaces. However, specific algorithms are needed for the numerical implementation regarding the coupling between two yield surfaces. The number of parameters in these models is generally high. For this reason, some authors proposed plastic models with a single closed yield surface ([Lade and Kim, 1995]; [Ehlers, 1995]; A[Aubertin et al., 1999];

[Lewis and Khoei, 2001]; [Aubertin and Li, 2004]; [Khoei and Azami, 2005]). However, in the phenomenological models, the effect of porosity is not explicitly taken into account. In order to determine the effective strength criteria for porous materials, important advances have been obtained on micromechanical modeling during the last decades. Based on the homogenization techniques using analysis method or variational principles, a series of macroscopic strength criteria have been developed for various porous materials.

The pioneering work is the famous Gurson's criterion for porous materials with a solid matrix obeying von-Mises criterion and containing spherical pores [Gurson, 1977]. For porous geomaterials, the solid matrix generally exhibits a pressure dependency, and then a pressure-sensitive criterion is needed for a correct description of mechanical behaviour of porous materials. Various forms of macroscopic strength criteria have also been developed with different pressure-sensitive solid matrix ([Jeong, 2002]; [Guo et al., 2008]; [Maghous et al., 2009]; [Monchiet and Kondo, 2012]; [Shen et al., 2013], [Shen et al., 2014], [Shen et al., 2015]). Some extensions have also been proposed for anisotropic materials containing spheroidal voids. The advantage of these micromechanics-based models is that the effects of porosity and the plastic property of solid matrix are explicitly taken into account in the macroscopic yield and failure criteria. A single yield surface is obtained and able to describe both the plastic shearing and pore collapse. It is therefore possible to develop the model through a purely micro-macro approach for mechanical behaviour of porous rocks. Based on the micromechanics-based macroscopic criteria derived with different pressure-sensitive criteria of solid matrix, some micromechanics-based associated models are developed for porous rocks in drained condition ([Lin et al., 2012], [Shen et al., 2014]). Considering that, under a low confining pressure, these proposed models with associated rules are overestimated elastic limit, deviatoric strength, as well as the volumetric dilatancy, therefore, in the present work, some improvements will be proposed by extending plastic yield function and by introducing a non-associated plastic flow rule.

2 Elastic properties of porous rocks

With help of the Electronic scanning microscope (MEB), the microstructure of porous rocks can be characterized clearly as an assembly of solid grains with different kinds of contact surfaces and a connected macroscopic porosity [Schroeder, 2003]. The macroscopic mechanical behavior of porous rocks depends on the calcite grains, the contact surfaces and the porosity. Therefore, the macroscopic mechanical properties of porous rocks can be analyzed through two steps. As a first approximation for the purpose of macroscopic

ic modelling, an idealized configuration can be adopted. The solid grains with different kinds of contact surfaces can roughly be considered a solid matrix with different contacts. Further, the solid matrix with different contacts forms an equivalent solid matrix in mesoscopic scale. As a consequence, the macroscopic mechanical behavior of porous rocks depends on the equivalent solid matrix and the macroscopic porosity. Based on the Mori-Tanaka homogenization scheme for porous materials, macroscopic elastic properties of porous rocks porous can be estimated.

$$\begin{cases} k_0 = \frac{4(1-\phi)k_m\mu_m}{4\mu_m + 3\phi k_m} \\ \mu_0 = \frac{(1-\phi)\mu_m}{1 + 6\phi \frac{k_m + 2\mu_m}{9k_m + 8\mu_m}} \end{cases} \quad (\text{III .1})$$

Where $(k_0; \mu_0)$ denote, respectively, the macroscopic bulk and shear moduli of porous rocks, and $(k_m; \mu_m)$ denote, respectively, the bulk and shear moduli of solid matrix, ϕ the porosity of rocks.

3 Micromechanics-based model for porous rocks

3.1 Macroscopic yield criterion of porous rocks

Based on the micromechanics-based macroscopic criterion derived by [Shen et al., 2015] from the analysis of a hollow sphere whose matrix obeys to a Mises -Schleicher criterion, we propose an extension of this work in order to describe the poromechanical behavior of saturated porous rocks both in drained and undrained conditions. Some improvements are also proposed by introducing a non-associated plastic flow rule.

Consider now a porous material constituted by an isotropic solid matrix and spherical voids. The porosity is denoted by ϕ . The solid matrix obeys a Mises -Schleicher yield criterion, which reads:

$$\varphi(\sigma) = \sigma_{eq}^2 + 3\alpha\sigma_0\sigma_m - \sigma_0^2 \leq 0 \quad (\text{III .2})$$

$\sigma_m = tr(\bar{\sigma})/3$ being the mean stress and $\sigma_{eq} = \sqrt{3/2\bar{\sigma}_d : \bar{\sigma}_d}$ with $\bar{\sigma}_d = \bar{\sigma} - \sigma_m\bar{\delta}$ being the deviatoric stress of the local stress field in the solid matrix. In this criterion, σ_0 and α are related to the tensile yield stress, T , and absolute yield stress in compression, C , by

$$\sigma_0 = \sqrt{CT} \text{ and } \alpha = \frac{C - T}{\sqrt{CT}} \quad (\text{III .3})$$

Note that the Mises-Schleicher criterion predicts asymmetry between tension and com-

pression. σ_0 and α are two material parameters with the assumption that $\alpha \geq 0$ and which physically means that the yield stress in tension is lower than in compression. The parameter σ_0 is the material cohesion related to the pure shear yield stress of solid matrix while the parameter α acts as the pressure-sensitive coefficient.

Denote $\bar{\bar{\Sigma}}$ as the macroscopic stress tensor applied to the representative volume element (RVE) of the porous material. Using an appropriate homogenization technique, [Shen et al., 2015] determined an approximate closed form of the macroscopic yield criterion of the porous material as a function of porosity and plastic parameters of a Mises - Schleicher solid matrix.

$$\Phi = \frac{\Sigma_{eq}^2/\sigma_0^2}{B - 3\alpha C \Sigma_m/\sigma_0} + 2\Gamma \cosh \left(A \ln \left(1 - 3\alpha \frac{\Sigma_m}{\sigma_0} \right) \right) - 1 - \Gamma^2 = 0 \quad (\text{III .4})$$

$$\text{with} \left\{ \begin{array}{l} B = \frac{(1-\phi)^2}{(1-\Gamma)^2} \\ C = \frac{(1-\phi)}{(1-\Gamma)^2} \\ \Gamma = \left(\alpha^2 (W(\phi p) + 1)^2 - \alpha^2 \right)^A \\ A = \text{sign}(\Sigma_m) \left(\frac{4}{9\alpha} + \frac{\alpha (W(\phi p) + 1)^2 - \alpha}{18} \right) \end{array} \right. \quad (\text{III .5})$$

In the relations above, $\Sigma_m = \text{tr}(\bar{\bar{\Sigma}})/3$ is the macroscopic mean stress and $\Sigma_{eq} = \sqrt{3/2 \bar{\bar{\Sigma}}_d : \bar{\bar{\Sigma}}_d}$ with $\bar{\bar{\Sigma}}_d = \bar{\bar{\Sigma}} - \Sigma_m \bar{\bar{\delta}}$ is the macroscopic deviatoric stress. And W denotes the ‘‘Lambert W’’ function which satisfies $W(x) = e^{W(x)} = x$. $W(x)$ has two branches: $W_0(x) \geq -1$ upper branch and $W_{-1}(x) \leq -1$ lower branch (for $-e^{-1} \leq x < 0$). In the functions above, $W(\phi p) = W_{-1}(\phi p_-)$ for compression and $W(\phi p) = W_0(\phi p_+)$ for tension. The coefficient p_- and p_+ are functions of α and the expressions are given as follows.

$$\left\{ \begin{array}{l} p_+ = z_+ \exp(z_+), \quad z_+ = \frac{-\alpha + \sqrt{\alpha^2 + 1}}{\alpha} \\ p_- = z_- \exp(z_-), \quad z_- = \frac{-\alpha - \sqrt{\alpha^2 + 1}}{\alpha} \end{array} \right. \quad (\text{III .6})$$

The yield criterion given in (III .4) will be used to describe the plastic deformation of porous rocks. In order to improve the criterion adaptability, a more general C solution should be proposed for ensuring smoothness of macroscopic criterion at the point $\Sigma_m = 0$. Even though the expressions for the two slopes K_t and K_c of the tangent line to curve of macroscopic criterion have the same expression as follows, it is clear that the values of two

slopes are not equal to each other at the point $\Sigma_m = 0$ due to Γ being different function in tension and compression conditions (for the detail, see [Shen et al., 2015]).

These two different expressions of Γ are caused by the traction-compression dissymmetry of Mises - Schleicher criterion in the matrix.

$$K_t = -\frac{3\alpha C(1-\Gamma)^2}{2(1-\phi)} \Gamma \text{ is a function of } W_0(\phi p_+) \text{ for the case of tension} \quad (\text{III .7})$$

$$K_c = -\frac{3\alpha C(1-\Gamma)^2}{2(1-\phi)} \Gamma \text{ is a function of } W_{-1}(\phi p_-) \text{ for the case of compression} \quad (\text{III .8})$$

Accordingly, we can take $C = (1-\phi)^s / (1-\Gamma)^2$ with a parameter s determining the form of the yield criterion, then the two slops, K_t and K_c , are equal to each other at point $\Sigma_m = 0$ with $K_t = K_c = -\frac{3}{2}\alpha(1-\phi)^{s-1}$. Note that $\lim_{\phi \rightarrow 0} K_t = \lim_{\phi \rightarrow 0} K_c = -\frac{3}{2}\alpha$, these are the two slops for Mises-Schleicher solid matrix at $\Sigma_m = 0$.

Furthermore, in order to describe the plastic hardening, we assume that the yield stress of the solid matrix is a function of plastic deformation. Therefore, replacing the initial yield stress σ_0 by the current threshold $\bar{\sigma}$, in the present work, the macroscopic plastic yield function is adopted in the following form:

$$\Phi = \frac{\Sigma_{eq}^2}{\Theta \bar{\sigma}^2} + 2\Gamma \cosh \left(A \ln \left(1 - 3\alpha \frac{\Sigma_m}{\bar{\sigma}} \right) \right) - 1 - \Gamma^2 = 0 \quad (\text{III .9})$$

$$\text{with} \begin{cases} \Theta = \left(\frac{1-\phi}{1-\Gamma} \right)^2 - 3\alpha \frac{(1-\phi)^s \Sigma_m}{(1-\Gamma)^2 \bar{\sigma}} \\ \Gamma = \left(\alpha^2 (W(\phi p) + 1)^2 - \alpha^2 \right)^A \\ A = \text{sign}(\Sigma_m) \left(\frac{4}{9\alpha} + \frac{\alpha(W(\phi p) + 1)^2 - \alpha}{18} \right) \end{cases} \quad (\text{III .10})$$

3.2 Hardening function

The plastic hardening function is essentially determined from the experimental data of a hydrostatic compression test, which revealed an initial pore collapse yield stress, a strong plastic contractancy due to the pore collapse and a hardening phase due to the increase of contact surfaces between grains. Therefore, the following hardening function by [Xie and Shao, 2006]:

$$\bar{\sigma} = \bar{\sigma}_0 \left(1 + a(\varepsilon_M)^n e^{b\varepsilon_M} \right) \quad (\text{III .11})$$

The variable ε_M denotes an equivalent plastic strain of the solid matrix. Three parameters, a , b and n , describe the yield stress evolution rate of the solid matrix, and can be determined by simulating the hydrostatic test.

3.3 Evolution of porosity

The porosity evolution law is related to the macroscopic plastic volumetric strain and the plastic strain of the solid matrix. It can be derived from the microscopic relation as following:

$$d\phi = (1 - \phi) d\bar{E}_{kk}^p - \frac{1}{|\Omega|} \int_{\Omega_m} tr(d\bar{\varepsilon}^p) dV \quad (\text{III .12})$$

where \bar{E}^p denotes the macroscopic plastic strain tensor, Ω_m represents the matrix domain, and $|\Omega|$ represents the total cell volume. Using (III .12) in the second term of this expression, we have

$$\frac{1}{|\Omega|} \int_{\Omega_m} tr(d\bar{\varepsilon}^p) dV = \frac{1}{|\Omega|} \int_{\Omega_m} 3d\varepsilon_m dV = 3(1 - \phi)d\varepsilon_m \quad (\text{III .13})$$

Therefore, the porosity evolution becomes as follow:

$$d\phi = (1 - \phi) (d\bar{E}_{kk}^p - 3d\varepsilon_m) \quad (\text{III .14})$$

In Mises-Schleicher yield criterion, σ_{eq} and σ_m denote the equivalent von-Mises stress and the mean stress respectively. The strain rate is derived from associated flow rule.

$$d\bar{\varepsilon}^p = d\lambda \frac{\partial \varphi(\bar{\sigma})}{\partial \bar{\sigma}} = d\lambda (3\bar{\sigma}_d + \alpha \bar{\sigma} \bar{\delta}) \quad (\text{III .15})$$

As mentioned above, where $\bar{\sigma}_d$ is the deviatoric part of the local stress, $\bar{\delta}$ is the second order identity tensor. And α and $\bar{\sigma}$ are the parameters of solid matrix. $d\lambda$ is the plastic multiplier of solid matrix. The computation of the von-Mises equivalent strain rate, $d\varepsilon_{eq}^p$, and the mean part of the local strain rate, $d\varepsilon_m$, leads to:

$$d\varepsilon_{eq}^p = 2d\lambda \sigma_{eq}, d\varepsilon_m^p = d\lambda \alpha \bar{\sigma} \quad (\text{III .16})$$

The plastic multiplier $d\lambda$ being positive, the means strain rate is then positive, $d\varepsilon_m^p \geq 0$. Eliminating $d\lambda$ between the two equations above, one has:

$$d\varepsilon_m^p = \frac{\alpha \bar{\sigma}}{2\sigma_{eq}} d\varepsilon_{eq}^p \quad (\text{III .17})$$

The local dissipation potential in the solid matrix is given by

$$\pi(d\bar{\varepsilon}^p) = \bar{\sigma} : d\bar{\varepsilon}^p = \sigma_{eq} d\varepsilon_{eq}^p + 3\sigma_m d\varepsilon_m^p = (2\bar{\sigma}^2 - 3\alpha\bar{\sigma}\sigma_m) d\lambda \quad (\text{III .18})$$

Replacing now the plastic multiplier $d\lambda$ by $\frac{d\varepsilon_{eq}^p}{2\sigma_{eq}}$ and introducing the expression of the equivalent stress σ_{eq} obtained with Mises-Schleicher yield criterion, the local dissipation is then obtained, and the resulting expression reads:

$$\pi(d\bar{\varepsilon}^p) = \frac{(2\bar{\sigma}^2 - 3\alpha\bar{\sigma}\sigma_m)}{2\sqrt{\bar{\sigma}^2 - 3\alpha\bar{\sigma}\sigma_m}} d\varepsilon_{eq}^p \quad (\text{III .19})$$

According to the energy compatibility condition between the microscopic and macroscopic scales, the local plastic strain of the solid matrix can be related to the macroscopic plastic strain work by:

$$(1 - \phi) \bar{\sigma} d\bar{\varepsilon}^p = \bar{\Sigma} d\bar{\mathbb{E}}^p \quad (\text{III .20})$$

$\bar{\mathbb{E}}^p$ denotes the macroscopic plastic strain tensor. Therefore, the equivalent strain rate $d\varepsilon_{eq}^p$ of matrix reads,

$$d\varepsilon_{eq}^p = \frac{2\sqrt{\bar{\sigma}^2 - 3\alpha\bar{\sigma}\sigma_m}}{(1 - \phi)(2\bar{\sigma}^2 - 3\alpha\bar{\sigma}\sigma_m)} \bar{\Sigma} d\bar{\mathbb{E}}^p \quad (\text{III .21})$$

Accordingly, the local mean strain rate $d\varepsilon_m^p$ of matrix is then obtained by introducing the equivalent strain rate $d\varepsilon_{eq}^p$ and the equivalent stress σ_{eq} obtained with Mises-Schleicher yield criterion:

$$d\varepsilon_m^p = \frac{\alpha\bar{\sigma}}{2\sigma_{eq}} d\varepsilon_{eq}^p = \frac{\alpha\bar{\sigma}}{(1 - \phi)(2\bar{\sigma}^2 - 3\alpha\bar{\sigma}\sigma_m)} \bar{\Sigma} d\bar{\mathbb{E}}^p \quad (\text{III .22})$$

Finally, the porosity evolution is obtained by introducing the local mean strain rate $d\varepsilon_m^p$ and the expression of the local mean stress $\sigma_m = \Sigma_m / (1 - \phi)$:

$$d\phi = (1 - \phi) \left(d\bar{\mathbb{E}}_{kk}^p - \frac{3\alpha\bar{\sigma}}{2(1 - \phi)\bar{\sigma}^2 - 3\alpha\bar{\sigma}\Sigma_m} \bar{\Sigma} d\bar{\mathbb{E}}^p \right) \quad (\text{III .23})$$

3.4 Plastic multiplier

The macroscopic plastic yield function is given in (III .9), and the associated plastic flow rule is then written as follows

$$\bar{\mathbb{E}}^p_{ij} = d\Lambda \frac{\partial \Phi}{\partial \bar{\Sigma}_{ij}} \quad (\text{III .24})$$

The plastic multiplier $d\Lambda$ can be determined by the plastic consistency condition:

$$d\Lambda = \frac{\frac{\partial \Phi}{\partial \bar{\Sigma}} : \mathbb{C}^0 : d\bar{\mathbb{E}}}{\frac{\partial \Phi}{\partial \bar{\Sigma}} : \mathbb{C}^0 : \frac{\partial \Phi}{\partial \bar{\Sigma}} - H} \quad (\text{III .25})$$

$$H = \frac{\partial \Phi}{\partial \bar{\sigma}} \frac{\partial \bar{\sigma}}{\partial \varepsilon_M} \frac{1}{(1-\phi)\bar{\sigma}} \bar{\Sigma} \frac{\partial \Phi}{\partial \bar{\Sigma}} + \left(\frac{\partial \Phi}{\partial \phi} + \frac{\partial \Phi}{\partial \bar{\sigma}} \frac{\partial \bar{\sigma}}{\partial \phi} \right) \left((1-\phi) \text{tr} \left(\frac{\partial \Phi}{\partial \bar{\Sigma}} \right) - \frac{3\alpha\bar{\sigma}}{(2\bar{\sigma}^2 - 3\alpha\bar{\sigma}\bar{\Sigma}_m/(1-\phi))} \bar{\Sigma} \frac{\partial \Phi}{\partial \bar{\Sigma}} \right) \quad (\text{III .26})$$

The fourth order tensor \mathbb{C}^0 denotes the elastic stiffness tensor of the intact chalk

4 Sensibility analysis of the model

In the order to evaluate the capacity of proposed micromechanics-based model on description of the macromechanical behaviour of porous materials, a sensitivity analysis is proposed here to capture influences of some main parameters involved in the model. Three different features are analyzed in the section. The first analysis is conducted on the effect of parameters which define the initial yield strength of porous materials. The second analysis is devoted to investigate the influence of the confining pressure on the mechanical behavior. Finally, it is proposed to compare the simulation results obtained by the associated model with those by a non-associated model.

4.1 Influences of parameters on the initial yield strength

Four parameters, α , $\bar{\sigma}_0$, s and porosity ϕ , are first investigated for the influences on the plastic yield condition of porous materials. The reference values for these parameters used here are shown in Table III .1. In Figures III .1-III .4, the plastic yield surfaces

Table III .1: Model parameters used for sensitivity analysis

ϕ	$\bar{\sigma}_0(\text{bar})$	α	s
0.3	1.0E6	3.0	1.0

are compared by using different values for each of these four parameters. From these figures, one can see that the macroscopic yield surface of porous materials is asymmetric elliptic-like form and strongly influenced by the porosity of the porous materials. In Figure III .1, it is clearly shown that with the increase of the porosity, the hydrostatic compression yield strength is substantially reduced. This means that important plastic

strain can be produced under hydrostatic compression. With the increase of the porosity, this is experimentally observed in high porosity rocks. However, the effect of increasing porosity on the macroscopic hydrostatic tensile strength is much less important than the compression one. As an asymptotic situation, when the porosity tends to 0 ($\phi \rightarrow 0$), the yield surface becomes close to the Mises-Schleicher quadratic surface. Compared with the porosity, the influences of the pressure-sensitive coefficient α and the initial yield strength of solid matrix $\bar{\sigma}_0$ on the macroscopic yield surface seem to be less drastic. In Figures III .2, the effects of increasing the initial yield strength of solid matrix $\bar{\sigma}_0$ seem to increase the yield strength, but not to change the shape of the macroscopic yield surface. In Figures III .3, the effects of increasing the pressure-sensitive coefficient α increases also the yield strengths, but it strengthens the degree of asymmetry of the macroscopic yield surface. In particular, the parameter s does not affect the hydrostatic compression yield strength and the hydrostatic tensile yield strength, but affects the shear yield strength (Figure III .4).

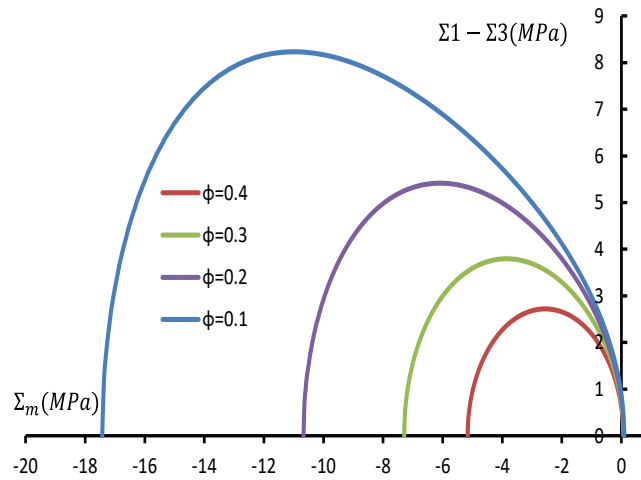


Figure III .1: Effect of porosity ϕ on the initial macroscopic yield strength

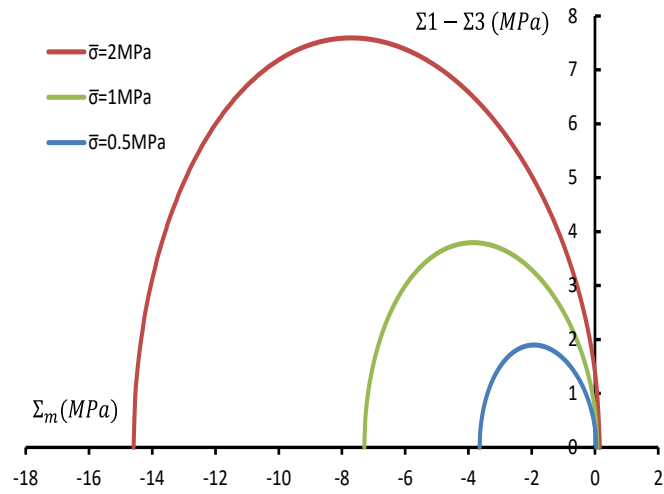


Figure III .2: Effect of initial yield strength of solid matrix $\bar{\sigma}_0$ on the initial macroscopic yield strength

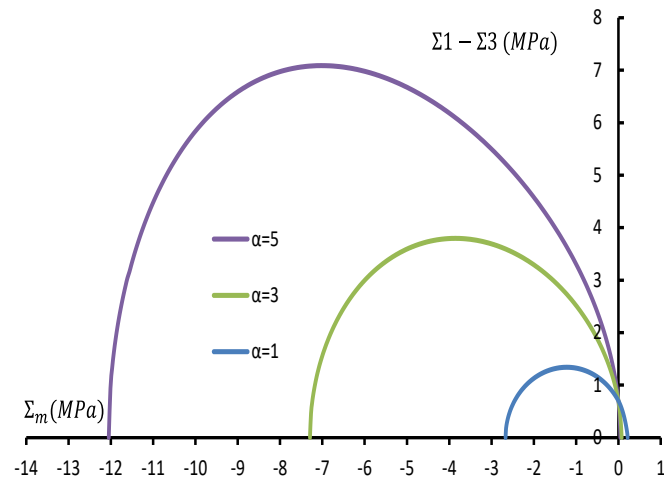


Figure III .3: Effect of pressure-sensitive coefficient α on the initial macroscopic yield strength

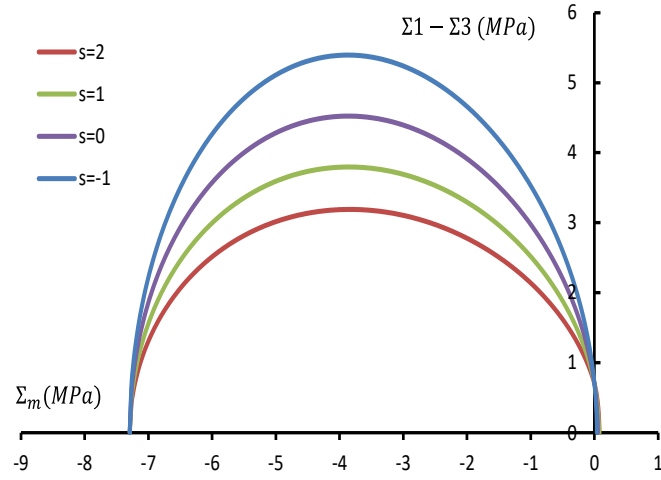


Figure III .4: Effect of parameter s on the initial macroscopic yield strength

4.2 Effect of confining pressure

In order to understand the effect of confining pressure on macromechanical behaviors of porous rocks, in particular, to reveal the effect of confining pressure on the evolution of porosity ϕ and volumetric strain E_v , the simulations of triaxial compression tests with two different confining pressures, say 0.5 and 6.0 MPa, The representative values of parameters used for these simulations are given in Table III .2.

Table III .2: Parameters used for the associated model

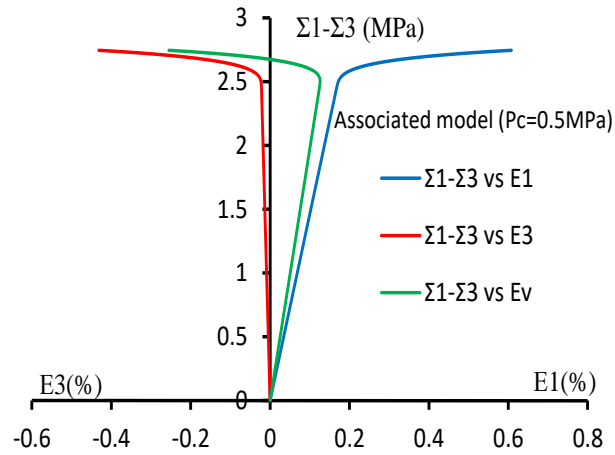
Parameters	
Porosity (ϕ)	0.43
Young's modulus of solid matrix (E_m , MPa)	3800
Initial Poisson's ratio of solid matrix (ν_m)	0.22
Initial yield stress of matrix ($\bar{\sigma}_0$, MPa)	0.936
Yield function parameter of matrix (α)	4.2
Form parameter of yield criterion (s)	1.45
Hardening parameter of yield stress of matrix (a)	0.55
Hardening parameter of yield stress of matrix (b)	1.23
Hardening parameter of yield stress of matrix (n)	0.3

Based on the simulation results, the evolutions of porosity ϕ and volumetric strain E_v versus axial strain E_1 are presented in Figure III .5 .

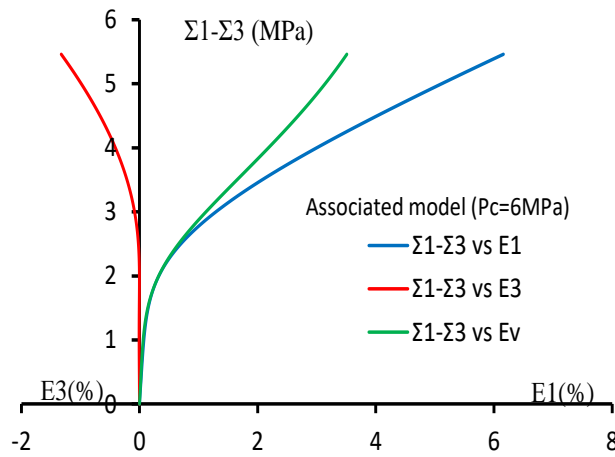
It can be noted that, for lower confining pressure, the volumetric dilatancy is important and the porosity ϕ increases; for higher confining pressure, the volumetric compaction is important and the porosity ϕ decreases. Generally, this is in agreement with most experimental data of porous rocks.

4.3 Comparison between associated and non-associated models

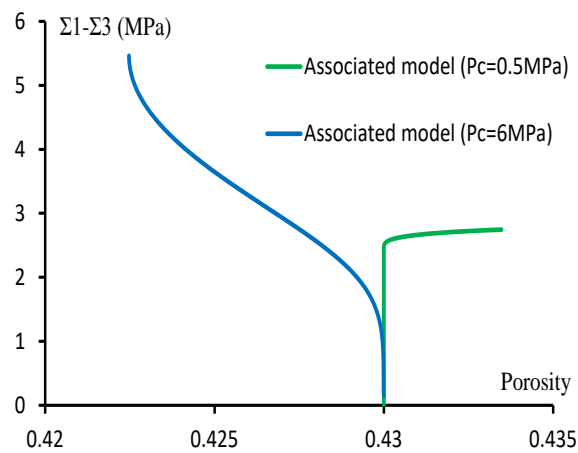
The micromechanics-based plastic model proposed earlier is based on the assumption that the plastic deformation of porous rock can be described by an associated flow rule. With the help of such an assumption, an analytical form of the macroscopic plastic criterion of porous rock was developed. However, in some cases, an associated model is not able to describe all features of mechanical behaviors of high-porosity rocks, for instance, the transition from volumetric compaction to dilatancy. The high-porosity rocks exhibits a volumetric compaction during deviatoric stress loading, even for the test under very low confining pressure [Xie and Shao, 2012]. As showing in Figure III .5, the associated model can't correctly describe the volumetric compaction of porous rock under low confining



(a) Stress-strain curves for a low confining pressure of 0.5MPa



(b) Stress-strain curves for high confining pressure of 6MPa



(c) Evolutions of porosity

Figure III .5: Effect of confining pressure simulated with the associated model

pressure; therefore, a non-associated flow rule should be considered to improve the model for a correct description of the volumetric deformation. In other words, it is needed to develop non-associated models.

For this purpose, in the context of rigorous micromechanical modelling, a non-associated plastic potential should be formulated through an appropriate homogenization procedure as that used for the determination of plastic criterion. However, some complex mathematical developments should be achieved to complete such a micro-macro modelling. For the sake of simplicity and as an approximation, a heuristic approach is adopted in the present work. Inspired by the previous works by [Maghous et al., 2009],[Shen et al., 2012],[Shen et al., 2013], [Ghorbanbeigi et al., 2016], a non-associated macroscopic plastic potential is directly proposed at the macroscopic scale by keeping a similar form as the macroscopic plastic criterion:

$$\Psi = \frac{\Sigma_{eq}^2}{\Theta_\psi \bar{\sigma}_\psi^2} + 2\Gamma_\psi \cosh \left(A_\psi \ln \left(1 - 3\alpha_\psi \frac{\Sigma_m}{\bar{\sigma}_\psi} \right) \right) \quad (\text{III .27})$$

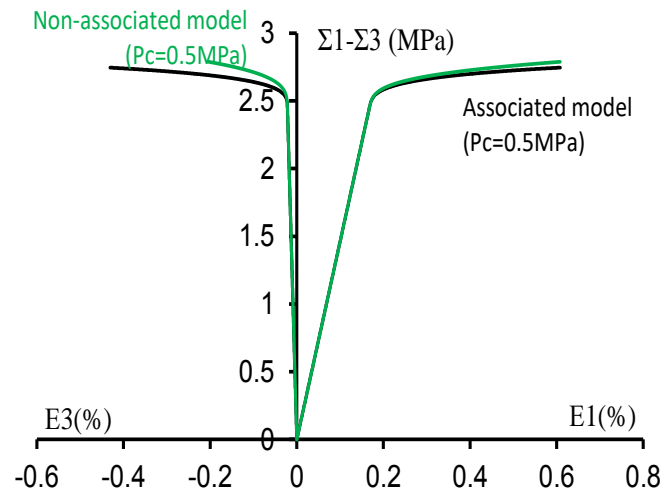
$$\text{with} \left\{ \begin{array}{l} \Theta_\psi = \left(\frac{1-\phi}{1-\Gamma_\psi} \right)^2 - 3\alpha_\psi \frac{(1-\phi)^s \Sigma_m}{(1-\Gamma_\psi)^2 \bar{\sigma}_\psi} \\ \Gamma_\psi = \left(\alpha_\psi^2 (W(\phi p) + 1)^2 - \alpha_\psi^2 \right)^{A_\psi} \\ A_\psi = \text{sign}(\Sigma_m) \left(\frac{4}{9\alpha_\psi} + \frac{\alpha_\psi (W(\phi p) + 1)^2 - \alpha_\psi}{18} \right) \end{array} \right. \quad (\text{III .28})$$

where $\bar{\sigma}_\psi$ and α_ψ are two parameters for defining the macroscopic plastic potential with parameter s and porosity ϕ . It is worth noticing that the values of $\bar{\sigma}_\psi$ and α_ψ control the final plastic volumetric strain. In order to show the sensitivity of porous material responses to the values of $\bar{\sigma}_\psi$ and α_ψ , we have studied the mechanical behaviors with two different values of $\bar{\sigma}_\psi$ and α_ψ in the triaxial compression tests with relative low and high confining pressures, say 0.5MPa and 6.0MPa, respectively. One group of $\bar{\sigma}_\psi$ and α_ψ are taken the same values with $\bar{\sigma}$ and α , the other group of $\bar{\sigma}_\psi$ and α_ψ are taken different values with $\bar{\sigma}$ and α . The two different values of $\bar{\sigma}_\psi$ and α_ψ are listed in Table III .3. In Figure III .5, the simulation results with associated model are presented, an important volumetric dilatancy is obtained for a low confining pressure of 0.5 MPa, in contrast, a plastic volumetric compaction for a high confining pressure of 6MPa. The numerical results obtained with the non-associated model are compared with those by the associated model in Figure III .6. In Figure III .7, the evolutions of porosity ϕ and volumetric strain E_v versus axial strain E_1 are presented for the two models. From these results, one can see that the mechanical response of porous rocks is strongly affected by the volumetric deformation or porosity change. More precisely, using a high value of α_ψ , one obtains an

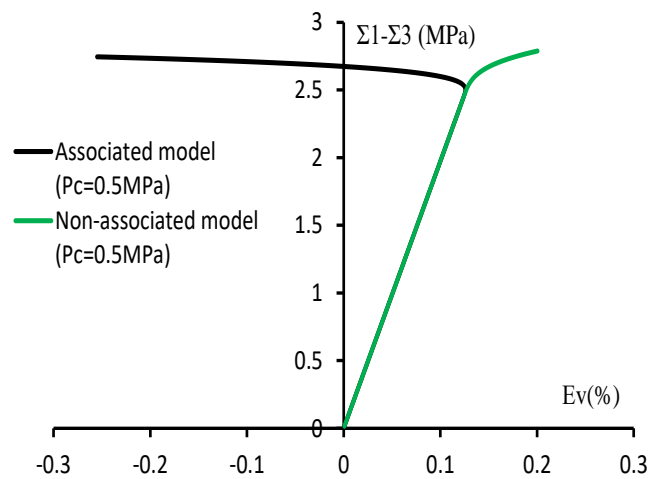
important volumetric dilatancy leading to an increase of porosity. As a consequence, there is a reduction of mechanical strength producing a material softening behavior because of the porosity increase. Therefore, the non-associated model provides a larger ability to describe complex volumetric strain evolutions than the associated one. Accordingly, the non-associated model has much more possibility to describe poromechanical behaviors of porous rocks than the associated one.

Table III .3: Different values of parameters defining the macroscopic plastic potential used in non-associated model for comparisons

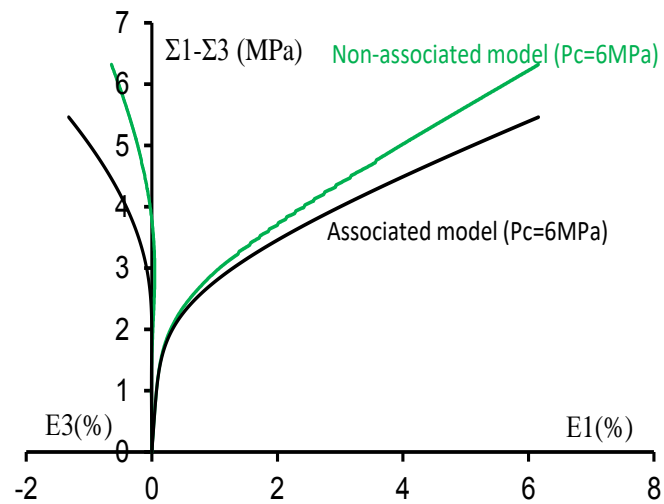
Group	$\sigma_{0\psi}$ (MPa)	α_ψ	NOTE
Groupe 1	0.936	4.2	Associated model
Groupe 2	6.5	0.38	Non-associated model



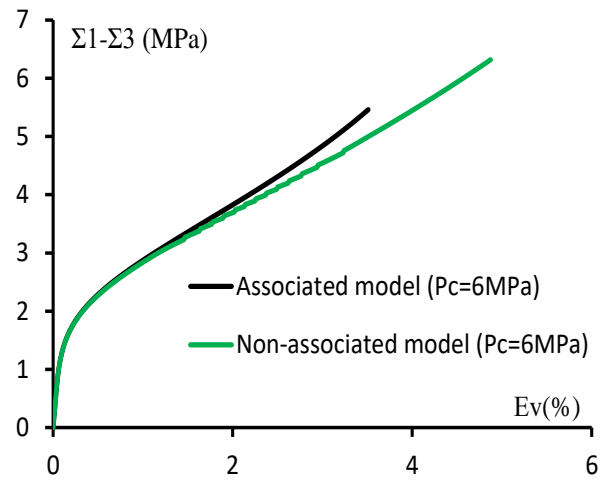
(a) Stress-strain curves for a low confining pressure of 0.5MPa



(b) Evolution of volumetric strain for a low confining pressure of 0.5MPa

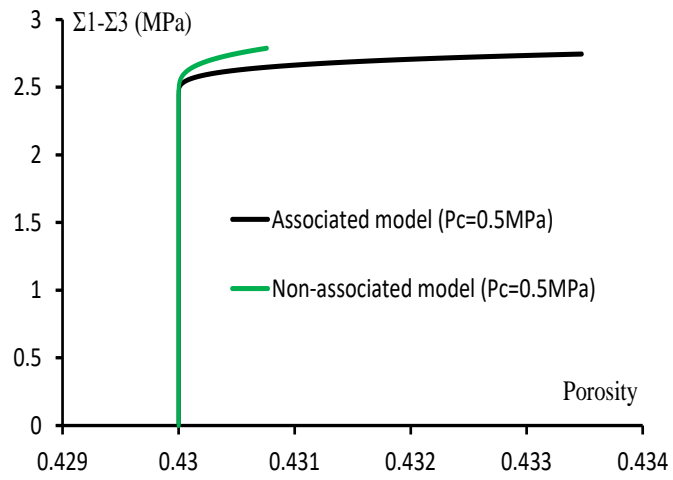


(c) Stress-strain curves for a high confining pressure of 6MPa

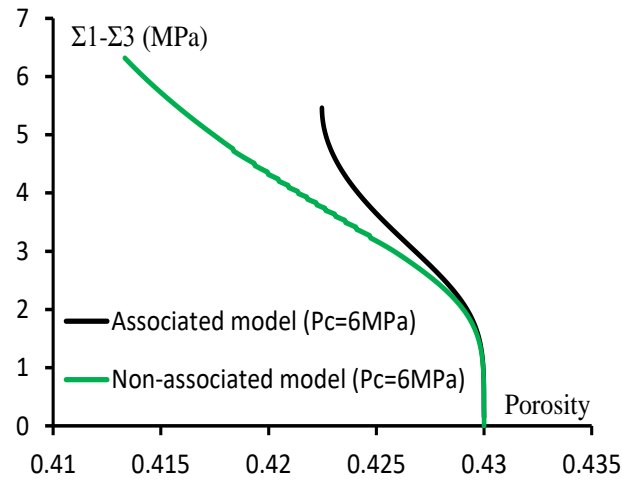


(d) Evolution of volumetric strain for a high confining pressure of 6MPa

Figure III .6: Stress-strain curves: comparison between associated non-associated models



(a) Deviatoric stress-porosity curves for a low confining pressure of 0.5MPa



(b) Deviatoric stress-porosity curves for a high confining pressure of 6MPa

Figure III .7: Simulated porosity evolutions: comparison between associated non-associated models

5 Conclusion

Based on the experimental data and the relevant micromechanical considerations, a micromechanics-based elastoplastic model has been proposed, taking into account the two plastic mechanisms in relation with the microstructure of porous rocks. The porous rock is represented by a two-phase porous composite, a equivalent matrix and a connected porosity. Two plastic parameters of the equivalent solid matrix, the plastic yield stress $\bar{\sigma}$ and the pressure-sensitive coefficient α , and the porosity ϕ are used as the fundamental parameters in the macroscopic plastic yield function. An associated model has been firstly developed for high porous rock, a non-associated flow rule is then proposed for building a non-associated model for porous rock.

Chapter IV

Applications for Porous Rocks: a Chalk and a limestone

Contents

1	Introduction	49
2	Simulations of drained mechanical behavior of Lixhe chalk	51
2.1	Basic mechanical behaviors of porous chinks	51
2.2	Simulation of drained laboratory tests	63
3	Simulations of undrained mechanical behavior of Lixhe chalk	66
3.1	General framework of the poroplastic modelling	66
3.2	Extension to poroplastic modelling	68
3.3	Simulation results of undrained laboratory tests	70
4	Simulations of mechanical behaviors Anstrude limestone	75
4.1	Hardening function for porous limestone	75
4.2	Simulation of drained laboratory tests	77
4.3	Simulations of undrained triaxial tests of porous limestone	81
5	Conclusion	86

1 Introduction

In this chapter, the micromechanics-based plastic model proposed in previous chapter will be applied to describe the elastoplastic behaviors of two porous rocks: a high-porosity chalk and a medium porosity limestone. A typical high-porosity chalk, Lixhe chalk. Based

on the experimental results of oil and water saturated chalk [Xie and Shao, 2012], influences of water saturation on the mechanical behavior are investigated. The porous rocks are represented by an equivalent solid matrix with different contacts and a connected porosity. Water saturation induces the diminution of capillary pressure in liquid contact and enhances the inter-granular pressure solution process in cemented contacts, leading to a weakening effect on mechanical behavior of porous chalk. The mechanical and poromechanical behaviors of oil and water saturated chalk are studied by adopting the proposed model. This work consists of two parts. In the first part, we propose an extension of this work in order to characterize water saturation effects on the mechanical behavior of chalk and to describe the basic mechanical behavior of saturated chalk under drained condition. In the second part, the proposed model will be extended to describe poromechanical behavior of porous chalk. Based on the experimental data and some relevant micromechanical considerations, the model is also extended to describe the poroplastic coupling effect by using the effective stress concept. Accordingly, the poroplastic behaviors of porous chalk are studied. And then, the proposed model is extended to describe the mechanical behavior of a medium-porosity limestone, Anstrude limestone. When the proposed model applied directly to the limestone, there is an important overestimation of strength of limestone under low confining pressure. Under low confining pressure, in contrast to the high-porosity chalk, the medium-porosity limestone exhibits a volumetric dilatancy and the porosity increases during the deviatoric stress loading. The increase of porosity will affect the plastic yield stress of solid matrix; therefore, the effect of plastic strains of solid matrix and the effect of porosity evolution should be taken into account in the hardening effect of solid matrix in the model for limestone. Accordingly, the proposed model is extended to describe the mechanical behavior of porous limestone under drained and undrained conditions. From a high-porosity chalk to a medium porosity limestone, the proposed model is verified in different loading conditions through comparisons between the numerical predictions and experimental data for both drained and undrained tests.

2 Simulations of drained mechanical behavior of oil and water saturated Lixhe chalk

2.1 Basic mechanical and poromechanical behaviors of porous chalks

Description of porous chalk

In this work, Lixhe chalk is chosen as a representative of highly porous rocks. This chalk is from Upper Campanian age and drilled in the CBR quarry near Liège (Belgium). It is a very pure chalk, composed of more than 98% of $CaCO_3$, and with less than 0.8% of SiO_2 and 0.15% of Al_2O_3 . The porosity of this chalk ranges from 42% to 44% with an average value of about 43%. The intrinsic permeability varies from $1 \times 10^{-16} m^2$ to $1 \times 10^{-15} m^2$. According to microscopic observations, this chalk can be considered as a homogeneous and isotropic material ([Homand and Shao, 2000]). This chalk has been studied in a series of previous experimental investigations because its mechanical behavior is qualitatively close to that of North Sea reservoir chalks ([Collin et al., 2002];[Schroeder, 2003]). In this section, the aim is to provide a brief account on the mechanical and poromechanical behaviors of Lixhe chalk.

Drained hydrostatic and triaxial compression tests

Hydrostatic and triaxial compression tests are performed basically to characterize the mechanical behavior of rock materials. A great number of drained hydrostatic tests were conducted on Lixhe chalk to investigate the plastic deformation of chalk due to pore collapse mechanism ([Shao and Henry, 1991];[Collin et al., 2002];[Xie and Shao, 2006];[Xie and Shao, 2012]). The basic response of the porous chalk under hydrostatic compression can be decomposed into three phases. There is a quasi-linear phase representing the elastic compressibility of the chalk skeleton at the beginning of loading. When the hydrostatic stress reaches some limit value, plastic pore collapse occurs and leads to an important plastic volumetric contractancy. The plastic pore collapse induces an increase of contact surfaces between solid grains and results in an increasing plastic hardening phase with a decreasing volumetric strain rate. Moreover, hydrostatic compression tests performed by [Collin et al., 2002] and [Schroeder, 2003] on Lixhe chalk saturated with different fluids show that the mechanical behavior of chalk under hydrostatic compression is highly sensitive to the nature of saturating fluid, and that the water content is the key factor for the mechanical behavior of this material. Moreover, all the results obtained can be classified in two families of behaviors: oil saturated chalk and water saturated chalk.

Therefore, oil and water saturated samples are generally taken as the two extremes for the mechanical response under hydrostatic compression stress. A typical hydrostatic stress versus volumetric strain curve for oil saturated Lixhe chalk is shown in Figure IV .1 ([Xie and Shao, 2012]).

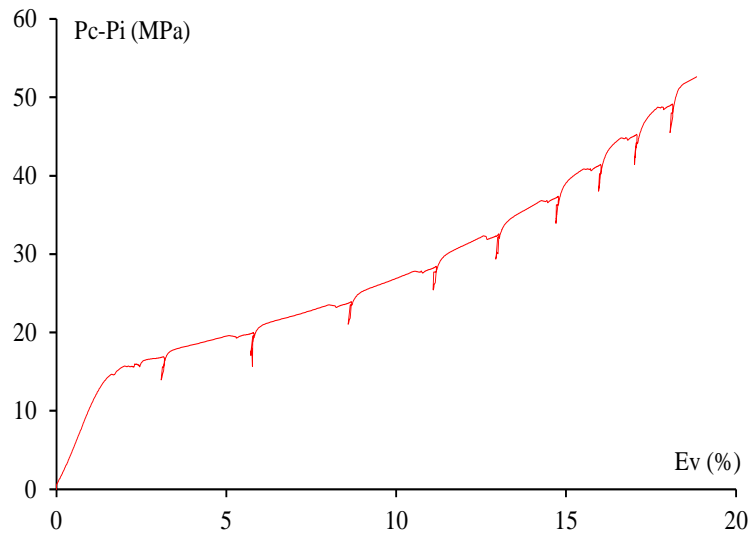


Figure IV .1: Hydrostatic stress versus volumetric strain curve for oil saturated Lixhe chalk[Xie and Shao, 2015]

In order to study mechanical behavior of chalk subject to deviatoric stress, drained triaxial compression tests are generally conducted with different confining pressures ([Shao and Henry, 1991];[Collin et al., 2002] ; [Xie and Shao, 2006];[Xie and Shao, 2012]). According to experimental results, the basic response of the porous chalk under deviatoric stress can be classified into two groups. Under low confining pressures, the basic behavior of chalk is elastic brittle or elastoplastic brittle. The brittle failure occurs with a material softening, and a peak deviatoric stress can be observed. Sample failure is classically produced by the formation of localized shear bands. There is a drastic transition from brittle to ductile behavior when the confining pressure increases. Under high confining pressures, no peak stress can be defined until very large value of axial strain. The slope of stress strain curve is continuously increasing with a concave form similar to that in hydrostatic compression test. This means that the applied deviatoric stress under high confining pressures enhances pore collapse process, leading to a plastic hardening due to the increase of contact surfaces. Accordingly, an important volumetric contraction is obtained due to the pore collapse. Material failure is manifested by complete destruction of

pore structure, transforming the cohesive chalk into a compacted powder after significant volumetric deformation. Drained triaxial compression tests performed by Homand (2000) and Xie (2005) on samples of Lixhe chalk saturated with different fluids show that the mechanical behavior of chalk under drained triaxial compression is highly sensitive to the nature of saturating fluid. Typical stress-strain curves for the water saturated Lixhe chalk are presented in Figure IV .2 [Xie and Shao, 2012]. In these tests, the confining pressures are applied with 0.5, 1, 3, 5, 6 and 7 MPa for revealing precisely the influence of confining pressure on mechanical behavior. For these triaxial tests, the experimental results show that the mechanical behavior of Lixhe chalk is strongly dependent on confining pressure due to its high porosity. Under low confining pressures (0.5 and 1 MPa), the chalk exhibited an elastic brittle behavior that is characterized by a peak deviatoric stress and a strain-softening phase. In particular, it needs to note that the chalk exhibited a volumetric compaction during deviatoric stress loading, even in the phase of post-peak for the test under very low confining pressure of 0.5 MPa. When the confining pressure became high, for instance higher than 3 MPa, we found an elastic-plastic response with a more and more important strain hardening phase. In particular, when the confining pressure was close to or higher than 5 MPa, important plastic strains were observed as soon as the deviatoric stress was applied. In this case, both pore collapse and deviatoric shearing phenomena occurred simultaneously and in a coupled way. There was no peak deviatoric stress, and the material failure was characterized by a diffuse compaction mode related to the destruction of cemented contacts between mineral grains.

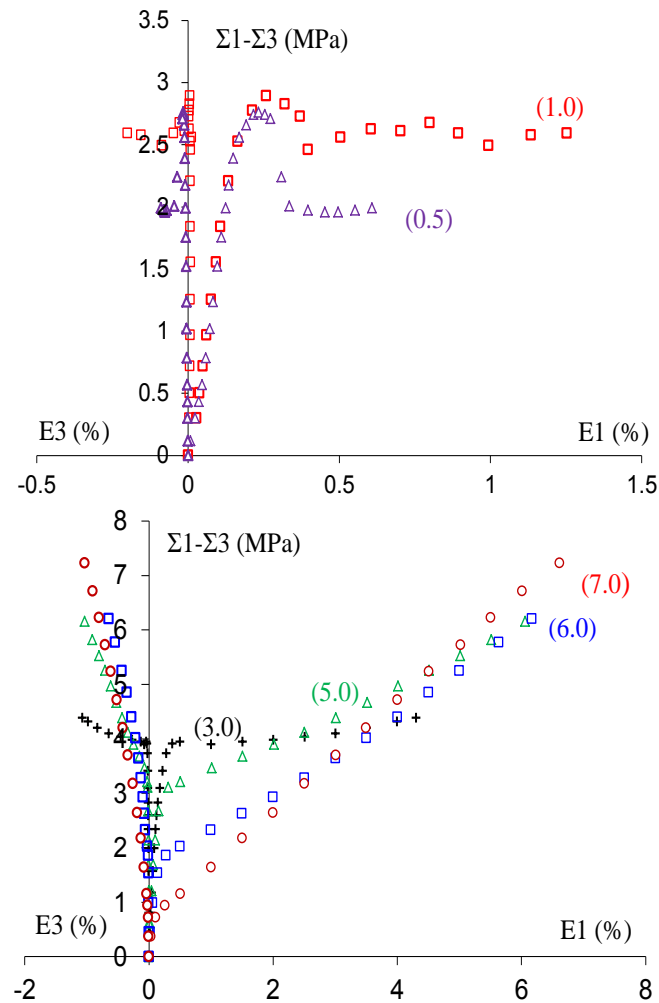


Figure IV .2: Stress-strain curves of drained triaxial tests for the water saturated Lixhe chalk (Values of confining pressure are marked in the brackets), ([Xie and Shao, 2015])

Undrained Triaxial Compression Tests

Based on the previous studies on porous rocks ([Yamada et al., 1981];[Kerbouche et al., 1995]), a hydrostatic poromechanical test composed of a series of poromechanical cycles was performed on oil saturated Lixhe chalk ([Xie and Shao, 2012]). Comparing the evolutions of plastic volumetric strain and plastic porosity versus hydrostatic stress, the plastic volumetric strain is nearly identical to the plastic porosity change.

For triaxial poromechanical tests, the previous experimental results show that the basic mechanical response of porous chalk under undrained condition is influenced by the initial effective confining pressure ([Xie and Shao, 2012]).

Under undrained condition, the evolution of interstitial pressure is clearly affected

by the initial confining pressure. Under low confining pressure, the interstitial pressure increases continuously during deviatoric stress loading. Only for a very low confining pressure, the interstitial pressure may decrease slightly after the post peak related to weak volumetric dilatancy induced by plastic shearing. Under high confining pressure, the interstitial pressure increases in a first elastic stage and then increases more importantly related to high volumetric contractancy induced by pore collapse. In particular, the variation of interstitial pressure is more important when the initial effective confining pressure is higher.

The effective stress path is clearly affected by the initial confining pressure. Under a low confining pressure, the effective mean stress is continuously increasing and the failure line is reached by the peak stress followed by a material softening behavior. In this case, the overall behavior of chalk is rather brittle in nature. Under a high confining pressure, in contrast to drained triaxial tests, a peak deviatoric stress can be obtained during deviatoric stress loading under undrained condition. This is the consequence of the increase of interstitial pressure leading to a decrease of the effective confining pressure. Accordingly, the effective mean stress increases in a first stage and then decreases in a second stage due to significant increase of interstitial pressure. The failure line is progressively approached with this decrease of effective mean stress. The peak deviatoric stress can be below the failure line and thus does not represent the material failure state. In this case, the post peak response is not related to material softening but induced by the decrease of effective confining pressure. Furthermore, the axial strain and the interstitial pressure at peak stress increase with the initial effective confining pressure and this shows the transition from brittle to ductile behavior.

In order to characterize the poromechanical behavior of chalk subjected to varying interstitial pressure, [Xie and Shao, 2012] have performed a set of undrained triaxial compression tests on both oil and water saturated samples of Lixhe chalk. The initial effective confining pressures are 2.0, 3.5 and 5.0 MPa for water saturated samples, and 4, 8 and 12 MPa for oil saturated samples respectively. Typical experimental results obtained are presented in Figure IV .3 and IV .4, showing axial and lateral strains as well as interstitial pressure versus deviatoric stress for different values of confining pressure.

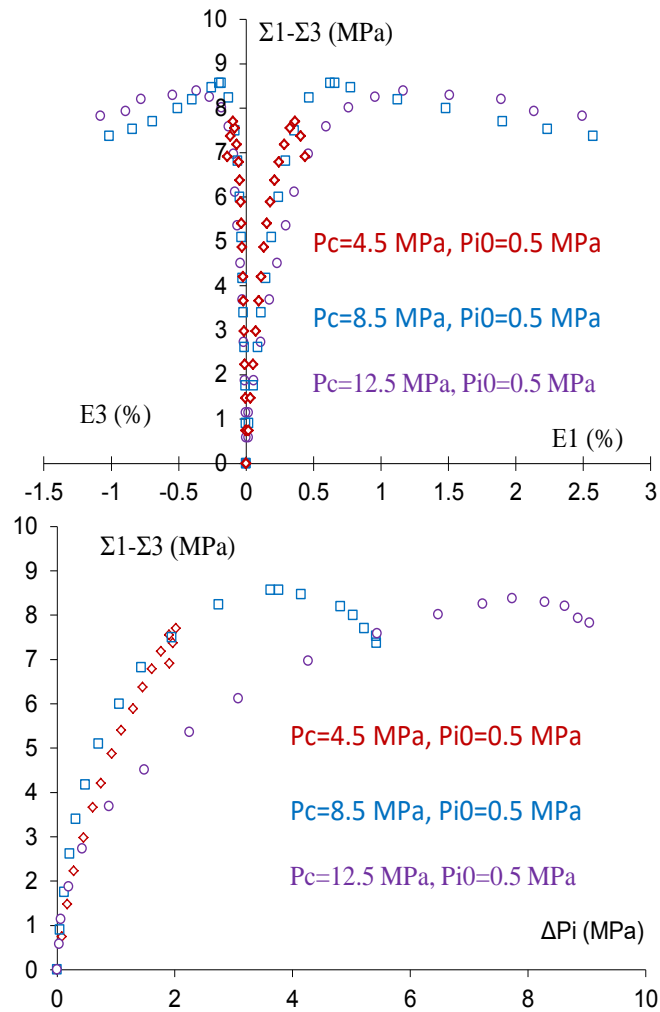


Figure IV .3: Deviatoric stress versus strains and interstitial pressure for undrained triaxial tests on oil saturated Lixhe chalk with different confining pressures and an initial interstitial pressure of 0.5 MPa (a, Deviatoric stress versus axial and lateral strains; b, Deviatoric stress versus interstitial pressure) (from [Xie and Shao, 2012])

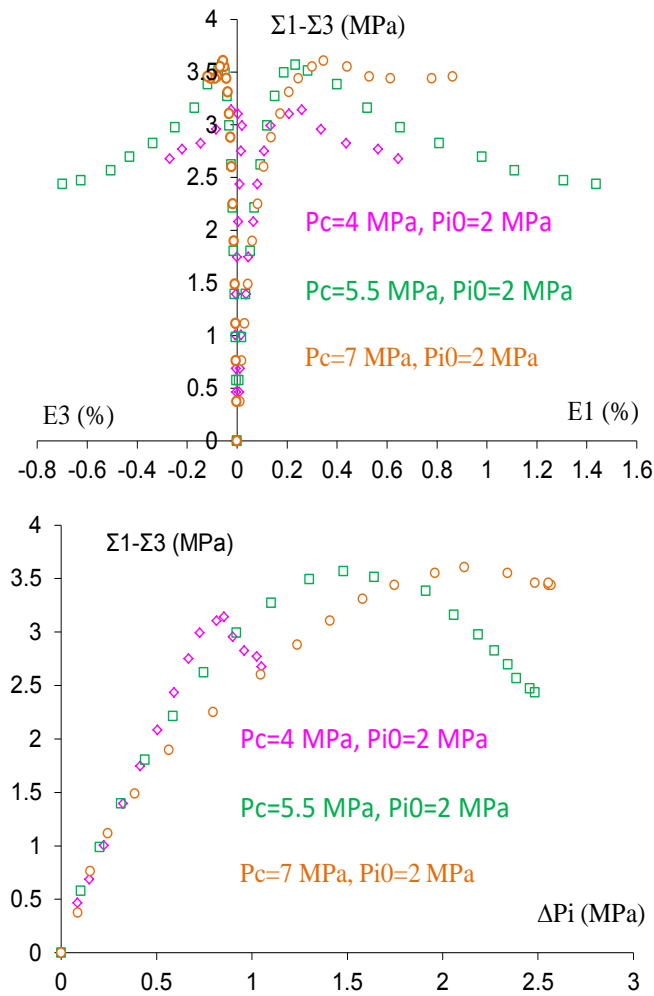


Figure IV .4: Deviatoric stress versus strains and interstitial pressure for undrained triaxial tests on water saturated Lixhe chalk with different confining pressures and an initial interstitial pressure of 2 MPa (a, Deviatoric stress versus strains; b, Deviatoric stress versus interstitial pressure) (from[Xie and Shao, 2012])

By comparing the results obtained respectively from the oil and water saturated samples, it is clear that the mechanical behavior of chalk under undrained triaxial compression is highly sensitive to the nature of saturating fluid. It is clear that there is a significant reduction of yield stress and failure strength due to water saturation. The general trends are similar for both saturating fluids. Such results are in agreement with those reported in the previous works.

Table IV .1: Typical values of parameters for oil and water saturated Lixhe chalk

Parameters	Oil saturated sample	Water saturated sample
Porosity (ϕ)	0.43	0.43
Young's modulus of solid matrix (E_m , MPa)	4900	3800
Initial Poisson's ratio of solid matrix (ν_m)	0.22	0.22
Initial yield stress of matrix ($\bar{\sigma}_0$, MPa)	2.55	0.936
Yield function parameter of matrix (α)	3.0	4.2
Form parameter of yield criterion (s)	0.6	1.45
Potential function parameter of matrix ($\sigma_{0\psi}$, MPa)	16.45	6.5
Potential function parameter of matrix (α_ψ)	0.18	0.38
Hardening parameter of yield stress of matrix (a)	0.55	0.55
Hardening parameter of yield stress of matrix (b)	1.23	1.23
Hardening parameter of yield stress of matrix (n)	0.3	0.3

Model parameter identifications

The proposed micromechanics-based model contains 11 parameters to describe basic elastic-plastic behavior of porous chalk. These parameters correspond to clearly identified deformation mechanisms and can be determined from conventional laboratory tests. The porosity ϕ is an important parameter in the model. The two elastic parameters of solid matrix, E_m and ν_m , are determined from the initial linear part of stress-strain curve during a conventional triaxial compression test. The two plastic parameters of the solid matrix, the initial yield stress $\bar{\sigma}_0$ and the pressure-sensitive coefficient α , can be determined from the results of tensile test and uniaxial compressive test accordingly. With the parameter s , determining the form of the macroscopic yield criterion, the two plastic parameters of solid matrix can also be obtained by fitting the initial macroscopic plastic yield surface to the initial yield stress data obtained from hydrostatic and triaxial compression tests, as shown in Figure IV .5. The three parameters used in the hardening law, say a , b and n can be fitted from hydrostatic compression test by drawing plastic volumetric strain versus hydrostatic stress. Finally, the parameters, α_ψ and $\bar{\sigma}_\psi$, are easily obtained from comparing the volumetric strain curves to the experimental data.

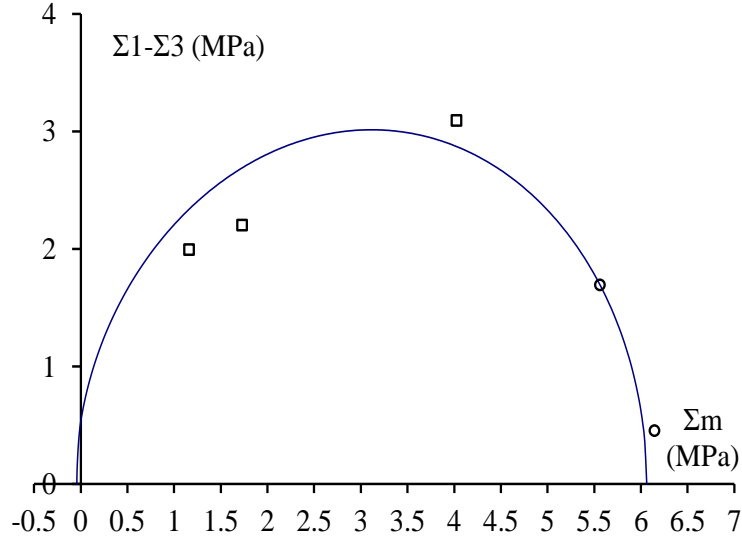


Figure IV .5: Yield surface of drained triaxial tests performed on water saturated Lixhe chalk

Influence of water saturation

It is clear that the macroscopic mechanical behavior of porous chalk depends on the mechanical properties of the equivalent solid matrix, which can be related to three principal kinds contact forces: cemented solid contact, frictional point contact and liquid contact due to capillary water. Among these contact forces, the liquid contact force related to the capillary effect plays an important role in porous chinks. Therefore, the initial yield stress $\bar{\sigma}_0$ and the pressure-sensitive coefficient s which can be influenced by water saturation degree.

Based on the experimental data reported by [Talesnick et al., 2001],[Collin et al., 2002],[Schroeder, 2003] and [Risnes et al., 2005], concerning the variations of the uniaxial compressive strength and tensile strength with the water saturation degree, the specific form of the function $\bar{\sigma}_0(S_W)$ proposed by [Xie and Shao, 2006] can be taken accordingly:

$$\bar{\sigma}_0(S_W) = \bar{\sigma}_0^{Water} + (\bar{\sigma}_0^{Oil} - \bar{\sigma}_0^{Water}) \exp\left(-B1 \frac{S_W}{1 - S_W}\right) \quad (IV .1)$$

The parameter α of the solid matrix can also be expressed by the ratio of uniaxial compressive yield limit to tensile yield limit, $\alpha = (C - T) / \sqrt{CT} = (C/T - 1) / \sqrt{C/T}$. Thus, the variation of parameter α with the water saturation degree $\alpha(S_W)$ can be determined from the ratio of uniaxial compressive yield limit to tensile yield limit under

different water saturation degree. However, this ratio is not available for different intermediary values of the water saturation degree. Based on the experimental data reported by [Talesnick et al., 2001], the ratio of compressive strength to tensile strength $R_{strength} = C_{Strength}/T_{Strength}$ varies with water saturation degree. Accordingly, the parameter ($\alpha_{Failure} = (R_{strength} - 1)/\sqrt{R_{strength}}$) varies with water saturation degree, and can be describe by taking the similar form as IV .1, the predicted parameter $\alpha_{Failure}$ and the experimental data obtained for a porous chalk [Talesnick et al., 2001] are presented in Figure IV .6

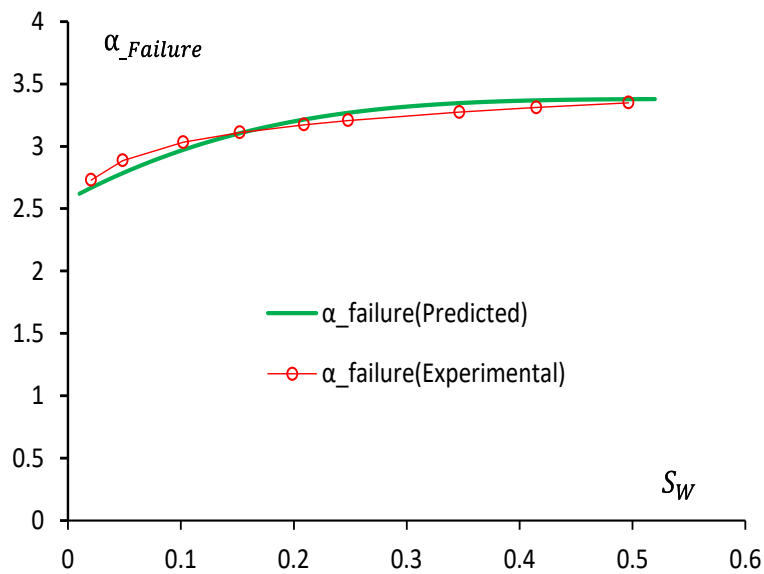


Figure IV .6: Predicted parameter $\alpha_{Failure}$ and experimental results of a porous chalk varied with water saturation (adapted from the ratio of compressive strength to tensile strength reported by [Talesnick et al., 2001])

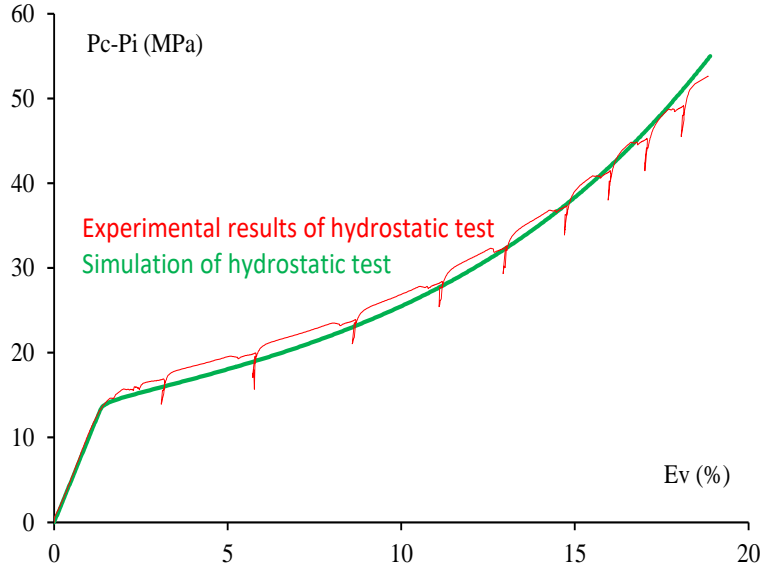


Figure IV .7: Simulation of drained hydrostatic compression test with oil saturated Lixhe chalk

Even though the ratio of strengths $R_{Failure}$ is not the ratio of yield limits $R_{yield} = C_{yield}/T_{yield}$, it is assumed that the tendencies of variations of two ratios with water saturation degree are similar. Accordingly, concerning the variation of ratio of the uniaxial compressive strength to the tensile strength with the water saturation degree, the form of the function $\alpha(S_W)$ can be taken as the similar as (IV .1):

$$\alpha(S_W) = \alpha^{Water} + (\alpha^{Oil} - \alpha^{Water}) \exp\left(-B2 \frac{S_W}{1 - S_W}\right) \quad (IV .2)$$

Figure III .1 also shows the comparison between the experimental data from the ratio of strengths and the theoretical approximation by the relation (IV .2). We can see that the parameter $\alpha(S_W)$ increases quickly with water saturation at low water saturation degree, and then tends towards a nearly constant value when the water saturation degree is greater than a certain limit value, $S_W = 0,3$ as here .

According to the yield surfaces shown in Figure IV .10, the parameter s is also affected by water saturation. Even though there are a lot of triaxial tests performed on chalk samples with different water saturation degree, the values of this parameter are not available for different intermediary values of the water saturation degree. Thus we cannot determine the continuous function for the variation of this parameter with water saturation. However, the physical mechanism of the water saturation effects is the same for the parameters of solid matrix and for the parameter s determining the form of the

macroscopic yield criterion. Thus, we assume that the variation of the parameter s can be described by the same function as that used for the variation of the parameters of solid matrix. Therefore, the following relation is proposed:

$$s(S_W) = s^{Water} + (s^{Oil} - s^{Water}) \exp\left(-B3 \frac{S_W}{1 - S_W}\right) \quad (\text{IV .3})$$

On the other hand, the stress strain curves, from hydrostatic compression tests respectively on oil and water saturated samples ([Homand and Shao, 2000],[Schroeder, 2003]), show that the general form of the plastic hardening process is not affected by water saturation degree. Therefore, it is assumed that the water saturation degree will not affect the three parameters used in the hardening law, say a , b and n . Thus, the hardening function for partially water saturated chalk can be expressed as follows:

$$\bar{\sigma}(S_W) = \bar{\sigma}_0(S_W) \left(1 + a(\varepsilon_M)^n e^{b\varepsilon_M}\right). \quad (\text{IV .4})$$

Finally, the experimental results show that the Young's modulus of porous chalk is also reduced by water saturation, and that the Poisson's ratio seems to be not affected by water saturation. Therefore, for the isotropic chalk, only the Young's modulus is assumed to be affected by the water saturation. This comes to say that the bulk modulus and the shear modulus are affected by the water saturation in the same way. In other words, the Young's modulus of porous chalk is affected by the water saturation through degradation of contact force of equivalent matrix of porous chalk. For convenience, it is proposed to use the same form of variation for the elastic modulus as for the plastic parameters:

$$E_0(S_W) = E_0^{Water} + (E_0^{Oil} - E_0^{Water}) \exp\left(-B4 \frac{S_W}{1 - S_W}\right) \quad (\text{IV .5})$$

The functions of S_W , such as $\bar{\sigma}_0(S_W)$, $\alpha(S_W)$, $s(S_W)$ and $E(S_W)$, vary from the asymptotic values for fully oil saturated chalk ($S_W = 0$), to the asymptotic values for fully water saturated chalk ($S_W = 1$). These extreme particular values can be determined from laboratory tests (including uniaxial compression tests, tensile tests, triaxial tests and hydrostatic tests), performed respectively on oil and water saturated samples. For the chalk studied here, the initial yield stress $\bar{\sigma}_0$ and the Young's modulus E_0 are reduced from values in the oil saturated chalk to the values in the water saturated one; in contrast, the parameters α and s are increased (see Table IV .1). The four parameters B1, B2, B3 and B4 should be determined from experimental data performed at different water saturation degrees. When such data are not available for the studied chalk, as a first approximation, it seems reasonable to take $B4=B3=B2=B1=1$.

By taking into account the influence of water saturation, the total strain increment due to applied stresses and water saturation change can be expressed as follows:

$$d\bar{\bar{\mathbf{E}}} = d\bar{\bar{\mathbf{E}}}^e + d\bar{\bar{\mathbf{E}}}^p = d\bar{\bar{\mathbf{E}}}^{e\sigma} + d\bar{\bar{\mathbf{E}}}^{eS} + d\bar{\bar{\mathbf{E}}}^{p\sigma} + d\bar{\bar{\mathbf{E}}}^{pS} \quad (\text{IV .6})$$

$$d\bar{\bar{\mathbf{E}}}^{e\sigma} = \mathbb{S}(S_W)d\bar{\bar{\Sigma}}, d\bar{\bar{\mathbf{E}}}^{p\sigma} = \frac{1}{-H} \frac{\partial \Phi}{\partial \bar{\bar{\Sigma}}} : d\bar{\bar{\Sigma}} : \frac{\partial \Psi}{\partial \bar{\bar{\Sigma}}} \quad (\text{IV .7})$$

$$d\bar{\bar{\mathbf{E}}}^{eS} = \frac{\partial \mathbb{S}}{\partial S_W} \bar{\bar{\Sigma}} dS_W, d\bar{\bar{\mathbf{E}}}^{pS} = \frac{1}{-H} \left(\frac{\partial \Phi}{\partial \bar{\sigma}} \frac{\partial \bar{\sigma}}{\partial S_W} + \frac{\partial \Phi}{\partial \alpha} \frac{\partial \alpha}{\partial S_W} + \frac{\partial \Phi}{\partial s} \frac{\partial s}{\partial S_W} \right) \frac{\partial \Psi}{\partial \bar{\bar{\Sigma}}} dS_W \quad (\text{IV .8})$$

In these relations, $d\bar{\bar{\mathbf{E}}}^{e\sigma}$ and $d\bar{\bar{\mathbf{E}}}^{p\sigma}$ denote respectively the increments of elastic and plastic strains due to the applied increment of stresses; while $d\bar{\bar{\mathbf{E}}}^{eS}$ and $d\bar{\bar{\mathbf{E}}}^{pS}$ correspond respectively to the additional increments of elastic and plastic strains induced by the change of water saturation degree. The fourth order tensor $\mathbb{S}(S_W)$ is the elastic compliance tensor which is a function of water saturation degree. Accordingly, the influence of water saturation on the mechanical behavior of chalk can be correctly reproduced by the proposed model.

2.2 Simulation of drained laboratory tests

Using the values of parameters given in Table (IV .1), simulations of hydrostatic and triaxial compression tests on oil and water saturated samples have been performed.

The simulation of drained hydrostatic compression test with oil saturated Lixhe chalk is presented in Figure IV .7, there is a good agreement between the numerical simulations and experimental data. The plastic deformation related to the pore collapse and the plastic hardening process due to increasing frictional contact surfaces are well described by the model.

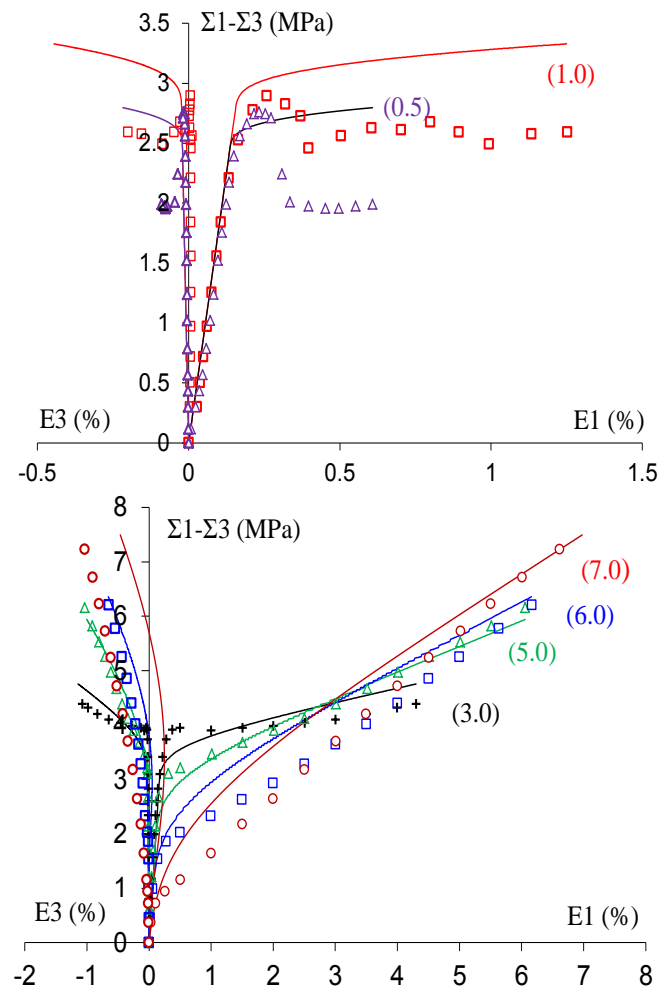


Figure IV .8: Simulations of drained triaxial compression tests with different confining pressures for water saturated Lixhe chalk (Values of confining pressure are marked in the brackets)

The numerical results by the proposed model are also compared with the experimental data for the drained triaxial compression tests on water saturated samples, both for low and high confining pressures, and are presented in Figures IV .8. At very low confining pressures, say 0.5 MPa and 1.0 MPa, a brittle failure is observed, with a small softening regime and the material failure occurs with a small value of the axial strain. Under such low confining pressures, the chalk exhibits a brittle failure with a strain softening regime. The plastic deformation is dominated by the plastic shearing. Note that the softening behavior generally implies formation of microcracks, defined as damages, and induced stiffness decreasing. Suitable method is that the damage evolution should be taken into

account in formulation of micromechanics-based model for porous chalk behavior. This feature is beyond the scope of the present work and is not discussed here. Therefore, the softening behavior of chalk at very low confining pressure is not taken into account in the present modelling; it is approached by an asymptotic perfect plastic regime. However, at slightly higher confining pressure, say 3MPa, we obtain a typical ductile failure mechanism characterized by an asymptotic perfectly plastic regime. The axial strain corresponding to the failure state is much higher. The axial strain corresponding to the failure state is much higher. Moreover, three other triaxial compression tests with different confining pressures (5, 6 and 7 MPa) are simulated and also presented in Figure IV .8 . Again, a good agreement between the numerical simulations and experimental data is obtained. The deviatoric stress enhanced pore collapse is correctly predicted by the proposed model. The porosity evolutions are presented in Figure IV .9, under low confining pressures (0.5, 1MPa), the porosity increase with the deviatoric loading due to plastic shear, when the confining pressure is above 3MPa, the porosity decrease with the deviatoric loading due to pore collapse.

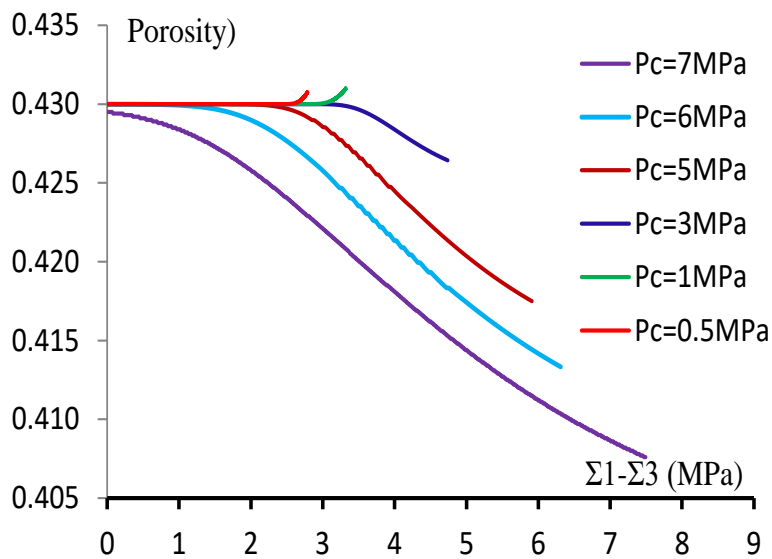


Figure IV .9: Simulated porosity evolutions of drained triaxial compression tests with different confining pressures and without pore pressure ($P_c=0$) for water saturated Lixhe chalk

In a general way, the proposed model is able to describe the main features of the mechanical behavior of porous chalk for all the range of confining pressure.

3 Extension to poroplastic modeling of saturated chalk

In this section, the focus is on modeling of the plastic behavior of saturated porous chalk with variation of pore pressure.

3.1 General framework of the poroplastic modelling

The plastic model presented above is formulated for the porous rocks with different water saturation degrees under interstitial pressure constant condition. In addition to being saturated by interstitial fluids, in practice, the porous rocks are subjected to the variation of interstitial pressure, which affects the plastic deformation of material. In the general framework of thermodynamics of open systems, the interstitial pressure acts as an independent conjugate force associated with the irreversible change of interstitial fluid mass. Accordingly, the macroscopic yield criterion of a saturated porous rocks should be reformulated as a function of macroscopic stresses and pore pressure:

$$\Phi \left(\bar{\bar{\Sigma}}, p, A_k \right) = 0 \quad (\text{IV .9})$$

A_k denotes the set of conjugate forces associated with the set of internal variables V_k describing the plastic deformation state of material. In a similar way, the plastic potential should also be expressed with the macroscopic stresses and interstitial pressure. The plastic flow rule is then written as:

$$\begin{aligned} d\bar{E}^p &= d\Lambda \frac{\partial \Psi \left(\bar{\bar{\Sigma}}, p, A_k \right)}{\partial \bar{\bar{\Sigma}}} \\ d\phi^p &= d\Lambda \frac{\partial \Psi \left(\bar{\bar{\Sigma}}, p, A_k \right)}{\partial p} \\ dV_k &= d\Lambda h \left(\bar{\bar{\Sigma}}, p, A_k \right) \end{aligned} \quad (\text{IV .10})$$

The plastic multiplier $d\Lambda \geq 0$ is determined with the plastic consistency condition. The function $h \left(\bar{\bar{\Sigma}}, p, A_k \right)$ is a pseudo dissipation potential related to the plastic hardening law. The positive intrinsic dissipation is written as:

$$\bar{\bar{\Sigma}} d\bar{E}^p + p d\phi^p - A_k dV_k \geq 0 \quad (\text{IV .11})$$

According to the general framework of poroplastic modeling defined above, the specific forms of the yield function, plastic potential and hardening law should be determined on the basis of experimental data. However, the experimental determination of these func-

tions for saturated porous materials is often very difficult. Moreover, the formulation of poroplastic model also needs suitable simplified theoretical framework. The basic idea is to formulate these functions for dry materials or saturated materials without interstitial pressure, and then make an extension to saturated materials with interstitial pressure variation by introducing relevant assumptions on the effects of interstitial pressure on plastic deformation. The principle of stress equivalence is thus introduced and stipulates that the plastic functions of the saturated porous medium remain the same as for the dry skeleton material by replacing the total stress tensor by a plastic effective stress tensor ([Coussy, 1995b],[Coussy, 2004]; [Lydzba and Shao, 2000],[Lydzba and Shao, 2002]). This principle is implicitly used in soil mechanics through the classical Terzaghi's effective stress concept [Terzaghi, 1944]. However, in cohesive geomaterials, the validity of such a principle is so far not fully proven, experimentally or theoretically. It is still an open issue of investigation. Some micromechanical studies have been devoted to the existence and definition of effective stress tensors in the plastic domain and in the strength criteria ([De Buhan and Dormieux, 1996],[De Buhan and Dormieux, 1999];[Lydzba and Shao, 2000],[Lydzba and Shao, 2002]; [Lydzba et al., 2007];[Shen and Shao, 2017]). These works provided a partial demonstration of the validity of the effective stress concept. On the macroscopic approach, based on a kinematic assumption of the relation between the plastic porosity change and macroscopic plastic volumetric strain, $d\phi^p = \beta d\bar{\bar{E}}_{kk}^p$, [Coussy, 1995b] proposed an extension of the classical Biot's effective stress in poroelasticity to poroplasticity. The positiveness of intrinsic dissipation becomes:

$$\left(\bar{\bar{\Sigma}} + \beta p \bar{\bar{\delta}}\right) d\bar{\bar{E}}^p - A_k dV_k = \bar{\bar{\Sigma}}^{ep} d\bar{\bar{E}}^p - A_k dV_k \geq 0 \quad (\text{IV .12})$$

The stress tensor $\bar{\bar{\Sigma}}^{ep} = \bar{\bar{\Sigma}} + \beta p \bar{\bar{\delta}}$ appears as the thermodynamic force associated with the plastic strain tensor, and acts as the effective stress tensor for the plastic flow rule

$$\Psi \left(\bar{\bar{\Sigma}}, p, A_k\right) = \Psi \left(\bar{\bar{\Sigma}}^{ep}, A_k\right) \quad (\text{IV .13})$$

However, for most geomaterials for which a non-associated flow rule is needed, an additional assumption is still needed, by assuming that the yield function can also be formulated with such an effective stress tensor. For porous rocks such as chalk, some experimental studies have been conducted for the characterization of poroelastic properties ([Kerbouche et al., 1995],[Xie and Shao, 2012]), and the results demonstrated the validity of this stress equivalence principle for some particular loading paths. Moreover, their results have shown that the poroplastic coefficient is close to unity, $\beta \approx 1$. Consider that the Biot coefficient

is also close to unity due to the obviously difference between the drained compressibility modules of the skeleton and the solid matrix for these high porosity rocks. This means that the classical Terzaghi's effective stress concept for elastic deformations can be used in the plastic modeling of saturated porous chalks. The experimental data performed on saturated Lixhe chalk by [Xie and Shao, 2012] also confirm the validity of this concept.

3.2 Extension to poroplastic modelling

In the preceding paragraphs, we discussed the general framework of the poroplasticity of saturated porous media, including the validity of the concept of effective stresses for the description of poroplastic behavior. For porous rocks such as chalk, it has been shown, at least in part, that the Terzaghi's effective stresses can be used to define the loading function and the plastic potential. We will then adopt this modeling framework and accept the validity of the effective plastic stress.

Thus, the plastic loading function and the plastic potential, proposed in the previous section for the two plasticity mechanisms, are now expressed as a function of the plastic effective stresses defined by the relation $\bar{\Sigma}^{ep} = \bar{\Sigma} + \beta p \bar{\delta}$.

Therefore, in the following, the plastic effective stress tensor will be used in the plastic yield function and the plastic potential:

$$\Phi = \frac{\Sigma_{eq}^2}{\Theta \bar{\sigma}^2} + 2\Gamma \cosh \left(A \ln \left(1 - 3\alpha \frac{\Sigma_m^{ep}}{\bar{\sigma}} \right) \right) - 1 - \Gamma^2 = 0 \quad (\text{IV .14})$$

$$\text{with} \left\{ \begin{array}{l} \Sigma_m^{ep} = \Sigma_m + \beta p, \quad \beta = 1 \\ \Theta = \left(\frac{1 - \phi}{1 - \Gamma} \right)^2 - 3\alpha \frac{(1 - \phi)^s \Sigma_m^{ep}}{(1 - \Gamma)^2 \bar{\sigma}} \\ \Gamma = \left(\alpha^2 (W(\phi p) + 1)^2 - \alpha^2 \right)^A \\ A = \text{sign}(\Sigma_m^{ep}) \left(\frac{4}{9\alpha} + \frac{\alpha (W(\phi p) + 1)^2 - \alpha}{18} \right) \end{array} \right. \quad (\text{IV .15})$$

and

$$\Psi = \frac{\Sigma_{eq}^2}{\Theta_\psi \bar{\sigma}_\psi^2} + 2\Gamma_\psi \cosh \left(A_\psi \ln \left(1 - 3\alpha_\psi \frac{\Sigma_m^{ep}}{\bar{\sigma}_\psi} \right) \right) \quad (\text{IV .16})$$

$$with \left\{ \begin{array}{l} \Theta_\psi = \left(\frac{1-\phi}{1-\Gamma_\psi} \right)^2 - 3\alpha_\psi \frac{(1-\phi)^s}{(1-\Gamma_\psi)^2} \frac{\Sigma_m^{ep}}{\bar{\sigma}_\psi} \\ \Gamma_\psi = \left(\alpha_\psi^2 (W(\phi p) + 1)^2 - \alpha_\psi^2 \right)^{A_\psi} \\ A_\psi = sign(\Sigma_m^{ep}) \left(\frac{4}{9\alpha_\psi} + \frac{\alpha_\psi (W(\phi p) + 1)^2 - \alpha_\psi}{18} \right) \end{array} \right. \quad (IV .17)$$

Assuming an isotropic material, the constitutive relations of saturated porous chalk are written as:

$$\bar{\Sigma} - \bar{\Sigma}^0 = 2\mu_b(\bar{E} - \bar{E}^p) + (k_b - \frac{2}{3}\mu_b)tr(\bar{E} - \bar{E}^p)\bar{\delta} - bp\bar{\delta} \quad (IV .18)$$

$$(p - p_0) = M \left[-btr(\bar{E} - \bar{E}^p) + \left(\frac{m}{\rho_f^0} - \phi^p \right) \right] \quad (IV .19)$$

In these equations, the two parameters, μ_b and k_b , are respectively the macroscopic shear modulus and bulk modulus in drained conditions. Consequently, for an isotropic linear poroelastic material, four independent parameters are to be determined, the two elastic parameters of the porous medium under drained conditions (μ_b and k_b), and the two coupling parameters, b and M , as scalar Biot's coefficient of isotropic porous medium and Biot's modulus ([Biot, 1941]), respectively. the incremental variation of fluid mass dm is decomposed into elastic part dm^e and plastic part dm^p , with $dm = dm^e + dm^p$. ρ_f^0 is the referential volumetric mass of interstitial fluid and ϕ^p , defined by $d\phi^p = dm^p / \rho_f^0$, denotes the plastic variation of porosity.

The elastic parameters are determined by the classical methods of linear elasticity theory. Coupling parameters can also be determined from specific laboratory tests [Shao and Giraud, 2002]. In addition, micromechanical analyzes make it possible to determine the relationships between the coupling parameters and the properties of the constituents of the porous medium ([Auriault and Sanchez-Palencia, 1977],[Cheng, 1997],[Lydzba and Shao, 2000]). For isotropic materials, we have the following relationships

$$b = 1 - \frac{k_b}{k_m}, \quad \frac{1}{M} = \frac{b - \phi}{k_m} + \frac{\phi}{k_f} \quad (IV .20)$$

In these relations, k_m and k_f are the compressibility modulus of solid matrix and interstitial fluid, respectively. ϕ denotes the total connected porosity of porous rock.

Finally, the plastic strain increment can be determined through the plastic flow rule:

$$d\bar{\bar{E}}^p_{ij} = d\Lambda \frac{\partial \Psi(\bar{\bar{\Sigma}}^{ep}, A_k)}{\partial \bar{\bar{\Sigma}}^{ep}_{ij}} \quad (\text{IV .21})$$

The plastic multiplier $d\Lambda$ can be determined by the plastic consistency condition:

$$\frac{\partial \Phi}{\partial \bar{\bar{\Sigma}}^{ep}} : d\bar{\bar{\Sigma}}^{ep} + \frac{\partial \Phi}{\partial \varepsilon_M} d\varepsilon_M + \frac{\partial \Phi}{\partial \phi} d\phi = 0 \quad (\text{IV .22})$$

Note that after the determination of plastic strains, the variation of interstitial pressure in the undrained condition can be evaluated easily by using the constitutive relations of saturated porous rocks.

3.3 Simulation results of undrained laboratory tests

In order to verify the capacity of the proposed model to describe the poromechanical behavior of saturated porous rocks subjected to varying interstitial pressure, based on the experimental data on Lixhe chalk reported by [Xie and Shao, 2012], a set of undrained triaxial compression tests are simulated in this study. The parameters determined from the drained tests and given in Table (III .2) remain unchanged in the simulation of undrained tests. That means that the simulation of undrained tests represents an interesting validation of the model. Further, according to the previous investigations [Xie and Shao, 2012], the value of Biot's coefficient is nearly equal to unity, $b=1$. The value of Biot's modulus is calculated by $\frac{1}{M} = \frac{b-\phi}{k_m} + \frac{\phi}{k_f}$ with the values of equivalent solid matrix compressibility k_m , fluid compressibility k_f and initial porosity ϕ . The typical coupling parameters are listed in table (IV .2). In Figure IV .10 we compared the initial yield surfaces and the effective stress paths during the deviatoric loading for three undrained triaxial compression tests respectively water and oil saturated samples. The numerical results obtained with the proposed model are presented and compared with the experimental data in Figures IV .11-IV .12 for the oil-saturated samples, and Figures IV .13-IV .14 for the water-saturated samples.

Table IV .2: Coupled parameters for oil and water saturated Lixhe chalk

Parameters	Oil saturated sample	Water saturated sample
Biot coefficient (b)	0.99	0.99
Biot modules(M,MPa)	4650	4630
Plastic effective stress coefficient(β)	0.99	0.99

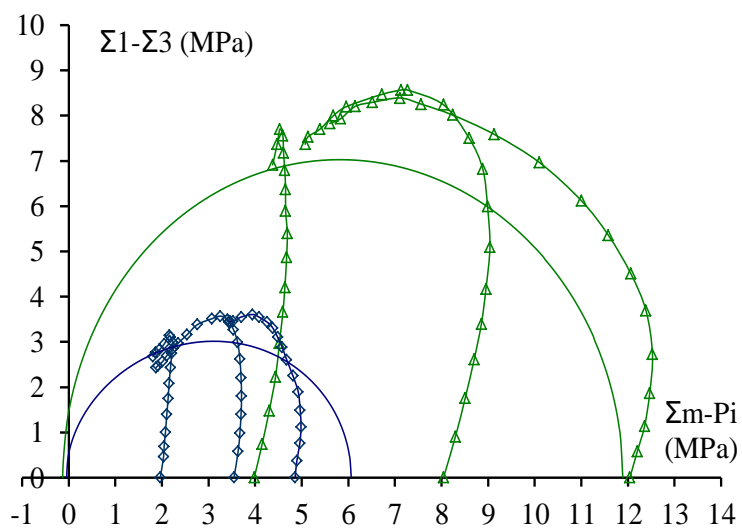


Figure IV .10: Effective stress paths during undrained triaxial compression tests in water (blue) and Oil (green) saturated samples, respectively

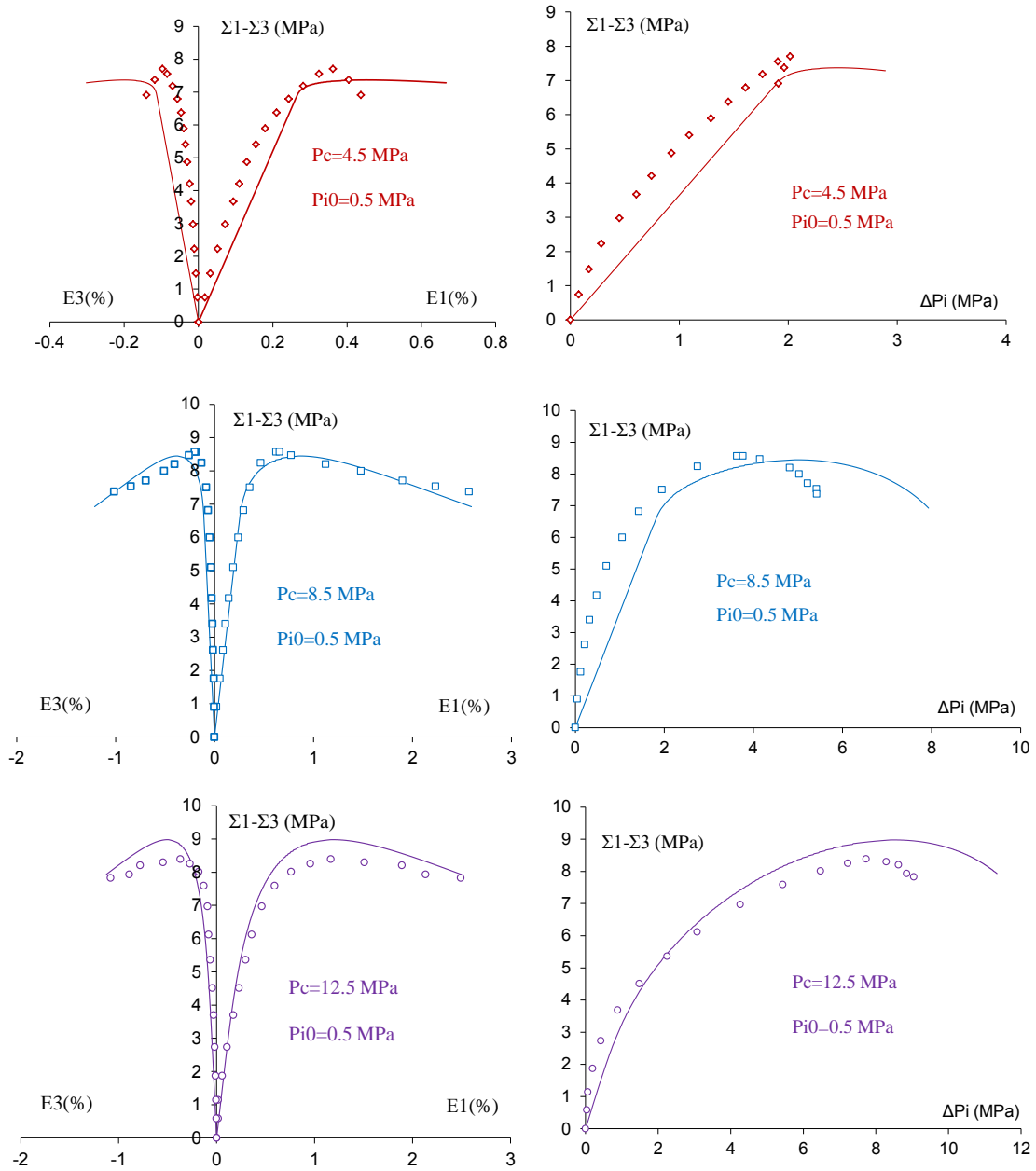


Figure IV .11: Simulations of undrained triaxial compression tests with different confining pressures and an initial interstitial pressure of 0.5 MPa for oil saturated Lixhe chalk

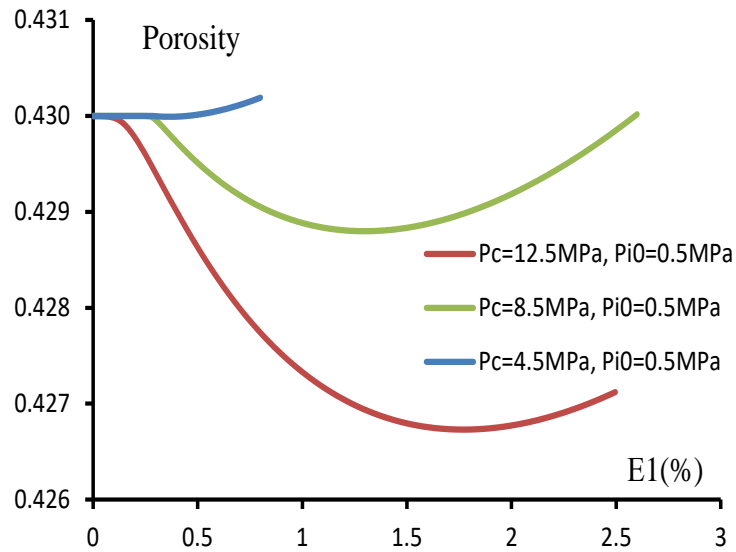


Figure IV .12: Simulated porosity evolutions of undrained triaxial compression tests with different confining pressures and an initial interstitial pressure of 0.5 MPa for oil saturated Lixhe chalk

It is observed that there is a good correspondence between the numerical simulations and the experimental data both for the stress-strain curves and for the interstitial pressure variations, and for the two saturating fluids. In particular, the drop of deviatoric stress due to the diminution of effective confining pressure or the increase of interstitial pressure is correctly described by the proposed model. Note that there is no strain softening law introduced in the proposed model. Therefore, the deviatoric stress drop is typically a consequence of plastic coupling effects. Similar to the drained tests, a brittle-ductile transition is also described clearly from low initial effective confining pressure to high initial effective confining pressure. Concerning the variation of interstitial pressure during undrained loading, there is a good quantitative agreement between the numerical simulations and the experimental data for both oil-saturated samples and water-saturated samples. The porosity evolutions are presented in Figure IV .12 and IV .14 for oil and water saturated samples respectively. The porosity evolutions correspond to the plastic mechanisms. Accordingly, the proposed micromechanics-based model correctly describes the poroplastic behavior of saturated chalk under undrained condition.

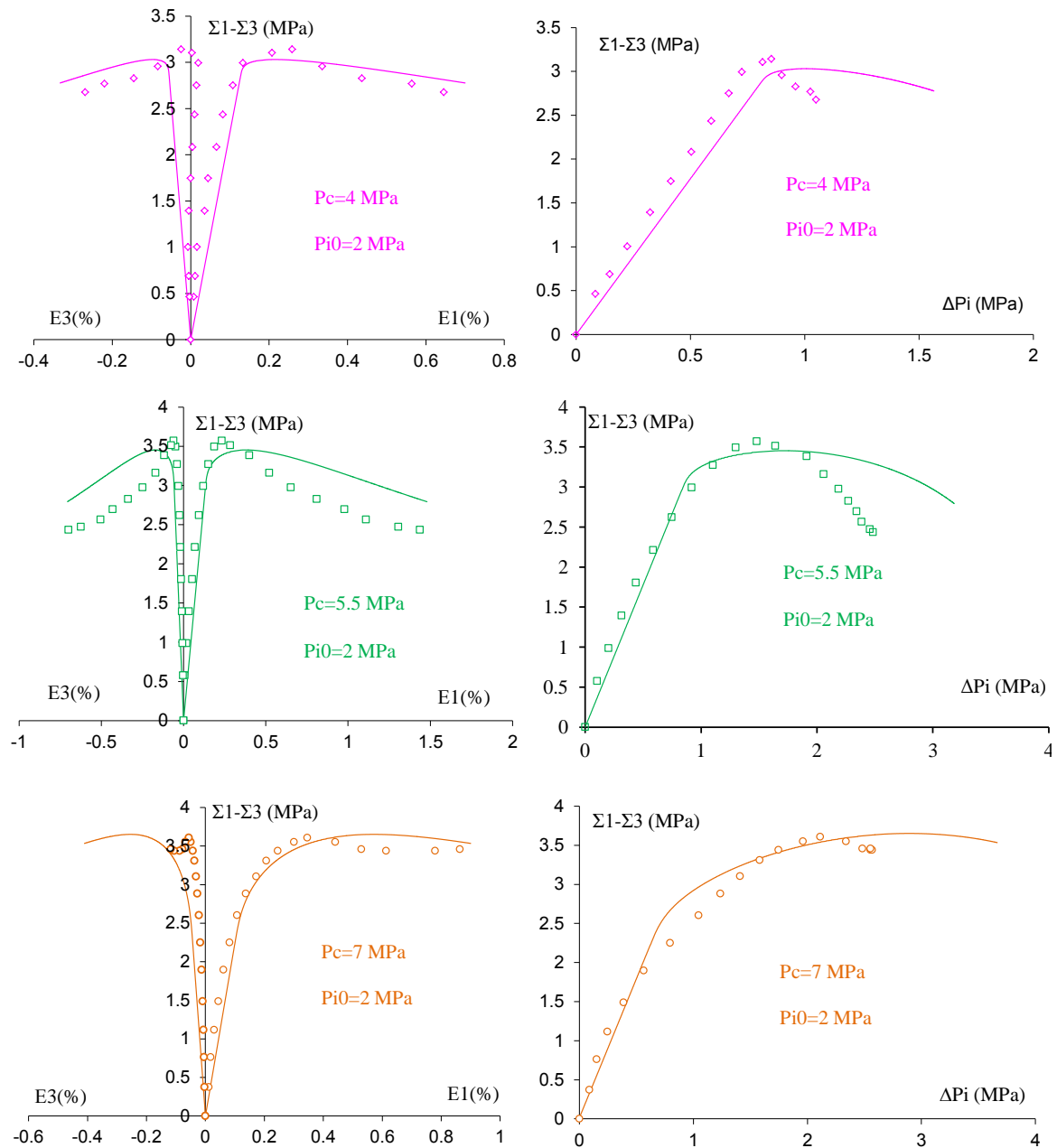


Figure IV .13: Simulations of undrained triaxial compression tests with different confining pressures and an initial interstitial pressure of 2 MPa for water saturated Lixhe chalk

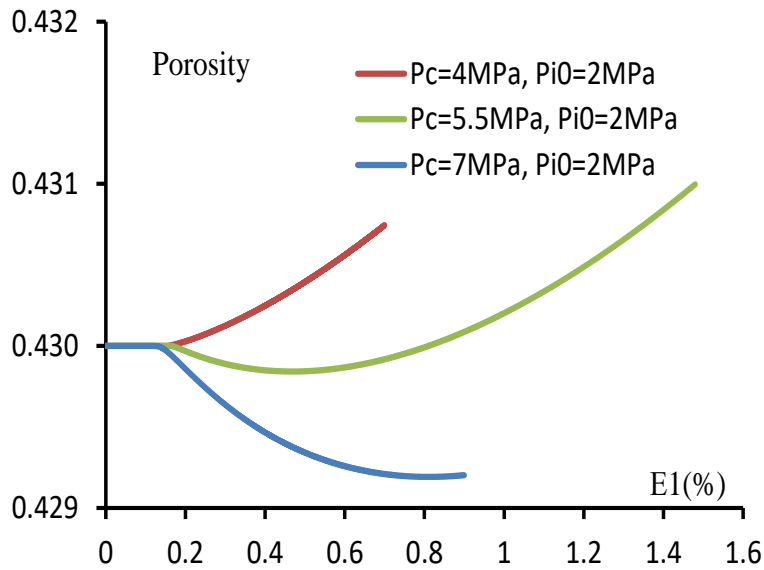


Figure IV .14: Simulated porosity evolutions of undrained triaxial compression tests with different confining pressures and an initial interstitial pressure of 2 MPa for water saturated Lixhe chalk

4 Simulations of mechanical and poromechanical behaviors of saturated Anstrude limestone

In the preceding chapter, a micromechanics-based model with a non-associated plastic flow rule is proposed for porous rocks for improving the overestimations under low confining pressure. But for the porous limestone with a relatively low porosity, the deviatoric strength is still overestimated significantly. In the present work, we propose an improvement of this model in order to characterize mechanical behavior of porous limestone both in drained and undrained conditions by introducing the porosity evolution to the hardening law.

4.1 Hardening function for porous limestone

According to the previous studies, the macroscopic mechanical behavior of porous rock depends on the mechanical properties of the porosity and the type of the equivalent solid matrix, [Xie and Shao, 2006]. The property matrix plays an important role in porous limestone, which is affected by the evolution of the plastic volumetric deformation.

According to the previous experimental results, the basic mechanical behavior of limestone shows the effect of the pressure dependence. Under a low confining pressure, the

limestone exhibits an elasto-plastic brittle behavior. The elastic limit stress increases with the increase of confining pressure. The sample failure is marked by a sharp strain softening phase. In addition, it is found that there is a clear transition from volumetric compaction to dilatancy during the deviatoric loading, and that the plastic volumetric dilatancy threshold nearly coincides with the plastic shearing threshold. It is known that the volumetric dilatancy in brittle rocks under compressive stresses is generally related to normal opening of micro-cracks during frictional sliding along rough crack surfaces [Hori and Nemat-Nasser, 1985]. For the tests under high confining pressures, the limestone exhibits an elastic-plastic ductile behavior. The elastic limit stress decreases with the increase of confining pressure. After the elastic limit stress, there is an important volumetric compaction due to the plastic pore collapse, followed by a clear transition from compaction to dilatancy. The volumetric strain is strongly influenced by the confining pressure. In contrast to the elastic limit stress, the deviatoric stress corresponding to the transition from compaction to dilatancy increases with the increase in confining pressure.

Accordingly, the contact force of equivalent solid matrix is assumed to be affected by the plastic volumetric compaction and dilatancy. The effect of the plastic volumetric compaction leads to increase of the contact force of equivalent solid matrix, which can be describe by the equivalent plastic strain of the solid matrix. In contrast to the plastic volumetric compaction, when limestone is reached elastic limit under low confining pressure, the plastic volumetric dilatancy leads to an increase of porosity, and to a reduction of the contact force of the solid matrix. Therefore, the plastic volumetric dilatancy leads to a diminution of plastic yield stress of the solid matrix. Accordingly, the effect of plastic volumetric dilatancy leads to reduction of the contact force, which can be described by the increase of the porosity. For a high porous chalk, the following hardening function is proposed by [Xie and Shao, 2006]:

$$\bar{\sigma} = \bar{\sigma}_0 \left(1 + a(\varepsilon_M)^n e^{b\varepsilon_M} \right) \quad (\text{IV .23})$$

The variable ε_M denotes an equivalent plastic strain of the solid matrix. Three parameters a , b and n , describe the yield stress evolution rate of the solid matrix. The plastic hardening function is essentially determined from the experimental data of a hydrostatic compression test, which revealed an initial pore collapse yield stress, a strong plastic contractancy due to the pore collapse and a hardening phase due to the increase of contact surfaces between grains. Due to the weak plastic dilatancy for the triaxial tests under low confining pressures, only the effect of the equivalent plastic strain of the solid matrix is taken account in this hardening function. For the studied porous limestone, apart from

the hardening effect of the equivalent plastic strain of the solid matrix, the hardening (softening) effect of porosity evolution on the mechanical properties of the equivalent solid matrix needs to be taken into account. Accordingly, a hardening function is proposed in this study:

$$\bar{\sigma}(\phi, \varepsilon_M) = \bar{\sigma}_0 (1 + \eta(\phi_0 - \phi)) \left(1 + a(\varepsilon_M)^n e^{b\varepsilon_M}\right) \quad (\text{IV .24})$$

$$\text{with } \begin{cases} \eta = \eta_0 & \text{if } \phi \geq \phi_0 \\ \eta = 0 & \text{if } \phi \leq \phi_0 \end{cases}$$

The parameter ϕ_0 denotes an initial porosity of porous material. The parameter η describes the yield stress evolution of the solid matrix with the variation of porosity of porous material, and can be determined by simulating the triaxial tests under low confining pressures.

4.2 Simulation of drained laboratory tests

The proposed micromechanics-based model contains 12 parameters to describe basic elastic–plastic behavior of porous limestone. The parameter η_0 can be determined from fitting the stress strain curves of triaxial compression tests under low confining pressure, the other 11 parameters can be determined as these of porous chalk.

Using the values of parameters given in Table IV .3, simulations of drained triaxial compression tests on water saturated limestone have been performed. The yield surface of drained triaxial tests performed on water saturated Anstrude limestone is presented in Figure IV .15.

The numerical results with the proposed model are compared with the experimental data for the drained triaxial compression tests on water saturated Anstrude limestone, both for low and high confining pressures, and presented in Figures IV .16. At low confining pressures, say 3.0, 6.0 and 10.0 MPa, a brittle failure is observed, with a small softening regime and the material failure occurs with a small value of the axial strain. Under such low confining pressures, the limestone exhibits a brittle failure with a strain softening regime. The plastic deformation is dominated by the plastic shearing. Therefore, the softening behavior of porous limestone at low confining pressure is taken into account in the present modelling by introducing the effect of porosity evolution. The strains and deviatoric strength are correctly predicted by the proposed model. Moreover, four other

triaxial compression tests with different confining pressures (15, 25, 35 and 50 MPa) are simulated and also presented in Figure IV .16. Again, a good agreement between the numerical simulations and experimental data is obtained. The deviatoric stress enhanced pore collapse is correctly predicted by the proposed model. In addition, the porosity evolutions are presented in Figure IV .17. Under low confining pressure, after the elastic limit, the porosity increases during the deviatoric loading due to the plastic shearing. Under high confining pressure, after the elastic limit stress, the porosity reduces due to the plastic pore collapse, followed by a transition from diminution to augmentation with the increase in deviatoric stress. Therefore, the porosity evolution is directly related to the plastic mechanisms. The increase of porosity is mainly induced by the plastic shearing process while the decrease of porosity is induced by the plastic pore collapse.

In a general way, the proposed model is able to describe the main features of the mechanical behavior of porous limestone for all the range of confining pressure.

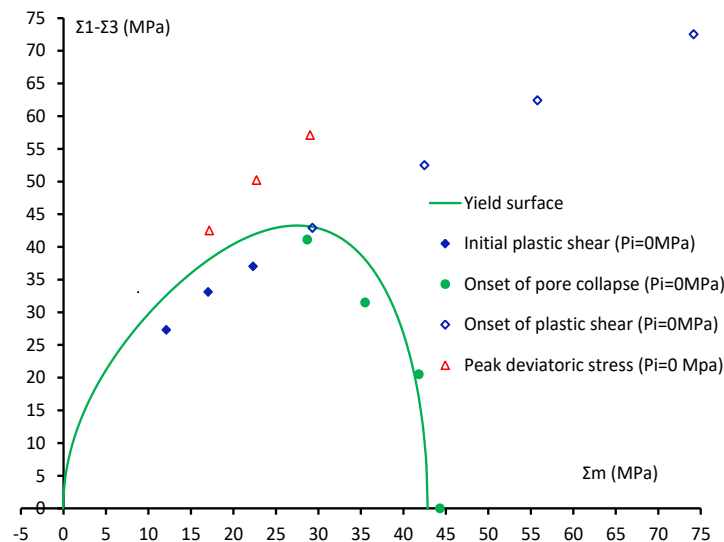


Figure IV .15: Yield surface of drained triaxial tests performed on water saturated Anstrude limestone

Table IV .3: Values of parameters for water saturated Anstrude limestone

Parameters	Water saturated sample
Porosity (ϕ)	0.2
Young's modulus of solid matrix (E_m , MPa)	22000
Initial Poisson's ratio of solid matrix (ν_m)	0.25
Initial yield stress of matrix ($\bar{\sigma}_0$, MPa)	2.25
Yield function parameter of matrix (α)	5.4
Form parameter of yield criterion (s)	-4.0
Potential function parameter of matrix ($\sigma_{0\psi}$, MPa)	4.5
Potential function parameter of matrix (α_ψ)	1.08
Hardening parameter of yield stress of matrix (a)	0.6
Hardening parameter of yield stress of matrix (b)	1.0
Hardening parameter of yield stress of matrix (n)	0.36
Hardening parameter of yield stress of matrix (η_0)	40

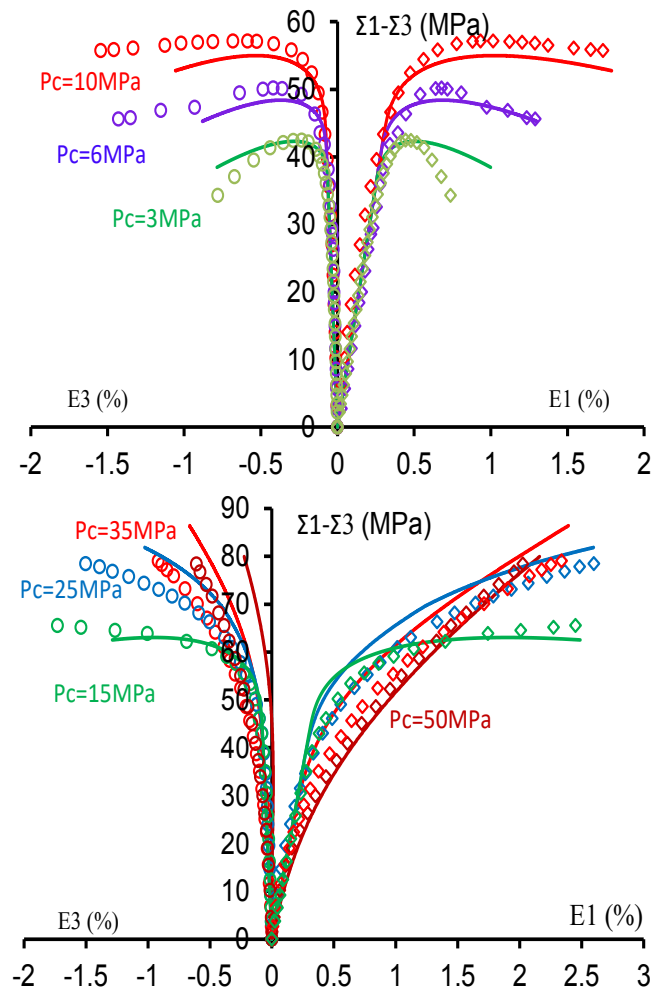


Figure IV .16: Simulations of drained triaxial compression tests with different confining pressures for water saturated Anstrude limestone

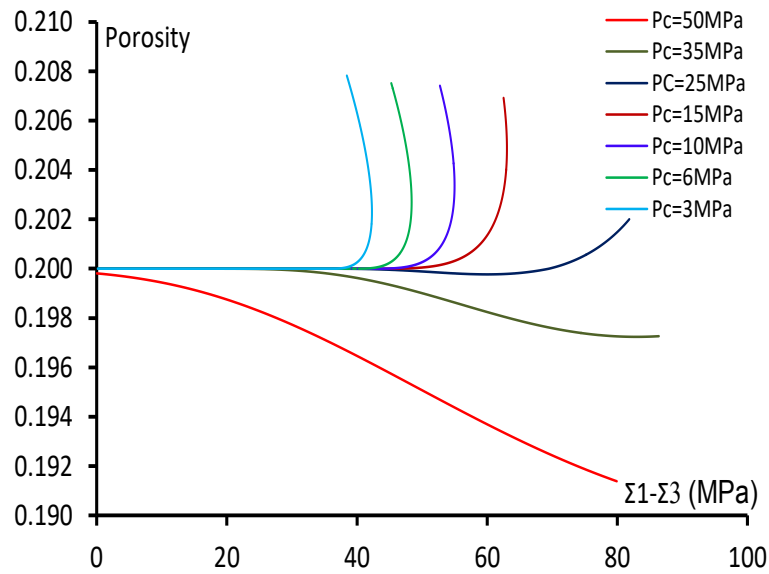


Figure IV .17: Evolution of porosity during deviatoric loading with different confining pressures for water saturated Anstrude limestone

4.3 Simulations of undrained triaxial tests of porous limestone

In order to verify the capacity of the proposed model to describe the poromechanical behavior of saturated porous rocks subjected to varying interstitial pressure, based on the experimental data on Anstrude limestone performed by [Han et al., 2018], a set of undrained triaxial compression tests are simulated in this study. The parameters determined from the drained tests and given in Table IV .3 remain unchanged in the simulation of undrained tests. That means that the simulation of undrained tests represents an interesting validation of the model. In Figure IV .18, the effective stress paths during the undrained tests are illustrated with respect to the yield surface of drained triaxial tests performed on water saturated Anstrude limestone. It can be seen that the mechanical response of limestone during undrained triaxial compression tests is influenced by effective mean stress or by the confining pressure and pore pressure. The typical coupling parameters for porous limestone are listed in table IV .4. The simulations of four undrained triaxial tests for the water-saturated samples are performed with the proposed model. In Figure IV .19, we present the curves of the deviatoric stress versus the axial and lateral strains as well as the pore pressure separately for each value of confining pressure.

Table IV .4: Coupled parameters for water saturated Anstrude limestone

Parameters	Water saturated sample
Biot coefficient (b)	0.8
Biot Modules (M, MPa)	8240
Plastic effective stress coefficient (β)	0.99

It is observed that there is a good correspondence between the numerical simulations and the experimental data both for the stress–strain curves and for the pore pressure evolutions. In particular, the increase of deviatoric stress due to the increase of effective confining pressure or the decrease of pore pressure is correctly described by the proposed model. It is interesting to note that there is a softening law introduced in the proposed model, but the deviatoric stress continues to increase until the porosity decreases near to zero. Therefore, the deviatoric stress increase is typically a consequence of poroplastic coupling effects. Concerning the evolution of pore pressure during undrained loading, there is a good quantitative agreement between the numerical simulations and the experimental data for water-saturated samples. In addition, the porosity evolutions are presented in Figure IV .20, and shown that the plastic shear mechanism is dominated the plastic deformation during undrained triaxial loading. Accordingly, the proposed micromechanics-based model can correctly describe the poroplastic behavior of saturated porous limestone under undrained condition.

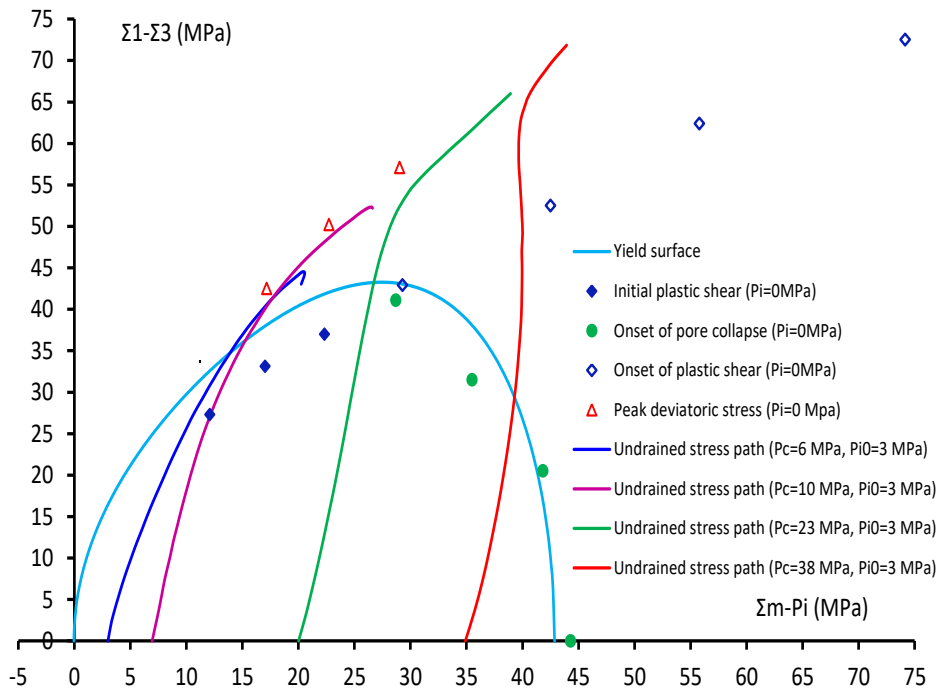
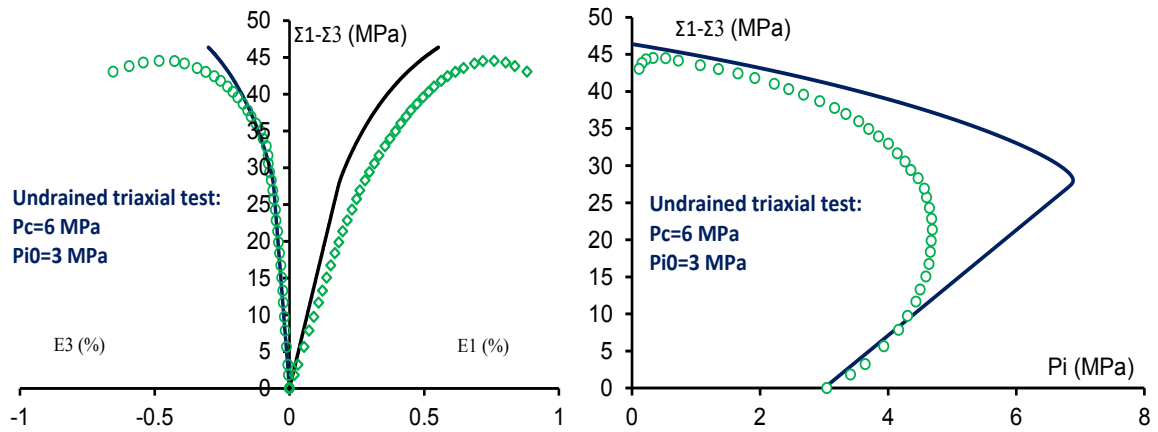
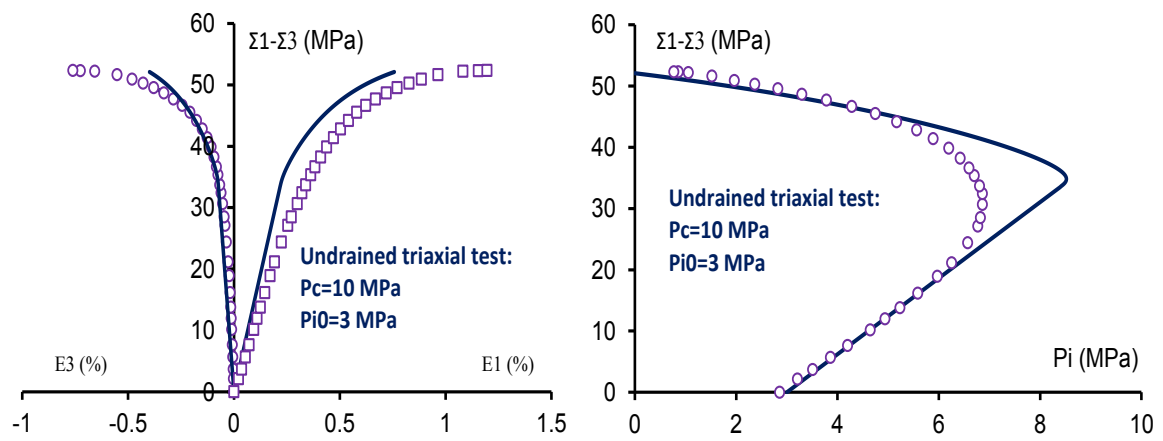
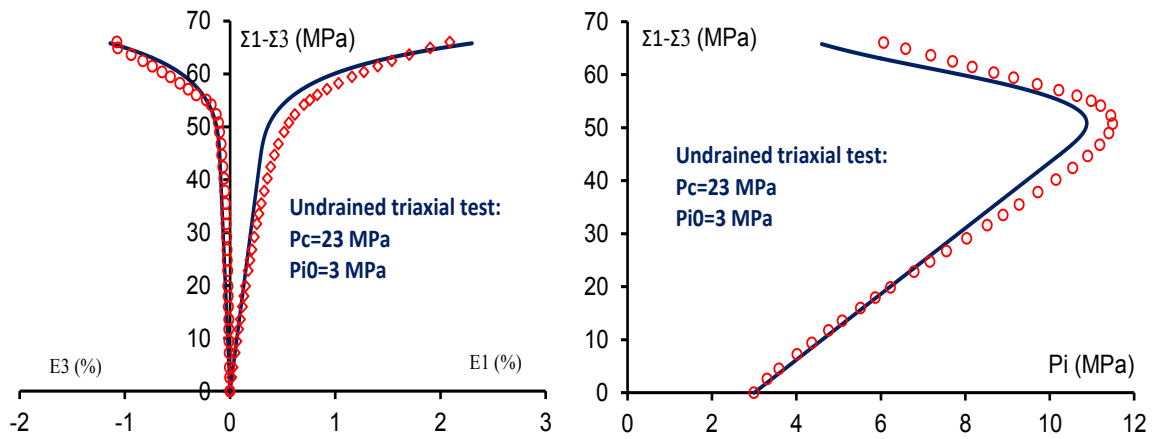
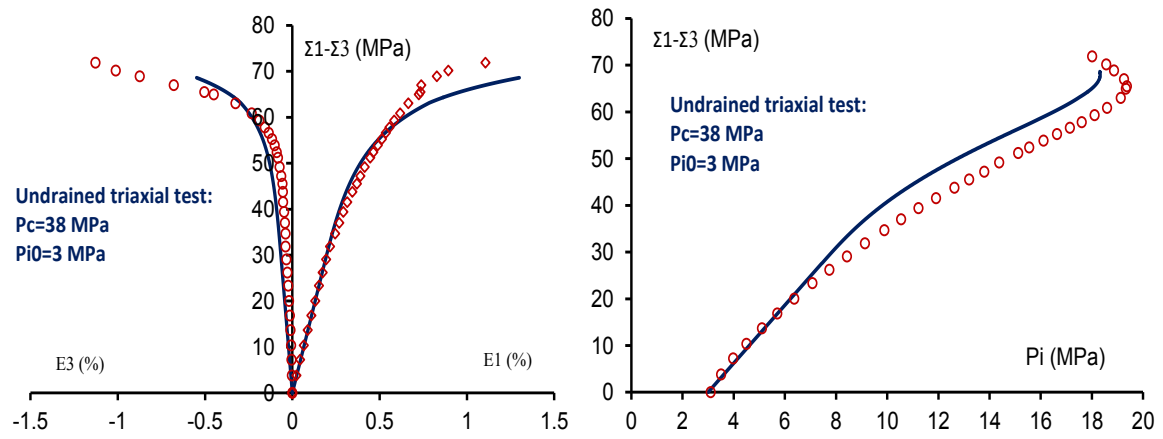


Figure IV .18: Stress paths in undrained triaxial compression tests with respect to initial plastic shearing surface, pore collapse surface and peak strength surface determined from triaxial compression tests without pore pressure

(a) Confining pressure $P_c = 6 \text{ MPa}$ and initial interstitial pressure $P_{i0} = 3 \text{ MPa}$ (b) Confining pressure $P_c = 10 \text{ MPa}$ and initial interstitial pressure $P_{i0} = 3 \text{ MPa}$



(c) Confining pressure $P_c = 23\text{MPa}$ and initial interstitial pressure $P_{i0} = 3\text{MPa}$



(d) Confining pressure $P_c = 38\text{MPa}$ and initial interstitial pressure $P_{i0} = 3\text{MPa}$

Figure IV .19: Simulations of undrained triaxial compression tests with different confining pressures and an initial interstitial pressure of 3.0 MPa for water saturated Anstrude limestone

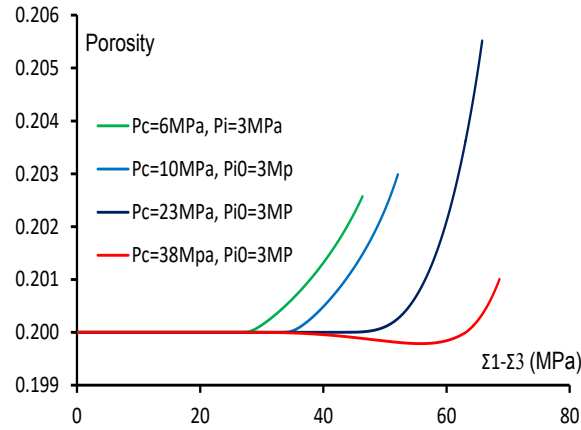


Figure IV .20: Evolution of porosity during deviatoric loading with different confining pressures for water saturated Anstrude limestone

5 Conclusion

Based on the model proposed in preceding chapter, the simulations of the mechanical behaviors of oil and water saturated chalk have been firstly carried out. The water effects on the mechanical behavior of porous chinks, due to the reduction of capillary force in liquid contact surfaces and the enhancement of inter-granular pressure solution process, have been studied by taking into account the water saturation degree. The elastic modulus on the macroscopic scale and the plastic parameters on the microscopic scale are expressed as functions of water saturation degree. Based on the effective stress concept, the micromechanics-based model is then extended to formulate poroplastic model for describing the poromechanical behaviors of porous chalk. According to the mechanical behavior of prous limestone, the proposed model is improved by taking effect of porosity evolution on the contact force of solid matrix. The drained mechanical behavior of porous limestone is studied by the improved model. At the same time, based on the effective plastic stress concept, the undrained mechanical behavior of porous limestone is also studied by adopting the improved model. Finally, the improved model is applied to simulate drained and undrained triaxial compression tests for the studied limestone. In a general way, the numerical results are in good agreement with experimental data for both of the high-porosity chalk and the medium-porosity limestone. The proposed model is able to describe not only basic mechanical responses of porous rocks in drained conditions but also in coupled poroplastic conditions.

Chapter V

Conclusions and Perspectives

The present work has been done with the aim of characterizing and modeling the mechanical behavior of porous rocks under drained and undrained conditions. Different types of tests have been carried out, including drained triaxial tests with and without permeability measurement, drained triaxial tests with and without constant pore pressure, water injection tests and undrained triaxial tests. The tests were used to characterize the behavior of the limestone.

First of all, the experimental results have confirmed that the studied limestone has two modes of plastic deformation: plastic deformation due to pore collapse and plastic deformation due to deviatoric plastic shearing. And the experimental results obtained have confirmed the effect of confining pressure on plastic behavior and failure property in most porous rocks, especially, the transition from brittle to ductile behavior can be explained as an effect of the pore collapse with the increase in confining pressure.

And next, the experimental results revealed that the permeability evolution is affected by the two the plastic processes. Under low confining pressure, with increase of deviatoric loading, the permeability is enhanced by the volumetric dilatancy due to the plastic shearing. However, under high confining pressure, the permeability evolution is strongly affected by the pore collapse process and continues to decrease or becomes nearly constant even after the compaction–dilatancy transition.

And then, the experimental results have shown that the effects of pore pressure on mechanical behavior are complex. Comparing the experimental results of drained triaxial tests without pore pressure and with pore pressure of 5 MPa, effects of constant pore pressure on mechanical behavior have been investigated. For the tests with pore pressure of 5MPa, both plastic deformation and strength are lower than those without pore pressure for a same effective confining pressure, especially for the tests under low confining pressure.

The water injection induces an increase in pore pressure and then a decrease in effective confining pressure. This enhances the plastic shearing process, volumetric dilatancy and shearing failure. Further only the plastic shearing is activated in such a loading path. The pore pressure evolution in undrained triaxial tests is also influenced by two plastic processes. Under low confining pressure, the deviatoric stress induces plastic dilatancy due to shearing process and then a decrease in pore pressure. But under high confining pressure, the deviatoric stress induces a plastic compaction due to pore collapse and enhances the increase in pore pressure. The pore collapse dominates the pore pressure evolution during the first stage of loading, while the plastic shearing dominates the peak strength and pore pressure evolution during the second stage. Based on the experimental results, finally, the concept of effective stress for plastic deformation and peak strength has been revisited.

For modeling mechanical behavior of porous rock, the high-porosity Lixhe chalk is firstly studied. According to previous study, chalk is presented as a typical porous rock composed of an equivalent solid matrix and connected porosity. A micromechanics-based plastic model is firstly proposed on basis of a recent Gurson-type model of porous material with a Mises–Schleicher matrix [Shen et al., 2015]. Two plastic parameters of the equivalent solid matrix, the plastic yield stress and the pressure-sensitive coefficient, and the porosity are used as the fundamental parameters in the macroscopic plastic yield function. Considering that the high-porosity rock exhibits a volumetric compaction under low confining pressure, a non-associated model is then proposed for high porous rock. Based on the proposed model, the elastoplastic behaviors of two porous rocks, a high-porosity chalk and a medium porosity limestone, are studied in this work. Firstly, the proposed model is applied to describe the drained mechanical behaviors of a high-porosity chalk saturated by oil and water respectively. The influences of water saturation are taken into account in modeling of porous chalk. And then, the model is extended to describe the poroplastic coupling effect by using the plastic effective stress concept, and the poroplastic behaviors of chalk are studied. Finally, the proposed model is improved for a medium-porosity limestone by taking the effect of porosity evolution on the hardening law, and the simulations of the mechanical and poromechanical behaviors of studied limestone are carried out with the improved model. In a general way, from a high-porosity chalk to a medium porosity limestone, the proposed model is verified in different loading conditions through comparisons between the numerical predictions and experimental data for both drained and undrained tests, and the proposed model is able to describe the mechanical and poromechanical behaviors for all the range of confining pressure.

Further works remain to be carried out for modeling of permeability evolution of porous

limestone under compression condition, and for extending the model to other porous geomaterials, such as porous sandstone.

Bibliography

- [Aubertin and Li, 2004] Aubertin, M. and Li, L. (2004). A porosity-dependent inelastic criterion for engineering materials. *International Journal of Plasticity*, 20(12):2179–2208.
- [Aubertin et al., 1999] Aubertin, M., Yahya, O. M. L., and Julien, M. (1999). Modeling mixed hardening of alkali halides with a modified version of an internal state variables model. *International Journal of Plasticity*, 15(10):1067–1088.
- [Auriault and Sanchez-Palencia, 1977] Auriault, J.-L. and Sanchez-Palencia, E. (1977). Etude du comportement macroscopique d’un milieu poreux saturé déformable. *Journal de mécanique*, 16(4):575–603.
- [Baud et al., 2000] Baud, P., Schubnel, A., and Wong, T.-f. (2000). Dilatancy, compaction, and failure mode in solnhofen limestone. *Journal of Geophysical Research: Solid Earth*, 105(B8):19289–19303.
- [Biot, 1941] Biot, M. A. (1941). General theory of three-dimensional consolidation. *Journal of applied physics*, 12(2):155–164.
- [Biot, 1973] Biot, M. A. (1973). Nonlinear and semilinear rheology of porous solids. *Journal of Geophysical Research*, 78(23):4924–4937.
- [Byerlee, 1968] Byerlee, J. D. (1968). Brittle-ductile transition in rocks. *Journal of Geophysical Research*, 73(14):4741–4750.
- [Cheng, 1997] Cheng, A.-D. (1997). Material coefficients of anisotropic poroelasticity. *International Journal of Rock Mechanics and Mining Sciences*, 34(2):199–205.
- [Collin et al., 2002] Collin, F., Cui, Y. J., Schroeder, C., and Charlier, R. (2002). Mechanical behaviour of lixhe chalk partly saturated by oil and water: experiment and modelling. *International journal for numerical and analytical methods in geomechanics*, 26(9):897–924.
- [Coussy, 1995a] Coussy, O. (1995a). *Mechanics of porous continua*. Wiley.
- [Coussy, 1995b] Coussy, O. (1995b). *Mechanics of porous continua 1995*.
- [Coussy, 2004] Coussy, O. (2004). *Poromechanics*. John Wiley & Sons.

- [De Buhan and Dormieux, 1996] De Buhan, P. and Dormieux, L. (1996). On the validity of the effective stress concept for assessing the strength of saturated porous materials: a homogenization approach. *Journal of the Mechanics and Physics of Solids*, 44(10):1649–1667.
- [De Buhan and Dormieux, 1999] De Buhan, P. and Dormieux, L. (1999). A micromechanics-based approach to the failure of saturated porous media. In *Porous Media: Theory and Experiments*, pages 47–62. Springer.
- [De Gennaro et al., 2004] De Gennaro, V., Delage, P., Priol, G., Collin, F., and Cui, Y.-J. (2004). On the collapse behaviour of oil reservoir chalk. *Géotechnique*, 54:415–420.
- [Desai, 1980] Desai, C. S. (1980). A general basis for yield, failure and potential functions in plasticity. *International Journal for Numerical and Analytical Methods in Geomechanics*, 4(4):361–375.
- [Desai, 2000] Desai, C. S. (2000). *Mechanics of materials and interfaces: The disturbed state concept*. CRC press.
- [DiMaggio and Sandler, 1971] DiMaggio, F. L. and Sandler, I. S. (1971). Material model for granular soils. *Journal of Engineering Mechanics*.
- [Dormieux et al., 2006] Dormieux, L., Kondo, D., and Ulm, F.-J. (2006). *Microporomechanics*. John Wiley & Sons.
- [Ehlers, 1995] Ehlers, W. (1995). A single-surface yield function for geomaterials. *Archive of Applied Mechanics*, 65(4):246–259.
- [Elliott and Brown, 1985] Elliott, G. and Brown, E. (1985). Yield of a soft, high porosity rock. *Geotechnique*, 35(4):413–423.
- [Fortin et al., 2005] Fortin, J., Schubnel, A., and Guéguen, Y. (2005). Elastic wave velocities and permeability evolution during compaction of bleurswiller sandstone. *International Journal of Rock Mechanics and Mining Sciences*, 42(7-8):873–889.
- [Fredrich et al., 1989] Fredrich, J. T., Evans, B., and Wong, T.-F. (1989). Micromechanics of the brittle to plastic transition in carrara marble. *Journal of Geophysical Research: Solid Earth*, 94(B4):4129–4145.
- [French et al., 2012] French, M., Boutt, D., and Goodwin, L. (2012). Sample dilation and fracture in response to high pore fluid pressure and strain rate in quartz-rich sandstone and siltstone. *Journal of Geophysical Research: Solid Earth*, 117(B3).

- [Gens, 1993] Gens, A. (1993). Conceptual bases for a constitutive model for bonded soils and weak rocks. *Geotechnical engineering of hard soils-soft rocks*, pages 485–494.
- [Ghabezloo et al., 2009] Ghabezloo, S., Sulem, J., Guédon, S., and Martineau, F. (2009). Effective stress law for the permeability of a limestone. *International Journal of Rock Mechanics and Mining Sciences*, 46(2):297–306.
- [Ghorbanbeigi et al., 2016] Ghorbanbeigi, H., Shen, W., Yurtdas, I., and Shao, J.-F. (2016). A micromechanics-based model for concrete materials subjected to carbonation. *International Journal for Numerical and Analytical Methods in Geomechanics*, 40(8):1203–1218.
- [Gueguen and Bouteca, 1999] Gueguen, Y. and Bouteca, M. (1999). Mechanical properties of rocks: pore pressure and scale effects. *Oil & Gas Science and Technology*, 54(6):703–714.
- [Guo et al., 2008] Guo, T., Faleskog, J., and Shih, C. (2008). Continuum modeling of a porous solid with pressure-sensitive dilatant matrix. *Journal of the Mechanics and Physics of Solids*, 56(6):2188–2212.
- [Gurson, 1977] Gurson, A. L. (1977). Continuum theory of ductile rupture by void nucleation and growth: Part i?yield criteria and flow rules for porous ductile media. *Journal of engineering materials and technology*, 99(1):2–15.
- [Han et al., 2018] Han, B., Shen, W., Xie, S., and Shao, J. (2018). Influence of pore pressure on plastic deformation and strength of limestone under compressive stress. *Acta Geotechnica*, pages 1–11.
- [Han et al., 2016] Han, B., Xie, S., and Shao, J. (2016). Experimental investigation on mechanical behavior and permeability evolution of a porous limestone under compression. *Rock Mechanics and Rock Engineering*, 49(9):3425–3435.
- [Hart and Wang, 2001] Hart, D. and Wang, H. (2001). A single test method for determination of poroelastic constants and flow parameters in rocks with low hydraulic conductivities. *International Journal of Rock Mechanics and Mining Sciences*, 38(4):577–583.
- [Homand and Shao, 2000] Homand, S. and Shao, J. (2000). Mechanical behaviour of a porous chalk and water/chalk interaction. part i: experimental study. *Oil & Gas Science and Technology*, 55(6):591–598.

- [Horii and Nemat-Nasser, 1985] Horii, H. and Nemat-Nasser, S. (1985). Compression-induced microcrack growth in brittle solids: Axial splitting and shear failure. *Journal of Geophysical Research: Solid Earth*, 90(B4):3105–3125.
- [Hu et al., 2010] Hu, D., Zhou, H., Zhang, F., and Shao, J.-F. (2010). Evolution of poroelastic properties and permeability in damaged sandstone. *International Journal of Rock Mechanics and Mining Sciences*, 47(6):962–973.
- [Jeong, 2002] Jeong, H.-Y. (2002). A new yield function and a hydrostatic stress-controlled void nucleation model for porous solids with pressure-sensitive matrices. *International journal of solids and structures*, 39(5):1385–1403.
- [Kerbouche et al., 1995] Kerbouche, R., Shao, J., Skoczylas, F., and Henry, J. (1995). On the poroplastic behaviour of porous rock. *European Journal of Mechanics, A/Solids*, 14(4):577–587.
- [Khoei and Azami, 2005] Khoei, A. and Azami, A. (2005). A single cone-cap plasticity with an isotropic hardening rule for powder materials. *International Journal of Mechanical Sciences*, 47(1):94–109.
- [Lade, 1977] Lade, P. V. (1977). Elasto-plastic stress-strain theory for cohesionless soil with curved yield surfaces. *International Journal of Solids and Structures*, 13(11):1019–1035.
- [Lade, 1997] Lade, P. V. (1997). Modelling the strengths of engineering materials in three dimensions. *Mechanics of Cohesive-frictional Materials: An International Journal on Experiments, Modelling and Computation of Materials and Structures*, 2(4):339–356.
- [Lade and Kim, 1995] Lade, P. V. and Kim, M. K. (1995). Single hardening constitutive model for soil, rock and concrete. *International Journal of Solids and Structures*, 32(14):1963–1978.
- [Lewis and Khoei, 2001] Lewis, R. W. and Khoei, A. R. (2001). A plasticity model for metal powder forming processes. *International Journal of Plasticity*, 17(12):1659–1692.
- [Lin et al., 2011] Lin, J., Shao, J.-F., and Kondo, D. (2011). A two scale model of porous rocks with drucker–prager matrix: Application to a sandstone. *Mechanics Research Communications*, 38(8):602–606.

- [Lin et al., 2012] Lin, J., Xie, S., Shao, J.-F., and Kondo, D. (2012). A micromechanical modeling of ductile behavior of a porous chalk: Formulation, identification, and validation. *International Journal for Numerical and Analytical Methods in Geomechanics*, 36(10):1245–1263.
- [Lion et al., 2004] Lion, M., Skoczylas, F., and Ledésert, B. (2004). Determination of the main hydraulic and poro-elastic properties of a limestone from bourgogne, france. *International Journal of Rock Mechanics and Mining Sciences*, 41(6):915–925.
- [Lisabeth and Zhu, 2015] Lisabeth, H. P. and Zhu, W. (2015). Effect of temperature and pore fluid on the strength of porous limestone. *Journal of Geophysical Research: Solid Earth*, 120(9):6191–6208.
- [Lockner and Stanchits, 2002] Lockner, D. A. and Stanchits, S. A. (2002). Undrained poroelastic response of sandstones to deviatoric stress change. *Journal of Geophysical Research: Solid Earth*, 107(B12).
- [Lydzba et al., 2007] Lydzba, D., Pietruszczak, S., and Shao, J.-F. (2007). Intergranular pressure solution in chalk: a multiscale approach. *Computers and Geotechnics*, 34(4):291–305.
- [Lydzba and Shao, 2000] Lydzba, D. and Shao, J. (2000). Study of poroelasticity material coefficients as response of microstructure. *Mechanics of Cohesive-frictional Materials: An International Journal on Experiments, Modelling and Computation of Materials and Structures*, 5(2):149–171.
- [Lydzba and Shao, 2002] Lydzba, D. and Shao, J.-F. (2002). Stress equivalence principle for saturated porous media. *Comptes Rendus Mecanique*, 330(4):297–303.
- [Ma and Zoback, 2017] Ma, X. and Zoback, M. D. (2017). Laboratory experiments simulating poroelastic stress changes associated with depletion and injection in low-porosity sedimentary rocks. *Journal of Geophysical Research: Solid Earth*, 122(4):2478–2503.
- [Maghous et al., 2009] Maghous, S., Dormieux, L., and Barthélémy, J. (2009). Micromechanical approach to the strength properties of frictional geomaterials. *European Journal of Mechanics-A/Solids*, 28(1):179–188.
- [Monchiet and Kondo, 2012] Monchiet, V. and Kondo, D. (2012). Exact solution of a plastic hollow sphere with a mises–schleicher matrix. *International Journal of Engineering Science*, 51:168–178.

- [Paterson, 1958] Paterson, M. (1958). Experimental deformation and faulting in wombeyan marble. *Geological Society of America Bulletin*, 69(4):465–476.
- [Paterson and Wong, 2005] Paterson, M. S. and Wong, T.-f. (2005). *Experimental rock deformation-the brittle field*. Springer Science & Business Media.
- [Perić and Ayari, 2002] Perić, D. and Ayari, M. A. (2002). On the analytical solutions for the three-invariant cam clay model. *International Journal of Plasticity*, 18(8):1061–1082.
- [Pietruszczak et al., 1988] Pietruszczak, S., Jiang, J., and Mirza, F. (1988). An elastoplastic constitutive model for concrete. *International Journal of Solids and Structures*, 24(7):705–722.
- [Pimienta et al., 2017] Pimienta, L., Fortin, J., and Guéguen, Y. (2017). New method for measuring compressibility and poroelasticity coefficients in porous and permeable rocks. *Journal of Geophysical Research: Solid Earth*, 122(4):2670–2689.
- [Risnes, 2001] Risnes, R. (2001). Deformation and yield in high porosity outcrop chalk. *Physics and Chemistry of the Earth, Part A: Solid Earth and Geodesy*, 26(1-2):53–57.
- [Risnes and Flaageng, 1999] Risnes, R. and Flaageng, O. (1999). Mechanical properties of chalk with emphasis on chalk-fluid interactions and micromechanical aspects. *Oil & Gas science and technology*, 54(6):751–758.
- [Risnes et al., 2005] Risnes, R., Madland, M., Hole, M., and Kwabiah, N. (2005). Water weakening of chalk—mechanical effects of water-glycol mixtures. *Journal of Petroleum Science and Engineering*, 48(1-2):21–36.
- [Schroeder, 2003] Schroeder, C. (2003). Mechanical behaviour of partially and multiphase saturated chalks and fluid-skeleton interaction: Main factor of chalk oil reservoirs compaction and related subsidence. *Final report of the EU project (PASACHALK2)*.
- [Shao, 1998] Shao, J. (1998). Poroelastic behaviour of brittle rock materials with anisotropic damage. *Mechanics of materials*, 30(1):41–53.
- [Shao and Giraud, 2002] Shao, J. and Giraud, A. (2002). Comportement poromécanique des roches saturées lois incrémentales viscoplasticité et endommagement, modèles de comportement des sols et des roches.
- [Shao and Henry, 1991] Shao, J. and Henry, J. (1991). Development of an elastoplastic model for porous rock. *International Journal of plasticity*, 7(1-2):1–13.

- [Shen et al., 2013] Shen, W., Kondo, D., Dormieux, L., and Shao, J. (2013). A closed-form three scale model for ductile rocks with a plastically compressible porous matrix. *Mechanics of Materials*, 59:73–86.
- [Shen et al., 2014] Shen, W., Lanoye, E., Dormieux, L., and Kondo, D. (2014). Homogenization of saturated double porous media with eshelby-like velocity field. *Acta Geophysica*, 62(5):1146–1162.
- [Shen and Shao, 2016] Shen, W. and Shao, J. (2016). An incremental micro-macro model for porous geomaterials with double porosity and inclusion. *International Journal of Plasticity*, 83:37–54.
- [Shen and Shao, 2017] Shen, W. and Shao, J. (2017). Some micromechanical models of elastoplastic behaviors of porous geomaterials. *Journal of Rock Mechanics and Geotechnical Engineering*, 9(1):1–17.
- [Shen et al., 2012] Shen, W., Shao, J.-F., Kondo, D., and Gatmiri, B. (2012). A micro-macro model for clayey rocks with a plastic compressible porous matrix. *International journal of plasticity*, 36:64–85.
- [Shen et al., 2015] Shen, W. Q., Shao, J.-F., Kondo, D., and De Saxce, G. (2015). A new macroscopic criterion of porous materials with a mises-schleicher compressible matrix. *European Journal of Mechanics-A/Solids*, 49:531–538.
- [Stover et al., 2003] Stover, S., Ge, S., and Screatton, E. (2003). A one-dimensional analytically based approach for studying poroplastic and viscous consolidation: Application to woodlark basin, papua new guinea. *Journal of Geophysical Research: Solid Earth*, 108(B9).
- [Talesnick et al., 2001] Talesnick, M., Hatzor, Y., and Tsesarsky, M. (2001). The elastic deformability and strength of a high porosity, anisotropic chalk. *International Journal of Rock Mechanics and Mining Sciences*, 38(4):543–555.
- [Terzaghi, 1944] Terzaghi, K. (1944). *Theoretical soil mechanics*. Chapman And Hali, Limited John Wiler And Sons, Inc; New York.
- [Thompson and Willis, 1991] Thompson, M. and Willis, J. (1991). A reformation of the equations of anisotropic poroelasticity. *Journal of Applied Mechanics*, 58(3):612–616.

- [Viesca and Rice, 2012] Viesca, R. C. and Rice, J. R. (2012). Nucleation of slip-weakening rupture instability in landslides by localized increase of pore pressure. *Journal of Geophysical Research: Solid Earth*, 117(B3).
- [Viesca et al., 2008] Viesca, R. C., Templeton, E. L., and Rice, J. R. (2008). Off-fault plasticity and earthquake rupture dynamics: 2. effects of fluid saturation. *Journal of Geophysical Research: Solid Earth*, 113(B9).
- [Warpinski and Teufel, 1992] Warpinski, N. and Teufel, L. (1992). Laboratory measurements of the effective-stress law of carbonate rocks under deformation. Technical report, Sandia National Labs., Albuquerque, NM (United States).
- [Wiborg and Jewhurst, 1986] Wiborg, R. and Jewhurst, J. (1986). Ekofisk subsidence detailed and solutions assessed. *Oil & Gas Journal*, 84(7):47–51.
- [Wong et al., 1997] Wong, T.-f., David, C., and Zhu, W. (1997). The transition from brittle faulting to cataclastic flow in porous sandstones: Mechanical deformation. *Journal of Geophysical Research: Solid Earth*, 102(B2):3009–3025.
- [Wong et al., 1992] Wong, T.-f., Szeto, H., and Zhang, J. (1992). Effect of loading path and porosity on the failure mode of porous rocks. *Applied Mechanics Reviews*, 45(8):281–293.
- [Xie et al., 2012] Xie, N., Zhu, Q., Shao, J., and Xu, L. (2012). Micromechanical analysis of damage in saturated quasi brittle materials. *International Journal of Solids and Structures*, 49:918–928.
- [Xie and Shao, 2012] Xie, S. and Shao, J. (2012). Experimental investigation and poroplastic modelling of saturated porous geomaterials. *International Journal of Plasticity*, 39:27–45.
- [Xie et al., 2011] Xie, S., Shao, J., and Xu, W. (2011). Influences of chemical degradation on mechanical behaviour of a limestone. *International Journal of Rock Mechanics and Mining Sciences*, 48(5):741–747.
- [Xie and Shao, 2006] Xie, S. and Shao, J.-F. (2006). Elastoplastic deformation of a porous rock and water interaction. *International Journal of Plasticity*, 22(12):2195–2225.
- [Xie and Shao, 2015] Xie, S. and Shao, J.-F. (2015). An experimental study and constitutive modeling of saturated porous rocks. *Rock Mechanics and Rock Engineering*, 48(1):223–234.

- [Yamada et al., 1981] Yamada, S., Schatz, J., Abou-Sayed, A., and Jones, A. (1981). Elasto-plastic behaviour of porous rock under undrained conditions. *International Journal of Rock Mechanics and Mining Science*, 18(2).
- [Yarushina and Podladchikov, 2015] Yarushina, V. M. and Podladchikov, Y. Y. (2015). (de) compaction of porous viscoelastoplastic media: Model formulation. *Journal of Geophysical Research: Solid Earth*, 120(6):4146–4170.
- [Zhang et al., 1990] Zhang, J., Wong, T.-F., and Davis, D. M. (1990). Micromechanics of pressure-induced grain crushing in porous rocks. *Journal of Geophysical Research: Solid Earth*, 95(B1):341–352.
- [Zhu et al., 1997] Zhu, W., Montesi, L. G., and Wong, T.-f. (1997). Shear-enhanced compaction and permeability reduction: Triaxial extension tests on porous sandstone. *Mechanics of Materials*, 25(3):199–214.
- [Zhu and Wong, 1997] Zhu, W. and Wong, T.-f. (1997). The transition from brittle faulting to cataclastic flow: Permeability evolution. *Journal of Geophysical Research: Solid Earth*, 102(B2):3027–3041.